BIOPHYSICAL INTERACTIONS: INFLUENCE OF WATER FLOW ON NUTRIENT DISTRIBUTION AND NITRATE UPTAKE BY MARINE ALGAE

A THESIS SUBMITTED TO THE GRADUATE DIVISION OF THE UNIVERSITY OF HAWAIʻI AT MĀNOA
IN PARTIAL FULFILLMENT OF THE REQUIREMENTS FOR THE DEGREE OF

DOCTOR OF PHILOSOPHY
IN
OCEANOGRAPHY

DECEMBER 2017

By

Sherril G. Leon Soon

Thesis Committee:
Kathleen C. Ruttenberg, Chairperson
Matthew Church
Margaret McManus
Brian Powell
Megan Donahue

Acknowledgements

A simple thank you could never express my gratitude for those who have helped me along the way, yet for many of those folks, a simple thank you is more than they would ever even ask for.

Thank you to my dissertation committee for staying the course with me and guiding me through the unexpected, and often unbelievable, challenges and obstacles that appeared in my path. Kathleen Ruttenberg's unwavering dedication, support, and mentorship transformed my experience into one of both academic advancement and personal growth.

Drs. Barb Bruno, Ruth Gates, and Mark Merrifield deserve special mention. Reflection on my matriculation experiences affirms that these generous faculty entered my life exactly when I needed them the most. Thank you, Mark, for taking the time to review my data and also for offering support, via your staff, students, and equipment, for additional field work. Thank you, Barb, for being a constant example of strength and relentless pursuit of excellence, progress, and what is right. Thank you, Ruth, for your genuine and sound advice and for extending yourself in support in more ways than one.

I have also been fortunate to receive overwhelming kindness from the administration and support staff (office and shop) of the Oceanography Department and the Hawai'i Institute of Marine Biology. It has allowed me to develop professional and personal relationships that I will forever hold dear.

A special thank you to those that gave of their time and expertise to assist with field work and sample collection.

My experience at He'eia Fishpond can only be described as a gift. Because of the generosity, support, kindness, and warm hearts of all those that mālama that loko, I not only had the opportunity to

work in a beautiful and cherished place, but I gained a family and feel like I can make Hawai‘i my home. Words cannot express my gratitude.

Last, and certainly not least, the success of this dissertation was in no small part made possible by the support of my family and closest friends here in Hawai‘i and at home in Trinidad and Tobago. The unconditional support of true friends needs no definition, qualification, or explanation – thank you. Finally, mahalo to my mother whose constant support, reassurance, inspiration, drive, fearlessness, and love carried me.

ABSTRACT

Inorganic nutrients are required by primary producers for photosynthesis. Their distribution and availability therefore underpin the success of ecosystems. The relationship between primary production and inorganic nutrient concentration and speciation is complex and variable, based not only upon differences in algal physiologies, but also upon physical environmental factors. For example, physical factors such as water flow rate can impact transport of nutrients to algal uptake surfaces. In order to understand survival strategies employed by the algae, it is essential to understand the different stages and drivers of the nutrient uptake and assimilation processes, including the interplay between nutrient concentration and hydrodynamics. The series of studies described in this dissertation represent a three-tiered investigation into the nitrate uptake response of marine algae to variable water flow rates. First, the interaction of an individual organism with its local flow environment is assessed in the field; next, the response of an epiphyte community to variable water flow rates is evaluated in an experimental study. Finally, a combined field-modeling study scales up data obtained from smaller-scale experiments and timeseries observations, focused on individuals and communities, to an ecosystem level study. In this field-modeling study, the impact of interplay between nutrient concentrations and hydrodynamics on the rates of, and capacity for, nitrate uptake by the algal community is examined. All phases of the study take place in the southern portion of Kāneʻohe Bay, Oʻahu, in the waters surrounding Moku o Loʻe and in Heʻeia Fishpond, an ancient Hawaiian fishpond.

Investigation into the role that local hydrodynamics can play in nutrient uptake by the specific benthic algae targeted in this study reveals that each benthic component displays flow-mediated nitrate uptake. Field studies reveal that *Gracilaria salicornia*, an invasive Rhodophyte in Hawaiʻi that is characterized by a particularly rigid canopy, is effective at forming microhabitats within its canopy understory, where inorganic nutrient concentrations are significantly elevated above the water column exterior to the

canopies. Measurement of nitrate reductase (NR) activity in the tissue of this alga also suggests that it can respond quickly to its immediate nutrient concentration environment, on spatial scales of at least 2 cm. Thus, vertical gradients in NR activity within *G. salicornia* canopies are likely driven by the nutrient microenvironment that the alga, itself, creates. Model results indicate that within He'eia Fishpond, *G. salicornia* is the main driver of nitrate drawdown from the water column. Assessment of an epiphyte community, hosted by benthic alga resident in Kāne'ohe Bay, reveals that the cumulative responses of individual epiphyte species to elevated nitrate concentrations and nitrate flux can translate into shifts in primary producer community structure. Finally, successful application of a nitrate distribution model developed for He'eia Fishpond reveals that the total biomass of each of the members of the primary producer community is an important determining factor in nitrate distribution.

TABLE OF CONTENTS

Acknowledgements ii
Abstract iv
List of Figures ix
List of Tables xii
CHAPTER 1 – INTRODUCTION 1
CHAPTER 2 – INFLUENCE OF FLOW ON THE ESTABLISHMENT OF MARINE MICROHABITATS AND BIOLOGICAL RESPONSE WITHIN A BENTHIC ALGAL CANOPY 7
Abstract 8
1. Introduction 9
2. Methods 15
2.1. Site description and experimental design 15
2.2. Sample collection, storage, and analysis 17
3. Results 24
3.1. Canopy Morphometrics 24
3.2. Hydrodynamic Characterization 24
3.3. Biogeochemical Characterization 27
3.4. Biological Response 28
4. Discussion 28
4.1. Impact of Canopies on Hydrodynamics 29
4.2. Impact of Canopies on Biogeochemistry 33
4.3. Impact of Canopies on System Nutrient Budgets 39
4.4. Linking Canopy Structure to Species Maintenance and Biodiversity 39
5. Summary and Conclusions 41
CHAPTER 3 – MARINE EPIPHYTE COMMUNITY RESPONSE TO VARIABLE NITRATE FLUXES IN A TROPICAL SHALLOW REEF FLAT SYSTEM 53
1. Introduction 53
2. Methods 58
2.1. Background 58
2.2. Study Site and Study Organism 59

2.3. Flume Design and Set-up 60
2.4. Experimental Design & Rationale 60
2.5. Sampling Scheme & Analysis 61
2.6. Field Collection and Experiment Setup 62
2.7. Sample Preparation and Microarray Hybridization 64
2.8. Data Analysis 66
3. Results 69
3.1. Results of Hybridization 69
3.2. Diversity of Naturally Occurring Epiphyte Community (i.e. non-treatment assemblages) 69
3.3. Flume Experiment Results 70
4. Discussion 73
4.1. Diversity of Naturally Occurring Epiphyte Community (i.e. non-treatment assemblages) 74
4.2. Flume Experiment Results 75
5. Conclusions 83
CHAPTER 4 – BIOPHYSICAL INTERACTIONS ON THE ECOSYSTEM LEVEL: INVESTIGATING NITRATE DISTRIBUTION IN A SHALLOW COASTAL REEF FLAT SYSTEM USING A NUMERICAL MODEL 109
1. Introduction 109
2. Materials & Methods 113
2.1. Study Site 113
2.2. Primary Producer Distribution 114
2.3. Nitrate Uptake Assessments 116
2.4. Nitrate Distribution Model 122
3. Results 131
3.1. Primary Producer Distribution 131
3.2. Nitrate Uptake Assessments 132
3.3. Nitrate Distribution Model 133
4. Discussion 137
4.1. Primary Producer Distribution 137
4.2. Nitrate Uptake Assessments 139
4.3. Nitrate Distribution Model 141
5. Conclusion 150

CHAPTER 5 – CONCLUSION 176
Appendix I – Canopy Hydrodynamics Data Validation 181
Appendix II – Graphical Abstract 182
Appendix III – Flume Experiment Sampling Scheme 183
Appendix IV – Epiphyte vs. Macroalgae Host Enzyme Activity 184
Appendix V – Functional Gene Microarray Glossary 185
Appendix VI – Nitrate Distribution Model Variables and Parameters 186
References 190

List of Figures

Figure		Page
2.1.	Map showing Coconut Island and study sites	43
2.2.	Canopy-associated sampling locations	44
2.3.	Conceptual figure of a typical energy density spectrum	45
2.4.	(a) Root Mean Square (*uRMS*) and (b) Reynolds numbers (*Re*) at canopy sampling locations	46
2.5.	Mean nutrient concentrations at canopy sampling locations	47
2.6.	Correlation between the attenuation parameter, alpha, and canopy morphometric and nutrient concentration ratios	48
2.7.	Mean Nitrate Reductase (NR) enzyme activity at canopy sampling locations	49
3.1.	Map showing study site at Coconut Island (Moku o Lo‘e)	85
3.2.	**A.** *Padina thivyae* collection and preparation for flume experiments **B.** Flow chart illustrating experiment sample collection and processing	86
3.3.	Section of scanned hybridized slide	87
3.4.	**A.** Phylogenetic tree of epiphyte community based on gene sequences coding for Rubisco (rbcL)	88
	B. Phylogenetic tree of epiphyte community based on gene sequences coding for Nitrate Reductase (NR) enzyme	89
	C. Phylogenetic tree of epiphyte community based on gene sequences coding for a eukaryotic membrane-bound nitrate transporter protein (*Nrt2*)	90
3.5.	Barcharts showing community structure based on the rbcL gene marker	91
3.6.	Barcharts showing community structure based on the NR gene marker	92
3.7.	Barcharts showing community structure based on the *Nrt2* gene marker	93
3.8.	Barcharts illustrating how the representation of Classes in a community sample can change depending upon choice of gene marker	94

3.9. Barcharts showing the range of Shannon diversity indices …… 95

3.10. Timeseries of nitrate concentration of the flume water in the 10 µM experiment 96

3.11. Barcharts showing **A.** Day 0 sample epiphyte community structure and **B.** a timeseries of epiphyte community structure over the experimental period …… 97

3.12. Barcharts showing variations in epiphyte community structure based upon hybridization of the chromophyte nitrate reductase(NR)gene ……. 98

3.13. Epiphyte community structure based on hybridization of the chromophyte nitrate reductase (NR) gene at sampling timepoints for paired 10 µM experiments ……. 99

3.14. Daily rate of change of relative abundance based on hybridization of the chromophyte nitrate reductase (NR) gene ……. 100

3.15. Daily rate of change of relative abundance based on hybridization of the chromophyte RuBisCO (rbcL) gene ……. 101

3.16. Scatterplot showing RNA:DNA ratios based on chromophyte nitrate reductase (NR) …… 102

3.17. Scatterplot showing RNA:DNA ratios based on chlorohyte nitrate reductase (NR) . 103

3.18. Scatterplot showing RNA:DNA ratios based on cyanobacteria nitrate reductase (NR) …… 104

3.19. Scatterplot showing RNA:DNA ratios based on eukaryotic membrane transport protein (*Nrt2*) …… 105

3.20. Scatterplot showing RNA:DNA ratios based on RuBisCO (rbcL) ……. 106

4.1. Map showing study site at He‘eia Fishpond (Loko i‘a o He‘eia) ……. 152

4.2. Map of He‘eia Fishpond showing monthly and seasonal sampling locations for algal cover and biomass ……. 153

4.3. **A.** Map of He‘eia Fishpond and **B.** Plan view of field flume ……. 154

4.4. Schematic representation of the processes linking nitrogen reservoirs within each model cell ……. 155

4.5. Map showing a typical benthic algal distribution in He‘eia Fishpond for the Dry and Wet Seasons …… 156

4.6. Vertical profiles of RMS velocity in **A.** main (longitudinal), **B.** transverse (V), and vertical (Z) directions of flow …… 157

4.7. Two examples of nitrate drawdown time series data within the flume at two flow velocities: **A)** 0.015 ms^{-1} and **B)** 0.129 ms^{-1} …… 158

4.8. **A.** Nitrate uptake rate constant for entire community as a function of bulk velocity, U_b and **B.** Nitrate uptake rate constant normalized to % algal cover …… 159

4.9. Nitrate Uptake by **A.** *Gracilaria salicornia*, **B.** *Acanthophora spicifera*, **C.** microphytobenthic community, and **D.** phytoplankton community in relation to bulk velocity (U_b). **E.** Contrasting nitrate uptake by benthic algal components …….. 160

4.10. Relative contribution of individual components of primary producing community to total nitrate uptake capacity of the benthos …… 161

4.11. Percent decrease in ***N*** for each model simulation …… 162

4.12. Model output for Typical Dry Season algal coverage versus Typical Wet Season algal coverage under baseline nutrient conditions …… 163

4.13. Model output for 100 % Dry Season ***M*** converge versus 100% Wet Season ***M*** coverage under baseline nutrient conditions …… 164

4.14. Model output for **(i)** Typical Dry Season algal coverage versus 100 % Dry Season M converge under baseline nutrient conditions and **(ii)** Typical Wet Season algal coverage versus 100 % Wet Season ***M*** converge under baseline nutrient conditions …… 165

4.15. Model output for Typical Dry Season algal coverage under baseline nutrient conditions versus under nutrient pulse conditions …… 166

4.16. Model output for 100 %Dry Season M converge versus 100%Wet Season M coverage under nutrient pulse conditions …… 167

4.17. Model output for Typical Dry Season algal coverage under half-day nutrient pulse conditions versus 1-day nutrient pulse conditions versus 2-day nutrient pulse conditions …… 168

4.18. Timeseries of total N in the fishpond under 0.5-day nutrient pulse conditions ……. 169

4.19. Map of Dry Season and Wet Season algal distribution showing high flow regions .. 170

4.20. Bar charts showing seasonal differences in benthic algal cover for each algal species observed …… 171

List of Tables

Table		Page
2.1.	Site descriptors for the Leeward and Windward sides of Moku o Lo‘e	50
2.2.	A. Mean nutrient concentrations at sample locations	51
	B. Percent increase in nutrient concentration at the ***BC*** (bottom of the canopy) canopy sampling location	52
3.1.	Phytoarray description	107
3.2.	Species Richness, S, for four T0 samples	108
3.3.	Shannon Entropy, H' for four T0 samples	108
3.4.	“true diversity” for four T0 samples	108
4.1.	Nitrate reservoirs defined for model	172
4.2.	Summary of Model Simulations	173
4.3.	Comparison of algal cover in He‘eia Fishpond between Dry and Wet Seasons	174
4.4.	Nitrate drawdown summary for field flume experiments	175

CHAPTER 1 – INTRODUCTION

"… there is a strong scientific consensus that coastal marine ecosystems, along with the goods and services they provide, are threatened by anthropogenic global climate change (IPCC 2001)"

Harley et al. 2006

The coastal ocean is important for a variety of activities integral to the healthy functioning of modern society. While covering only approximately 10% of total ocean area, it is within these waters that 15% of oceanic primary production occurs (Giraud et al. 2008), which supports 95% of the total oceanic biomass (Trujillo & Thurman 2013). Coastal oceans are the locus of important fisheries, shipping, oil and gas extraction, recreation, nutrient cycling, waste treatment, species refuge, cultural activities, and critical services from coral reefs systems, such as biodiversity maintenance, coastal protection, flood control (Scavia et al. 2002). Globally, over a billion people live in low-lying coastal regions ("The battle for the coast" 2010), and expanding coastal infrastructure to accommodate this growing population is placing increasing pressure on coastal resources, giving rise to new management challenges. As a result of a rapidly changing climate and often-unchecked anthropogenic activities, coastal marine ecosystems are at risk of serious and irreversible degradation, which also endangers human health and welfare (Harley et al. 2006). Large and permanent shifts in average conditions in the coastal ocean (deviations from the mean or 'baseline') are manifest, and can be attributed to changes in land use within the watershed, coastal development, shipping and navigation channels, and species invasions. These activities are in part responsible for higher nutrient loads to the coastal ocean and changes in biological community structure. Thus, it is increasingly important to develop strategies for protecting coastal systems as part of a comprehensive and collaborative environmental management plan.

Changing dissolved nutrient patterns are a significant symptom of coastal transformations related to climate change and anthropogenic activity. Since the source of inorganic nutrients is in large part terrestrial, a nutrient concentration gradient typically exists from higher levels near coastlines to progressively lower levels with distance from the shore. These patterns are subject to modification by changes in both large- and small-scale process, such as intensification of coastal upwelling (physically forced nutrient fluxes), increased flux of terrestrial materials, and spreading dead zones and oxygen minimum zones (OMZs) (Diaz & Rosenberg 2008). For example, nitrogen delivery to coastal regions is projected to double by 2050, based on the 1990 business as usual values (Seitzinger et al. 2002), as a consequence of human population growth and increased food demand generating pressure on agriculture lands (increased use of fertilizers). Climate change-induced shifts in wind patterns may impact coastal upwelling, either enhancing it and increasing nutrient availability in surface waters (Harley et al., 2006), or promoting increased stratification resulting in a reduction of upwelled nutrients (Roemmich & McGowan 1995). Climate models predict an increase in extreme rainfall events, which can significantly increase the dissolved nutrient and sediment load delivered to coastal waters (Scavia et al. 2002). These features can have profound effects on both primary and secondary production, and thus the marine foodweb. Variation in nutrient distribution will impact patchiness of benthic algal cover and abundance, which will also affect overall production (Lotze & Worm 2002, Nielsen 2003 from Harley et al 2006.

Invasive species can disrupt the existing ecological balance of a system by affecting changes on the population level (e.g., via predation), and also on the community and ecosystem level (e.g., via space occupation, facilitation of other species invasions, and disproportionate use of resources, such as inorganic nutrients). These impacts can ultimately result in disruption of ecosystem services, including

the economy, the environment, and human health (Jacoby et al. 2004). The research described in this dissertation was designed, in part, to provide insight into mechanisms that drive nutrient uptake by invasive and native algae. Such insight may provide clues to ways in which management practices can bolster resilience of native species in the face of species invasions, and thus to preserve ecosystem function.

The research described in this dissertation investigates nutrient dynamics in a shallow coastal region of Oʻahu, Hawaiʻi, with particular focus on nitrate. The direct and indirect effects of anthropogenic activities on nutrient delivery to the coastal ocean are particularly apparent in Hawai'i because of the relatively short watershed (Ringuet & MacKenzie 2005; Cox et al. 2006; De Carlo et al. 2007). Additionally, coastal lands in Hawaiʻi have undergone numerous land-use changes in the past 35 years ("Hawaii Agricultural Land Use Study Released" 2016), which have resulted in alterations of nutrient discharge and sediment efflux patterns (Stimson & Larned 2000, Hoover & Mackenzie 2009)

Nitrate is an essential nutrient for primary production, and can be the limiting nutrient in many coastal areas. Nitrate can also drive eutrophication in coastal ecosystems (Howarth & Marino 2006). There has been a well-documented, worldwide increase in areal cover and biomass of algae correlated to increased nutrients (Valiela et al. 1997). The research presented herein focuses on biophysical interactions between algal communities and flowing water (and thus dissolved nutrients) in coastal systems. Response of various algae to changes in inorganic nitrate distribution and delivery to their uptake surfaces as a function of water flow rates, and how they in turn influence nutrient distribution patterns, is the central organizing focus of this dissertation work. Questions about nutrient uptake dynamics are investigated on three ecological scales. The Individual: In Chapter 2, we focus on the response on an individual benthic alga (*Gracilaria salicornia*) to its hydrodynamic environment, and its

physiological response to the local hydrodynamic regime. The Community: The response of an epiphyte community to variable nitrate flux to uptake surfaces is explored in Chapter 3, using a functional gene microarray. The Ecosystem: In Chapter 4, the concept of differential responses by members of the primary producing community to nitrate flux was scaled up to assess the ability of an ecosystem as a whole to respond to variable nitrate fluxes by developing a nitrate distribution model for He'eia Fishpond.

Chapter 2: The Individual.

Benthic algal canopies function as roughness elements and can modify the water flow regime across benthic landscapes. The magnitude of currents within algal canopies (the understory), and exchange between within-canopy water and surrounding water, are significantly attenuated. This chapter describes results of a field study which demonstrates that *Gracilaria salicornia* (benthic Rhodophyte) algal canopies can attenuate current speeds by as much as 98%, and documents significantly higher nitrate (up to 5-fold), ammonium (up to 24-fold), and phosphate (up to 5-fold) concentrations within the canopy compared to the immediately adjacent external environment. The observed nutrient distributions correlate well with the degree of flow attenuation by the canopies, and are likely maintained for time periods sufficient for well-defined canopy-associated microhabitats to form. Additionally, a vertical gradient in Nitrate Reductase enzyme activity is observed in *Gracilaria salicornia* canopy tissues, which is consistent with dissolved inorganic nitrogen gradients within the canopy. The interaction of organism morphology, hydrodynamics, and biological response creates complex physical and biogeochemical landscapes, and highlights the need to understand the drivers behind these interactions.

Chapter 3: The Community.

Epiphytes on marine macrophytes can play a large role in overall community nutrient uptake and nutrient cycling compared to their hosts, and can represent a significant proportion of total system productivity (Nelson 1997, Cornelisen & Thomas 2002, 2006). Epiphytes thus have the potential to affect the size of the inorganic nutrient reservoir, and thus the availability of nutrients to other organisms. Epiphytes also may play unique roles in the function of the ecosystems within which they are found, making their high metabolic rates even more consequential. Chapter 3 reports results from a laboratory study to track response of an epiphyte community from Kāneʻohe Bay to changes in nutrient flux. A functional gene approach was adopted to (1) determine the capability of detecting and assessing the epiphytic community structure in Kāneʻohe Bay using a custom-designed microarray chip, (2) assess the community structure and diversity of epiphytes associated with *Padina thivyae*, and (3) use the microarray to assess changes in the epiphyte community in response to variable nitrate flux (nitrate delivery to uptake surfaces). Three genetic markers that encode proteins essential for uptake and assimilation of nitrogen and carbon in primary producers were employed. The first of these is rbcL, which codes for the large subunit of the enzyme ribulose 1, 5 bisphosphate carboxylase/oxygenase (RuBisCO). RuBisCo is the enzyme involved in the first step of carbon fixation by primary producers. The second is NR, which codes for Nitrate Reductase, which is the enzyme that catalyzes the reduction of nitrate to nitrite. The third is a marker for EukNrt, which codes for the membrane-bound nitrate transporter protein in eukaryotes. In brief, the measured RNA:DNA ratios of whole epiphyte community samples indicated upregulation of NR by the epiphytes in response to increases in the rate of nitrate delivery to their uptake surfaces.

Chapter 4: The Ecosystem.

Chapter 4 describes the development and application of a one-dimensional numerical model for nitrate uptake by the primary producer community in He‘eia Fishpond, an ancient Hawaiian fishpond in He‘eia, Ko‘olaupoko, O‘ahu. The objective of the model was to investigate the nitrate uptake capacity and distribution of a community consisting of phytoplankton, microphytobenthos (MPB), and two invasive benthic algal species common in Hawai‘i (*Gracilaria salicornia* and *Acanthophora spicifera*) under different environmental conditions. Several model scenarios were employed in order: (i) to assess the effect of seasonal changes in algal cover on the total nitrate uptake by primary producers, (ii) to assess the nitrate uptake capacity of He‘eia Fishpond primary producers in the absence of the invasive macroalgae, and (iii) to evaluate the response of the primary producers within the fishpond to pulses of elevated nitrate levels which simulate a post-storm nutrient environment. Results of the model reveal that *Gracilaria salicornia* is the primary determinant in total nitrate removed from the water column in the fishpond, under all conditions. Additionally, phytoplankton are the most responsive to rapid increases in nutrient delivery, such as those experienced during increased run-off after a storm.

CHAPTER 2 – INFLUENCE OF FLOW ON THE ESTABLISHMENT OF MARINE MICROHABITATS AND BIOLOGICAL RESPONSE WITHIN A BENTHIC ALGAL CANOPY

Leon Soon, Sherril G.[1,2] (Corresponding author)
leonsoon@hawaii.edu

Ruttenberg, Kathleen C.[2,3]
kcr@hawaii.edu

Merrifield, Mark A.[2]
markm@soest.hawaii.edu

Thomas, Florence I.M.[1]
fithomas@hawaii.edu

[1]Hawai'i Institute of Marine Biology, University of Hawai'i at Mānoa, P.O. Box 1346, Kāne'ohe, Hawai'i 96744 U.S.A.

[2]Department of Oceanography, University of Hawai'i, SOEST, Honolulu, Hawaii 96822 U.S.A.

[3]Department of Geology and Geophysics, University of Hawai'i, SOEST, Honolulu, Hawaii 96822 U.S.A.

For submission to Limnology & Oceanography as a Research article.

Abstract

Benthic algal canopies function as roughness elements and can modify the water flow regime across benthic landscapes. The magnitude of currents within the canopy (understory) and exchange between within-canopy water and surrounding water are significantly attenuated. This alteration of local hydrodynamic patterns may result in spatial and temporal patchiness of various geochemical parameters, such as dissolved nutrients, thereby establishing canopy-associated microhabitats. The present study demonstrates that *Gracilaria salicornia* (benthic Rhodophyte) algal canopies can attenuate current speeds by as much as 98% and documents significantly higher nitrate (up to 5-fold), ammonium (up to 24-fold), and phosphate (up to 5-fold) concentrations within the canopy compared to the adjacent external environment. The observed nutrient distributions correlate well with the degree of flow attenuation by the canopies, and are likely maintained for time periods sufficient for well-defined canopy-associated microhabitats to form. Additionally, we observed a vertical gradient in Nitrate Reductase enzyme activity in *Gracilaria salicornia* canopy tissues that is consistent with dissolved inorganic nitrogen gradients. The interaction of organism morphology, hydrodynamics, and biological response creates complex physical and biogeochemical landscapes, and highlights the need to understand the drivers behind these interactions.

Keywords

microhabitat formation; hydrodynamics; *Gracilaria salicornia*; nutrient distribution; nitrate reductase; Kāneʻohe Bay, Hawaiʻi

1. Introduction

Microhabitats can play a major role in community structure, and their persistence and variability in space and time can provide information about species distribution and productivity (e.g., Fonseca et al. 2011). Microhabitats are small-scale niches in space and/or time in which environmental conditions are distinct from the immediately adjacent surroundings. When they encompass the physical requirements of a particular organism or population, microhabitats provide conditions that can support a distinct flora and/or fauna. Woodbury (1933) described microhabitats as "[the] ultimate division of the habitat including recognition of its modifying factors, occupied by morés or species". They may also be defined operationally as the space used daily, or over some defined period of time, by an organism(s) for a particular activity (Jorissen et al. 1995, Pittman & McAlpine 2003). Microhabitats have ecological importance because they provide physical shelter (Marx & Herrnkind 1985), refuge from predation (Vaudo & Heithaus 2013), grazing grounds (Pittman & McAlpine 2003), and breeding and/or nesting sites (Ormond et al. 1996). Microhabitat use can vary on multiple temporal and spatial scales (Ormond et al. 1996), and microhabitat type may determine the size distribution of organisms (Dahlgren & Eggleston 2001). In environments where background resource availability is low, such as in the tropics, the way in which organisms locate and exploit these microhabitats can be of critical importance (Seymour et al. 2009). Therefore, understanding how and where microhabitats arise, and how they are maintained, has implications for ecosystem function and management (Miller et al. 2012).

The formation and maintenance of microhabitats result from complex interactions among physical, geochemical, and biological processes. A hydrodynamic feature particularly relevant to the present study is the benthic boundary layer at the sediment-water interface (SWI) (see Burdige 2006, and citations therein, for a discussion of the benthic boundary layer). At the SWI, benthic processes of remineralization, irrigation, sedimentation, and resuspension are linked with processes in the overlying pelagic environment. This type of coupling, frequently referred to as bentho-pelagic coupling (Marcus & Boero 1998), is especially tight in shallow coastal systems where these interactions tend to be highly variable due to the short spatiotemporal scales over which they take place (Grebmeier et al. 1988). The benthic boundary layer, a gradient in flow typically found at the SWI (Berner 1980, Vogel 1996, Boudreau 1997), "intimately links the sediment to the water column" (Holtappels et al. 2011) and as such, structures (living and non-living) within it impact benthic and pelagic processes. The involvement of these structures in the formation of benthic microhabitats is therefore inherently complex.

Vegetated canopies form permeable structures that water must flow through and around, resulting in the development of distinct local hydrodynamic characteristics such as a shear layer at the canopy-water interface with associated vortices and the synchronous waving of flexible canopies (a phenomenon called monami) which can enhance the turbulent vertical transport of momentum (Ackerman & Okubo 1993, Ghisalberti & Nepf 2002). The average water velocity and wave energy within aquatic vegetation is typically reduced compared to that of

mainstream flow (Ackerman & Okubo 1993, Hurd 2000). The degree of flow attenuation depends upon multiple factors, including the submergence ratio (ratio of water depth to canopy height) (Paul et al. 2012), wave period (Hurd 2000), canopy size and morphology (Bouma et al. 2005, Paul et al. 2012), population density (i.e., number of canopies per area), and the dimensions of the canopy stand (Nepf 1999). The resulting flow attenuation can decrease nutrient uptake rates within the canopy due to reduced mass transfer (Wheeler 1980), and may modify the rates at which products of geochemical processes are exchanged between sediments and the overlying water column. The uneven distribution of benthic macroalgal structures (or roughness elements) creates a mosaic of flow patterns and may generate "patches" of water with distinct physical and geochemical characteristics. These distinct features fluctuate in space and time across the benthoscape (Zajac et al. 2013), drive community dynamics (production and biological structure) (Marcus & Boero 1998), and in turn affect organism distribution.

In addition to modifying the rate of mixing between water within the canopy understory and the overlying water column, macroalgae also affect within-canopy water chemistry through their own metabolic processes. Photosynthesis, respiration, waste elimination, and other processes associated with co-occurring vegetation and fauna all add and/or remove dissolved metabolites (e.g., nutrients) to and/or from the water column, modifying the water chemistry (Hurd 2000). In this way, the interaction of water flow and benthic vegetated canopies can create microhabitats. Algal canopies also have the potential to respond to the microhabitats

they create. For example, nutrient uptake rates and enzyme activity may respond to the local physicochemical environment (Young et al. 2005), resulting in feedback interactions between the alga and its environment.

Benthic algal cover in Hawai'i has recently undergone substantial modifications (Rodgers & Cox 1999, Stimson et al. 2001, Smith et al. 2002, 2004, Lapointe & Bedford 2011). Specifically, several species of non-indigenous marine algae have been introduced since the 1950s (Smith et al. 2004), and invasive species such as *Gracilaria salicornia* (*G. salicornia*) and *Acanthophora spicifera* (*A. spicifera*) outcompete and exclude native species of macroalgae (Lapointe & Bedford 2011). The native and introduced species can vary widely in morphology, resulting in a range of interactions with overlying water. *G. salicornia* is of particular interest as it tends to form dense mat- or carpet-like canopy morphologies with relatively thick, rigid thalli.

G. salicornia is a benthic Rhodophyte that was introduced intentionally from Hilo Bay to the reefs of Waikiki and Kāneʻohe Bay, Oʻahu circa 1978 (Smith et al. 2004). The rigid canopy of *G. salicornia* is different from that of its native congener, *Gracilaria coronopifolia*, which is instead characterized by a more flexible canopy. The thalli of *G. salicornia* are brittle, and adopt an interlocking branching morphology that is not flexible in flow (Figure 2.1a). *G. salicornia* is fast-growing, spreads clonally by fragmentation, and the geographic extent of its distribution from the point of introduction at Coconut Island in Kāneʻohe Bay has expanded rapidly since its introduction (Rodgers & Cox 1999, Smith et al. 2004).

Light and dissolved oxygen levels within *G. salicornia* canopies can differ significantly from that in the overlying water (Martinez et al. 2012). Therefore, different parts of the alga can be exposed to multiple geochemical environments simultaneously. Beach et al. (1997) observed that concentrations of light-absorbing pigments not only varied throughout *G. salicornia* canopies, but that this variation correlated with the irradiance gradient (established *in situ* by the branching morphology of the alga). The correlation between pigment concentration and the irradiance gradient suggests that the alga responds physiologically to the conditions created within its structure. Concentrations of solutes within the canopy, such as nutrients, differ from those in the overlying water (Larned 1998, Murphy 2012). The establishment of contrasting nutrient concentrations may be related to the rates of exchange between the water parcels within and outside of the canopy, which are driven by hydrodynamic interactions between the canopy and the overlying water column. The capacity for *G. salicornia* to form well-developed microhabitats has the potential to modify the physiochemical characteristics of its broader habitat. Its distribution and extent of cover is temporally variable, changing seasonally (Ruttenberg & Briggs 2012) and also on shorter time scales in response to physical disturbances (e.g., storms, high winds). As such, its impact on the habitat can be stochastic.

In this study, we determine the extent to which the chemical environment within the understory of *G. salicornia* canopies differs from the environment external to them, and explore factors that may control the formation of microhabitats within these canopies. Specifically, we measured the flow velocities within and external to the canopies, and relate

flow characteristics to biogeochemical patterns. Further, we determine whether the alga shows a biological response to the modified chemistry within its canopy. Here, the term 'canopy' refers to an isolated clump of *Gracilaria salicornia* that is easily distinguished from nearby algae or coral heads. While previous studies have observed the buildup of nutrients within canopies (e.g., Larned 1998, Murphy 2012), and numerous others have measured flow attenuation by algal canopies (reviewed in Hurd 2000), none to date have directly linked flow attenuation to the observed nutrient build-up within the algal canopies.

We hypothesize that the interaction between *G. salicornia* canopy morphology and water flow reduces exchange between within-canopy water and the surrounding water, and that this reduction in exchange influences the distribution of dissolved nutrients, giving rise to the establishment and maintenance of canopy-associated microhabitats. The canopy-associated microhabitats are characterized by higher levels of nutrients relative to the surrounding water column. We further hypothesize that even though these microhabitats may be variable in space and time (having multiple drivers including tides, winds, and light intensity), they are sustained for a long enough time period to elicit a correlated physiological response by the algae.

To investigate the interplay between the physical, geochemical, and biological processes of microhabitat formation and biological response in a shallow tropical coastal system, we (1) characterize hydrodynamic conditions within, and adjacent to, *G. salicornia* algal canopies, (2) characterize the distribution of dissolved inorganic nutrients in the water associated with *G.*

salicornia canopies, and (3) measure nitrate reductase (NR) enzyme activity throughout the canopy to determine its distribution. NR was selected as a biological indicator of macroalgal response to the modified conditions within its canopy structure because nitrate reduction is the rate-limiting first step in nitrate assimilation (Campbell 1999), and NR activity is affected by both nutrient concentration (nitrate and ammonium) and prevailing light conditions. Both nutrient concentration (Larned 1998, Murphy 2012) and light intensity (Martinez et al. 2012) have been shown to be significantly different within the canopy relative to outside. While other indicators, such as carbonic anhydrase activity, algal growth rates, or even the expression of stress proteins may also be used as indicators of biological response, NR has been shown to respond quickly to environmental fluctuations (Young et al. 2007), and assays for its activity are well established and reliable (Hurd et al. 1996, Young et al. 2005). For the reasons listed above, NR activity is useful as an indicator of biophysical interactions, specifically nutrient distribution within the system, providing a link between environment and physiology.

2. Methods

2.1. Site description and experimental design

The study site was located at Moku o Loʻe (Coconut Island – home of the Hawaiʻi Institute of Marine Biology), in Kāneʻohe Bay, Oʻahu, Hawaiʻi (21.4336°N, 157.7883°S). The prevailing winds at the site are the Northeast Trade Winds. Currents off the reef flat in the vicinity of Coconut Island, approximately 1 km away from the study site, typically range between 0.05 ms^{-1} and 0.08 ms^{-1} (Bathen 1968); currents associated with study site are of lower magnitude (see Table 2.1). Samples were taken on both the Leeward (Site A) and Windward (Site B) sides of the island

(Figure 2.1b). Hydrodynamic, geochemical, and morphological properties were measured for twelve (12) *G. salicornia* canopies evenly distributed across the two sites, and all canopies were located at least fifteen (15) meters from shore. Water depth was measured at each canopy and canopy dimensions were recorded.

The locations for sampling water, macroalgal tissue and/or measuring hydrodynamic parameters at each canopy (Figure 2.2), were designated as ***FS*** (freestream – 20 cm below air-water interface, 1 m away from the canopy), ***TC*** (tip of canopy – within the top 2 cm of the algal canopy), ***MC*** (middle of the canopy – the center 2 cm of the canopy), ***BC*** (bottom of the canopy – just above the SWI within the bottom 2 cm of the canopy understory), ***MA*** (adjacent to the canopy, 30 cm away in a direction perpendicular to mainstream flow at the same height as the ***MC*** *location*), and ***BA*** (adjacent to the canopy, 30 cm away in a direction perpendicular to mainstream flow at the same height above the SWI as the *BC* location). Each canopy was sampled only once. Due to the density and rigid structure of the *G. salicornia* thalli, taking replicate hydrodynamic, water, and tissue samples would have been disruptive to the canopy structure itself. To minimize the effects of changes in tide during the sampling period, all measurements and samples were taken during an incoming tide, and sampling at each canopy was accomplished within 20 minutes, a short enough time period to ensure uniform tidal activity. Sampling was completed between 09:00 and 14:00 each day, to limit the effects of varying light on observations.

2.2. Sample collection, storage, and analysis

2.2.1. Hydrodynamic characterization

Two assessments of flow were taken within and adjacent to the algal canopies: (1) within-canopy Dye Retention measurements and (2) hydrodynamic data collection using acoustic Doppler velocimeters (ADVs). The Dye Retention measurements allowed visualization and quantitative characterization of flow within the algal canopies, while the canopy-associated ADV data permitted a systematic and detailed assessment of the differences in flow characteristics among the designated sampling locations associated with the canopies (*MC, MA*, and *FS*).

For the Dye Retention measurements, fluorescein dye (5 ml) was injected into the center of the canopies, after which 5-ml subsamples of water were taken every 15 to 30 seconds at the injection site until the dye could no longer be detected by the naked eye in the sample volume. These samples were analyzed for fluorescein intensity on a Molecular Devices Spectra Max M2 spectrophotometer (490 nm and 525 nm excitation and read wavelengths, respectively). Based on exponential regression of the plotted data, a continuous dye decay rate (*k*), in units of second^{-1}, was determined for each canopy.

Hydrodynamic parameters were measured using Nortek Vectrino acoustic Doppler velocimeters (ADVs). A reference ADV, placed mid-water column at a central distance of 10 to 20 meters from the canopies under study, collected continuous data in order to assess general site conditions and to permit assessment of whether mean flow changed in any systematic way during the sampling period. The second ADV was used to measure flow at three locations

associated with each canopy, namely *MC*, *MA*, and *FS* (Figure 2.2). We used the differences between flow at the *MC* and *MA* locations, and between the *MC* and *FS* locations to determine the effect of the canopy on flow. The ADV probe was oriented down-looking, affixed to a stationary arm whose height could be adjusted. At each location, data were acquired for five (5) minutes at a sampling rate of 25 Hz in the stream-wise (*u*), cross stream (*v*), and vertical (*w*) directions. For each canopy, measurements were taken within a 20-minute period to reduce possible effects of changes in water flow over time. Because of small canopy size (Table 2.1; Supplemental Materials T1), it was only practical to take one measurement at the center of the canopy. Thus we used the mid-canopy location (*MC*) and its external counterpart, adjacent to the canopy (*MA*), for comparison. Sampling volume and transmit length were set to 7 mm and 1.8 mm, respectively.

The ADV output was processed using MATLAB (R2011b; The MathWorks, Inc.®; Matlab code developed by Oscar Guadayol o Roig (O. Guadayol o Roig pers. comm.)). Spikes (anomalous peaks in the data) were removed using the 3D phase-space thresholding technique outlined by Goring & Nikora (2002) and Wahl (2003), and as applied by Kregting et al. (2013). Velocity components with beam correlations of <60%, or below a threshold signal-to-noise (SNR) of 15 dB, were removed (McLelland & Nicholas 2000). The number of spurious data points excluded was small (0.04%), and linear interpolations were made to bridge the gaps left by the excluded data points.

To ensure that the data accurately represented flow along the stream-wise/cross-stream axes, empirical orthogonal function (EOF) analysis was used to correct slight misalignments of the probe during data collection. In this analysis, horizontal dimensions are re-oriented such that they are orthogonal to the dominant current. This treatment assumes that no changes in the orientation of the probe were made during data collection. All calculations from this point forward utilized parameters in the stream-wise (u) direction only, as this was defined as the principal axis of the horizontal current.

Flow parameters were calculated following methods in Stiansen & Sundby (2001) and Kregting et al. (2013). The velocity signal was decomposed into a low frequency mean velocity (*U*), a wave component (u_w), a turbulent component (u'), and an instrumental white noise component (u_{noise}):

$$u = U + u_w + u' + u_{noise} \qquad \text{Eq. 1}$$

The various components of the total signal were estimated by integrating different regions of the power density spectra of the signals (Figure 2.3a). The white noise component of the signal was identified using the flat segment at the highest frequencies in the spectra, while the inertial subrange was identified as the segment of the density spectrum that followed a $-5/3$ slope, after subtraction of white noise (Kregting et al. 2013). By integrating under the inertial subrange region of the spectrum, we determined the turbulent component of the signal. The wave component was estimated by integrating the peak (spike in energy density) that appears in the wave frequency. The total Root Mean Square (*uRMS*) current is:

$$uRMS = \sqrt{\overline{u^2}} = \sqrt{\overline{U^2} + \overline{u_w^2} + \overline{u'^2} + \overline{u_{noise}^2}} \quad \text{Eq. 2}$$

and the Reynolds number (Re) was calculated as follows:

$$Re = \frac{uRMS * l}{\nu} \quad \text{Eq. 3}$$

where l = characteristic length (water depth outside the canopy or mean space between thalli inside the canopy), and ν = kinematic viscosity.

Following Lowe et al. (2005) and Weitzman et al. (2013), we used the velocity ratio alpha (α) to assess the effect of the canopy on hydrodynamic and nutrient distributions. This ratio can be viewed as an attenuation parameter, as it compares the reduced velocity within the canopies to the velocities outside of the canopies. To facilitate visualization of the effects of increasing attenuation (the greater the attenuation, the larger the alpha) on nutrient buildup within the canopies, we chose alpha (α) to be OUT/IN for our study. Alpha (α) was calculated as the ratio between the values of $uRMS$ measured outside of the canopy (*MA*) to those measured inside the canopy (*MC*):

$$\alpha_{\mathrm{OUT/IN}} = \frac{uRMS_{\mathrm{OUT}}}{uRMS_{\mathrm{IN}}} \quad \text{Eq. 4}$$

A large $\alpha_{\mathrm{OUT/IN}}$ value indicates that flow within the canopy is greatly attenuated (OUT >>> IN). The relationships between $\alpha_{\mathrm{OUT/IN}}$ and canopy height, submergence ratio (water depth:canopy height), and dissolved nutrients were evaluated using Pearson's Correlation Coefficient.

Having considered the potential challenges of accurately measuring extremely low water flow rates within the algal canopies and the possibility of disruption of ADV data collection by the rigid thalli of the alga, several validation tests were conducted. These tests were used to assess the ability of the instrument to distinguish low flow rates from instrumental noise, and the possibility of artifacts in the data that might arise due to the interaction of the ADV transducer beams with alga thalli.

2.2.1.1. Validation of hydrodynamic (ADV) data

Three sets of ADV validation tests were conducted in both controlled and manipulated environments to (i) provide a reference point for confidently measuring low within-canopy water flow rates, and (ii) explicitly determine characteristic data features that correspond to direct interference by the alga in ADV data collection. In all validation tests, data were collected at the same sampling frequency (25 Hz) used for the canopy sampling locations, and we analyzed the same standard metrics used to assess the quality of hydrodynamic data: signal amplitude, beam correlation, and SNR. We also generated energy density spectra based on the *uRMS* time series data. A 'no-flow' reference point was obtained from a Bucket Test, in which ADV data were collected in still water with a probe oriented down-looking and affixed vertically to a stationary arm. Energy density spectra from these tests provide a reference range for instrumental white noise. Energy spectra above this lower range correspond to signals that can be confidently distinguished from the instrumental noise. A Freestream Flow Test provided a reference point for unobstructed flow. In this test, the down-looking sampling probe was positioned 0.15 m below the surface of the water at the study site, a distance far enough from

bottom elements (including macroalgal heads) that water is minimally influenced by obstructional features. Finally, to determine how transducer beam obstruction by the algae would manifest in ADV data, we purposefully positioned *G. salicornia* thalli within the path of the ADV transducers while collecting data in the Beam Obstruction Test.

Once anomalous data points associated with correlation and SNR values outside of threshold levels were filtered and removed (Materials and Methods 2.2.1), the inside-canopy amplitude, correlation, and SNR data were compared to these same parameters from the validation tests. We used the reference values obtained from the 'no-flow' Bucket, Freestream Flow, and Beam Obstruction Tests to evaluate whether the ADV data obtained within the algal canopies was robust, or whether there were artifacts in the data due to the extremely low flow rates within the algal canopies, and/or signs of bias in the data due to obstruction of the transducer beam path by the stationary alga. Validation test data are used as benchmarks against which the inside-canopy data were assessed for validity. Characterization of the inside-canopy data as valid was dependent upon whether the data fell within the ranges of the assessment parameters (noise floor, amplitude, SNR, and beam correlation percent) as defined by the validation tests and the manufacturer recommended cut-offs.

2.2.2. Biogeochemical characterization

Water samples were taken at the *TC*, *BC*, *BA*, and *FS* locations (i.e., both within and external to the canopy) using a 140 ml syringe fitted with a blunt-end needle. Only one water sample was taken at each sampling location in order to prevent the mixing and/or overlap of sampling locations (i.e., to maintain discrete sampling locations) within the relatively small canopy

volume. Samples for nutrient analysis were filtered through 0.2 µm Thermo Scientific™ Target2™ nylon syringe filters, and stored in 30 ml HDPE bottles at -80°C until analysis. All sampling equipment and storage containers were acid-washed in order to avoid contamination. Nitrate, nitrite, ammonium, phosphate, and silicate concentrations were determined following the protocols of the WOCE Hydrographic Program using a Technicon AAII system (University of Washington Marine Chemistry Laboratory, *http://www.ocean.washington.edu/story/Marine+Chemistry+Laboratory*).

For each nutrient, the ratio of the values measured outside of the canopy to those measured inside the canopy were calculated and compared to $\alpha_{\mathrm{OUT/IN}}$. A large OUT:IN ratio for a nutrient indicates that its concentration within the canopy is low relative to that outside of the canopy (OUT >>> IN). Conversely, a small OUT:IN ratio indicates a build-up of that component within the canopy relative to the outside (IN >>> OUT).

2.2.3. Biological response

After sampling for nutrients, a vertical trans-section of algal tissue was collected for enzyme activity analysis using a polypropylene syringe push core with beveled edges to cut through the algal tissue. The core was then sectioned into tip (*TC*, top 2 cm), middle (*MC*, center 2 cm), and bottom (*BC*, bottom 2 cm) sections. Tissue samples were immediately frozen in liquid nitrogen and stored at -80°C until analysis. Nitrate reductase activity of the *G. salicornia* tissue was assayed and values were normalized to gram frozen weight (gFW^{-1}), following Young et al. (2005).

3. Results

General site descriptors for both Site A and Site B are summarized in Table 2.1. All reported parameters at Site A were statistically indistinguishable from those at Site B, with the exception of water depth.

For all canopy sampling locations assessed (*FS*, *TC*, *MC*, *BC*, *MA*, and *BA*), the mean value of physical, chemical, and biological parameters measured were statistically indistinguishable between Site A and Site B. Therefore, throughout the rest of the paper, we report the mean values calculated over all twelve canopies sampled.

3.1. Canopy Morphometrics

Canopy dimensions ranged from 0.16 to 0.43 m in length, 0.14 to 0.33 m in width, and 0.065 to 0.165 m in height (Supplemental Materials T1). These canopy dimensions correspond to a range of canopy volumes from 0.0025 to 0.0199 m^3. The volume of water enclosed by each algal canopy defined the microhabitats for this study. None of the canopies occupied more than 30% of the water column depth, with submergence ratios ranging from 3.6 to 7.6.

3.2. Hydrodynamic Characterization

During the Dye Retention evaluations, the injected dye remained well-contained within the algal canopy, and was not visible at canopy outer edges until after approximately two minutes. Decay rate (k) ranged from -0.029 to -0.011 (Supplemental Materials T1) and correlated best with canopy width (Pearson's correlation coefficient, $r = 0.555$, $p = 0.061$).

Although mean *uRMS* at the reference ADVs were comparable between sites A and B, the variances surrounding those means were distinct (Table 2.1). On the leeward side of the island

(Site A), mean *uRMS* at the reference ADV during the sampling period was 0.015 ms^{-1} with a Root Mean Square Error (*RMSE*) of 0.015. On the windward side of the island (Site B), mean *uRMS* at the reference ADV was 0.017 ms^{-1} with a RMSE of 0.023. General flow conditions were relatively stable throughout the sampling period with mean *uRMS* remaining within +/- 20% of starting values at both Site A and Site B, and general flow conditions did not change systematically during sample collection.

At the canopy sampling locations, Root Mean Square velocity in the predominant direction of flow (i.e., *uRMS*) was significantly lower ($p < 0.0005$) inside (*MC*) (1.5×10^{-3} m s^{-1}) the *G. salicornia* canopies compared to the adjacent (*MA*) (1.1×10^{-2} m s^{-1}) and the above canopy (*FS*) (1.1×10^{-2} m s^{-1}) sampling locations (Figure 2.4a). The *uRMS* values at *MC* represent a mean reduction of 87.01 % (SD = ± 13.97) and 84.1 % (SD = ± 22.83) relative to *MA* and *FS*, respectively.

Reynolds numbers within the canopies (range = 1.12 to 25.70, mean = 7.11, SD = 8.78) are three to four orders of magnitude lower than those outside the canopy at the *MA* (1.21×10^3 to 9.38×10^3) and *FS* (3.64×10^3 to 1.12×10^4) locations ($p < 0.0005$) (Figure 2.4b).

In the time series of ADV data collected at sampling locations outside the algal canopies (*MA* and *FS*), the energy spectra showed well-defined $-5/3$ slopes (Figure 2.3b) indicating turbulent energy dissipation, and thus measureable turbulent flow. Mean turbulent *uRMS* was 0.4×10^{-2} m s^{-1} and 0.3×10^{-2} m s^{-1} at the *MA* and *FS* locations, respectively. The energy spectra generated from ADV data collected within the canopies showed decreased turbulent and wave energy

compared to those generated from data collected outside of the canopy (Figure 2.3c versus 3b). This is a clear indication that inside-canopy flow is significantly different from that external to the algal canopies. Within the canopy understory, flows are slower, less turbulent, and wave energy is suppressed. Thus, it is expected that mixing rates will be low inside relative to outside the algal canopies, which is corroborated by the Dye Retention evaluations.

3.2.1. Validation of hydrodynamic (ADV) data

SNR and beam correlation of all canopy-associated ADV data exceed the manufacturer-recommended cut-offs for good data (Nortek AS 2015) and are consistent with values published in other studies (e.g., (McLelland & Nicholas 2000, Kregting et al. 2013).

Under the 'no flow' conditions simulated by the Bucket Test, signal amplitudes ranged from 50 to 150, beam correlations ranged from 95% to 100%, and SNR ranged from 20 to 60. The corresponding energy density spectra generated from bucket test data had non-sloping portions that were centered at *ca.* 10^{-7} $ms^{-2}Hz^{-1}$. Freestream Flow Test amplitudes ranged from 50 to 70, correlation values were all above 80%, and SNR ranged from 10 to 50. Beam Obstruction Test amplitudes were elevated above those observed in the Bucket and Freestream Flow tests, ranging between 100 and 200 counts. Beam correlation values observed during the Beam Obstruction Test were highly variable, fluctuating across the full spectrum (i.e., between 0 and 100%); SNR values were elevated, registering between 25 and 75 (Supplemental Materials T2).

While Beam Obstruction Test amplitudes extended to 200 counts, none of the within-canopy amplitude data exceeded 180 counts. Within-canopy beam correlation values were constrained above 80% with one exception which was constrained above 60%; these are similar to the lower limit of ranges for the Bucket and Freestream Flow Tests, but notably distinct from the range observed in the Beam Obstruction Test, which spanned the full range from 0-100%. We were able to conclusively match the ADV data (amplitude, beam correlation, SNR) from five algal canopies to ranges observed in the Bucket (no-flow) and Freestream Flow (unobstructed-flow) validation tests. Five other inside-canopy ADV datasets fell entirely within one or two out of the three test parameter ranges set by the validation tests. Two inside-canopy datasets display ranges for all three parameters that fall within or below the validation test ranges. While the amplitude, beam correlation, and SNR data for these latter 7 canopies do not fall entirely within the ranges set by the validation tests, they largely overlap these ranges.

3.3. Biogeochemical Characterization

3.3.1. Nutrients

In general, mean nutrient concentrations across the twelve (12) algal canopies were significantly higher at the bottom of the canopy (*BC*, proximal to the sediment-water interface) than at all other sampling locations (Figure 2.5, Tables 2.2a and 2.2b). For nitrate, nitrite, ammonium, and phosphate, mean concentrations at the *BC* location were 1.07 ± 0.45 SD µM ($p < 0.0005$), 0.22 ± 0.08 SD µM ($p < 0.0005$), 1.43 ± 1.54 SD µM ($p = 0.011$), and 0.30 ± 0.16 SD µM ($p < 0.0005$) respectively. These mean nutrient values at *BC* represent concentrations that are 49—86% (nitrate), 105—147% (nitrite), 203—232% (ammonium), and 113—131% (phosphate)

higher than at the other sampling locations (*TC*, *BA*, and *FS*). Mean silicate concentration did not differ significantly between locations (mean concentration at *BC = 6.71; $F_{3,33}$ = 2.39; p = 0.086*). The pattern of higher nutrient concentration at the sediment-water interface was not seen outside the canopy over the bare sediment (*BA*) (Figure 2.5).

3.3.2. Attenuation parameter

Alpha ($\alpha_{OUT/IN}$) displayed a significant positive correlation with canopy height (r = +0.637; p = 0.026), but a significant negative correlation with submergence ratio (r = -0.715; p = 0.009). Alpha ($\alpha_{OUT/IN}$) also displayed a significant negative correlation with the OUT:IN ratios for nitrate ($NO_3^-{}_{OUT/IN}$; r = -0.761; p = 0.004), nitrite ($NO_2^-{}_{OUT/IN}$; r = -0.722; p = 0.008), ammonium ($NH_4^+{}_{OUT/IN}$; *r = -0.822; p = 0.001*), and phosphate ($PO_4^{3-}{}_{OUT/IN}$; r = -0.872; p <0.0005) (Figure 2.6). No significant relationship with silicate was observed, where Pearson's r = -0.083 and p = 0.798.

3.4. Biological Response

3.4.1. Nitrate Reductase activity

Assessment of the *G. salicornia* tissue for nitrate reductase (NR) activity revealed a vertical gradient in enzyme activity, with the tips (*TC*) having highest values (Figure 2.7). Mean NR activity decreased systematically from *TC* to *MC* to *BC*. Although, NR activity at *TC* and MC were not statistically different, both were significantly higher than NR activity at the *BC* location (*p <0.0005*) (Figure 2.7).

4. Discussion

The results of this study indicate that *Gracilaria salicornia* canopies markedly attenuate water flow. The observed attenuation correlates with differences in nutrient concentrations that characterize waters within and outside of the canopy. Further, the measured vertical gradient

in NR activity suggests that the alga is responding to the geochemical and physical environment created by the interaction between its morphology and water flow.

4.1. Impact of Canopies on Hydrodynamics

Dye Retention evaluations quite clearly demonstrated the effect of the algal canopies on water flow and thus on the advection and dissipation of dissolved components. The fact that the dye stayed within the canopy understories and was not visible at the canopy edges for at least two minutes provided a striking visual reflection of flow attenuation within the canopies. In fact, based on mean *uRMS* at the study site, a water molecule near the surface of the water column, in the absence of a canopy, would take approximately 16 seconds to travel a distance equivalent to that traveled by the dye within the canopies, from the injection site at the canopy center to the canopy edge. Thus, the water within the canopies travels 7.5 times more slowly than freestream flow. In addition, the positive correlation of decay rate, k, with canopy width ($p = 0.061$), suggests that the degree of the attenuation effect of the alga on inside-canopy water flow is dependent on canopy dimension. Parameter comparisons based on ADV data (Figure 2.6) corroborate this finding.

Mean flow (*uRMS*) at the leeward and windward sides of Coconut Island did not differ significantly (Table 2.1), but the more exposed (windward) site was characterized by higher variance about the mean (*RMSE*) than the leeward site. Even with this difference in variance between sites, the consistency in flow throughout the sampling period (flow remained within 20% of starting values, and no systematic changes were observed) and the similarity in mean velocity between the windward and leeward sites, allowed us to directly compare observations

made throughout the study, and to attribute differences to the presence of algal canopies. For example, the average difference between flow within the canopies (*MC*) and the adjacent site (*MA*) was 87%, and between *MC* and the above canopy sampling site (*FS*) was 84%; both are substantially greater than the ±20% variance in general flow recorded by the reference ADV during the entire sampling period.

The Reynolds number (*Re*) of a hydrodynamic regime is the ratio between inertial and viscous forces. High inertial forces favor turbulence while high viscous forces favor laminar (smooth) flow (Vogel 1996). As such, within a given system, lower Reynolds numbers indicate a tendency toward less turbulent flow while higher values indicate more turbulent flow. At the sampling frequency used (25 Hz), we could detect that both turbulence and wave energy were dampened within the canopy understories relative to flow outside of the canopy, and we observed low Reynolds numbers compared to those observed outside of the canopy (Figure 2.4b). In most cases the Reynolds numbers within the canopies indicate that water motion is approaching laminar flow where mixing is driven by molecular diffusion (self-diffusion coefficient on the order of 10^{-9} m^2 s^{-1}: Harris & Newitt 1997, Holz et al. 2000, Tofts et al. 2000) combined with low levels of turbulent mixing, and supplemented by small currents on the order of $10^{-3}ms^{-1}$ (See *uRMS* data in *Results – Hydrodynamic characterization*). This result is consistent with other studies demonstrating that turbulence and waves within submerged canopies are damped (Verduin & Backhaus 2000, Mendez & Losada 2004, Duarte et al. 2013). In contrast, estimated turbulent diffusion rates at sampling locations outside the canopy are on the order of

10^{-3} m^2s^{-1}, based on ADV data from above and outside the algal canopies (S. Leon Soon unpubl.), which greatly exceeds molecular diffusion rates by order 10^6. Overall, mixing rates within the canopies are greatly reduced relative to the turbulent mixing rates in the water column over bare sediment, where algal canopies are absent (Figure 2.4a and 2.4b). Cleary, the hydrodynamic environment of the canopy understories differs substantially from that of the surrounding water column, and this difference has implications for the distribution of both the dissolved components of the water (e.g., nutrients), as well as for any organismal activity linked to nutrient levels.

The proportion of the water column occupied by benthic structures (i.e., the submergence ratio) can significantly impact the flow environment. Our results reveal that the degree of attenuation of flow by *G. salicornia* canopies is highly correlated to submergence ratio (Figure 2.6), consistent with existing literature (Bouma et al. 2005, Prinos et al. 2010, Paul et al. 2012). This has relevance for how the hydrodynamic characteristics of the water (both within and external to a canopy) may change over tidal cycles as the water depth, and thus submergence ratio, fluctuates. As Kāneʻohe Bay experiences mixed tides, organisms must cope with fluctuations of their hydrodynamic environment multiple times per day.

Attenuation of mixing by *G. salicornia* canopies is likely to be more pronounced than attenuation by more flexible algal species, such as various *Padina* species and *Acanthophora spicifera*, both of which are commonly found in close proximity to *G. salicornia* canopies in Hawaiʻi, including at the current study site. Flexible canopies can exhibit coherent waving in a

flow field, a movement called the monami, which is a progressive, repeated deflection of the canopy (Ghisalberti & Nepf 2002, 2009). The repeated motion of the canopy can have the effect of disrupting the continuous buildup of nutrients within the canopy understory, as it increases the penetration of turbulent stress into the canopy. Unlike flexible canopies, the rigid thalli of *G. salicornia* do not bend in flow, and thus are more apt than their flexible counterparts to diminish flow and cause a build-up of nutrients.

4.1.1. Validation of Hydrodynamic (ADV) Data

The Bucket, Freestream Flow, and Beam Obstruction validation tests provide a context within which the hydrodynamic data from the four canopy-associated sampling locations can be viewed. The data ranges for amplitude, beam correlation and SNR from these tests provide metrics for assessing whether within-canopy data are negatively impacted by algal obstruction, and if not, whether they are consistent with uncompromised data collected under controlled conditions during the Bucket (no-flow) and Free Stream (unobstructed-flow) Tests. While the Bucket Tests allow us to assess instrument data collection in the absence of flow, the ADV is still able to detect small-scale motions such as convection currents, which are reflected in the energy density spectra and elevate the flat portion of the curve above the 'real' noise level of the instrument. As such, these data provide a conservative estimate of instrumental white noise.

A comparison of within-canopy data ranges of signal amplitude, beam correlation, and SNR to ranges observed in the validation tests indicates that (i) none of the canopies displayed data ranges that indicate algal obstruction, and (ii) all within-canopy data overlap the ranges

observed in the Bucket Test and the Freestream Flow Test. In addition, all inside-canopy data passed the initial screening tests consistent with industry standards and used in previous studies (McLelland & Nicholas 2000, Kregting et al. 2013), and met the constraints of a minimum of one out of the three validation tests. Thus, we include data from all canopies in the assessment and interpretation of biogeochemical data. We note the caveat, however, that while all inside-canopy hydrodynamic data met basic manufacturer-recommended standards for data quality, the overlap of some of the test parameter ranges did not allow us to conclusively rule out influence of the stationary canopy itself on the flow for all canopies.

4.2. Impact of Canopies on Biogeochemistry

The biogeochemistry of the water associated with the inside of the *G. salicornia* canopies is significantly different from the surrounding water (Table 2.2a). Specifically, while there is a clear difference in dissolved nutrient concentrations between *TC* and *BC*, there is no significant difference in nutrient concentration between the two-point vertical profile in the well-mixed column external to the canopy, i.e., between *FS* and *BA* (Figure 2.5; Table 2.2a). Thus, the 2-point vertical profile (*FS* to *BA*) provides a control against which the canopy nutrient profile can be assessed. In addition, nitrate, nitrite, ammonium, and phosphate concentrations were significantly correlated to flow attenuation (Figure 2.6). Collectively, these observations are consistent with our hypothesis that the interaction between flowing water and algal canopies with morphologies comparable to *G. salicornia* affects the distributions of dissolved nutrients, thereby establishing and maintaining microhabitats within the algal canopy.

The low mixing rates within the canopy understory offer a plausible explanation for the build-up of nutrients at the bottom of the canopies compared to concentrations measured in the surrounding water. It is the isolation of the water within the canopies that allows nutrients that are being released from sediments, from multiple processes such as remineralization (Boucher et al. 1994), groundwater seepage (Lewis 1987), as well as macrofaunal excretion (Williams & Carpenter 1988), to build up within the canopy understory. In the absence of the algal canopy, these nutrients would otherwise diffuse more quickly into the overlying water (Berner 1980), or be actively pumped out of the sediments via wave and tidal activity (Falter & Sansone 2000) or irrigating infauna (Aller 1994, Percuoco et al. 2015), and be subsequently mixed into the water column. The attenuated flow within the canopies inhibits the sub-canopy water from readily mixing into the water column (Larned 1998, Lapointe & O'Connell 1989, and suggested by Stimson et al. 1996 for *Dictyosphaeria cavernosa* in Kāneʻohe Bay). Although previous investigations of *G. salicornia* (Larned 1998) and other benthic macroalgae (Lapointe & O'Connell 1989, Larned & Stimson 1996, Stimson et al. 1996, Murphy 2012) have also observed nutrient build-up within canopy understories, because they did not pair hydrodynamic measurements (within and external to the algal canopies) with nutrient data, they were unable to explicitly demonstrate the role of biophysical interactions as a driver of the observed geochemical patterns.

The increases in nutrient concentrations at the base of the canopy (*BC*) correlate directly with attenuation parameter alpha (α) (Figure 2.6), and thus with the presence of *G. salicornia*

canopies. The clear relationship between the nutrient concentration OUT:IN ratios and α reinforces the link between attenuation of flow by *G. salicornia* canopies and the elevated nutrient concentrations within the canopy. Nutrient concentrations at the *BC* location were elevated by 71% to 203% over concentrations observed at the SWI adjacent to the canopies (*BA)*, and by 49% to 217% above those measured at the *FS* sampling location (Table 2.2b). Marine sediments have been shown to be a source of nutrients to the overlying water in Kāneʻohe Bay by Stimson & Larned (2000), Murphy (2012), and Briggs et al. (2013), and in similar tropical coral reef systems by Lewis (1987), Williams & Carpenter (1988), and Boucher et al. (1994). The rates at which these nutrients are mixed into the water column are affected by characteristics of water flow at the SWI (Huettel et al. 2003, Burdige 2006 and references therein). Our results indicate that the presence of *G. salicornia* canopies impacts flow characteristics at the SWI, resulting in increased nutrient concentrations within the canopy (Figure 2.5).

Living benthic structures not only interact physically with the water, but also biologically, as dissolved nutrients are utilized in physiological processes. Biological activity associated with the algal canopies may also drive the build-up of nutrients within the canopy via a reduction in the utilization of these nutrients. For example, under low light conditions, photosynthetic rates can drop to a tenth of the value expected in regular to high light conditions (Arnold & Murray 1980). The environment under the algal canopies is typically characterized by diminished light intensities relative to the immediately adjacent environment (Beach et al. 1997, Martinez et al.

2012). With lower rates of photosynthesis, a reduction of nutrient demand, and thus the rate at which inorganic nutrients are depleted via metabolism, is expected. Additionally, lower flow reduces mass transfer within the canopies, resulting in reduced nutrient uptake rates (Wheeler 1980, 1988, Hurd 2000). Together, the diminished nutrient demand and nutrient uptake capability minimize biological uptake as a significant sink for newly released nutrients under the canopies, and nutrients accumulate as a consequence. The magnitude and the relative importance of decreased nutrient demand versus decreased uptake capacity as biological drivers of nutrient buildup within the canopy understory cannot be resolved with the present dataset, and remains an intriguing and potentially important distinction.

4.2.1. Nitrate Reductase

The process of nitrate assimilation (nitrate reduction, nitrite reduction, and ammonium assimilation) can be regulated at multiple levels (i.e. molecular versus macro) and stages (i.e., points in time). Nitrate utilization is light-dependent and is highly positively correlated with photosynthetic activity. Specifically, NR is activated by the oxidized state of an electron transport component in the photosynthesis process (Sherameti et al. 2002), and photosynthesis provides the energy (ATP) for nitrate uptake and reduction (Flores et al. 2005). Light intensity is known to be attenuated by *G. salicornia* canopies, with the benthos receiving, on average, 0.2 to 4.9% of (i.e., 99.8 to 95.1% lower than) the amount of photosynthetically active radiation (PAR) received immediately above the canopies (Beach et al. 1997, Martinez et al. 2012). The higher NR activity observed at *TC* (Figure 2.7) is consistent with higher light levels at the top of the canopy, which would stimulate higher levels of NR. In contrast, reduced light at the canopy

interior is expected to slow NR enzyme activity rates, consistent with the relatively low rates observed at the bottom of the canopy (Figure 2.7). The intermediate NR activity observed in the middle of the algal canopy (*MC*) likely reflects intermediate light intensity at that location. The fact that *TC* and *BC* differ from each other but not from the mid-point (*MC*) is most likely because nutrient-light conditions at *MC* are more similar to *TC* than to *BC*. But, it is important to point out that the trend in *mean* NR values is one of monotonic decrease in NR from canopy top to bottom.

The vertical gradient in nitrate reductase (NR) activity between the outer edges (*TC*) and the bottom of the canopy (*BC*) indicates that the alga may be responding to the high nutrient environment within its understory in complex ways. Inorganic nitrate is known to induce the expression of nitrate assimilation genes (Flores et al. 1980, Ohashi et al. 2011), and thus the vertical distribution of nitrate concentration, higher at *BC* than at *TC* (Figure 2.6), would suggest that NR activity would be highest at the *BC* location. The fact that the observed trend in NR activity is exactly the opposite of that anticipated on the basis of nitrate concentrations alone suggests that additional factors are influencing the expression of NR by algal tissues. Ohashi et al. (2011) demonstrated that the presence of ammonium in growth media is sufficient to elicit inhibitory effects on nitrate assimilation regardless of the presence (or absence) of nitrate. We observe relatively higher ammonium concentrations at *BC* relative to *TC* (Figure 2.5). Thus, the contradiction between trends in nitrate concentration and NR activity can be reconciled by recognizing that ammonium assimilation inhibits nitrate utilization (uptake and reduction)

(Flores et al. 1980, Ohashi et al. 2011). Together, the higher ammonium concentration and lower light intensity at *BC* relative to *TC* and *MC* locations, may cause inhibition of NR activity and thus nitrate uptake.

The tips of *G. salicornia* thallus branches are the loci of meristematic tissue (Smith et al. 2002), and are therefore likely to have higher NR activity levels than regions without meristematic tissue (Granbom et al. 2004). These thalli tips are not restricted to the outer edges of the algal canopy, but are distributed throughout the strata of the alga. The fact that NR activity at the *TC* and *MC* canopy locations was not significantly different can be explained as a consequence of the overlapping, branching morphology of the alga, which exposes the meristematic tissue to gradients in light and ammonium concentration within the understory. The distribution of these determinant parameters (light, ammonium, and meristematic tissue) does not favor localization of NR activity at the canopy edges. Rather, NR is being synthesized within and expressed by tissues located within different geochemical environments; both high ammonium and nitrate concentrations at *BC*, and comparatively lower nitrate and ammonium levels at *TC* (Figure 2.7). Due to the dispersion of meristematic tissue throughout the canopy strata, the significant difference in NR activity between the top (*TC*) and the bottom of the canopies (*BC*) is not expected to correlate with a systematically vertical distribution of meristematic tissue. Thus, the final distribution of NR activity may be related to both the pervasive distribution of meristematic tissue as well as to differences in light intensity and nutrient concentrations within the established microhabitat.

4.3. Impact of Canopies on System Nutrient Budgets

Our results clearly indicate that *G. salicornia* canopies are able to break up the homogeneity of nutrient distribution in an otherwise well-mixed water column by establishing microhabitats. The formation of these microhabitats has substantial ecological implications. *G. salicornia* mats can be loosely attached to the substratum, and the alga often behaves like a "marine tumbleweed" once flows are high enough to dislodge the canopy from its attachment. At lower flows, such as those occurring in the habitats examined here, *G. salicornia* remains attached as a dense mat. The accumulated nutrients within the canopy understories may be released as pulses when canopies are dislodged by wave activity or high water flows. The tendency to break away from the substratum suggests that these algae may have an important role in pulsed release of nutrients to the water column and nutrient redistribution within the system. *G. salicornia* cover can also be ephemeral on seasonal scales in Kāneʻohe Bay (Ruttenberg & Briggs 2012). Given the high degree of nutrient enrichment within the canopy understories, seasonal changes in algal cover can have a particularly pronounced effect on nutrient budgets in small embayments or regions typified by low flow and reduced mixing.

4.4. Linking Canopy Structure to Species Maintenance and Biodiversity

The ability of *Gracilaria salicornia* to establish canopy-associated microhabitats, defined by heterogeneity in nutrient concentration and water flow, may be instrumental in the success of this species in Hawaiʻi. The relatively rapid rate of spread of *G. salicornia* observed in Kāneʻohe Bay (Smith et al. 2004) could be due, in part, to its ability to modify the relative concentrations of nutrients within its structure. The accumulation of essential nutrients in the canopy

understory, to levels over 200% higher than background concentrations, may effectively facilitate *G. salicornia* growth in oligotrophic systems, while impeding access to nutrients by other algal species. Because of its reduced state, uptake of ammonium is less energetically costly than uptake of nitrate, which must be reduced prior to assimilation (e.g., D'Elia & DeBoer 1978). Therefore, the high levels of ammonium as a nitrogen source may offer *G. salicornia* a competitive advantage over native macroalgae.

Benthic vegetation, such as *G. salicornia*, plays a role in the maintenance of higher biodiversity and abundance of benthic organisms compared to unvegetated sediments (Fonseca et al. 2011, Barnes & Barnes 2012). Additionally, Fukunaga et al. (2014) demonstrated that the morphology (and not only the presence) of benthic algal canopies can affect community structure – differences in epifauna density were observed between macroalgal species of contrasting morphologies, including *G. salicornia*, at Site A of the current study. They further illustrated a distinct pattern of variability in assemblage structure of epifaunal communities occupying invasive, native, and mixed-species algal canopies, with mixed canopies having intermediate variability between the native and invasive algal canopies. We have demonstrated that *G. salicornia* canopies create vertically and laterally distinct nutrient regimes, providing conditions which result in the establishment of multiple niches. Some organisms can exploit the patterns of heterogeneity in the environment that arise from the interplay of processes taking place on multiple scales (Levin 2000). Therefore, the existence of multiple nutrient regimes within an environment can greatly enhance the potential for elevated biodiversity. The results of this

study illustrate the direct effect of macroalgal morphology on water flow – an interaction that facilitates the development of canopy-associated microhabitats. This redistribution of resources (i.e., nutrients) may contribute to the coexistence of species (Levin 1981, 2000, Ellingsen et al. 2007) and account for the effect of morphological differences of macroalgae on biodiversity observed by Fukunaga et al. (2014).

5. Summary and Conclusions

Gracilaria salicornia canopies attenuate flow such that the hydrodynamic environment within their structures is significantly different from the external environment. Dye Retention experiments reveal that water flow is 7.5 times slower within the algal canopies as compared with freestream flow, and this flow attenuation effect scales with canopy dimension. Reynolds numbers and turbulence within the canopies are lower than outside of the canopies. This effect on hydrodynamics limits exchange of water between the canopy understory and the external water column, resulting in a modified sub-canopy geochemical environment. Specifically, nutrient concentrations within the canopies are substantially elevated compared to the surrounding water. Organisms living within the canopies can exploit an environment that otherwise would not exist in the absence of the alga. In addition, it is apparent that the alga itself is able to respond to the microenvironment it creates. A gradient in nitrate reductase (NR) activity was observed along vertical transects through the algal canopies, with relatively lower activities at the bottom of the canopy (*BC)* compared to the tip of the canopy (*TC*), a trend that correlates with high ammonium concentrations within the canopy understory; ammonium is an established inhibitor of NR activity. These interactions and the resulting correlated physical,

biological, chemical, and physiological patterns observed underscore the ability of *Gracilaria salicornia* to impact ecological processes. Together, these observations define the role of the alga in its new, non-native habitat, and offer initial insights as to how this invasive species outcompetes its native counterparts.

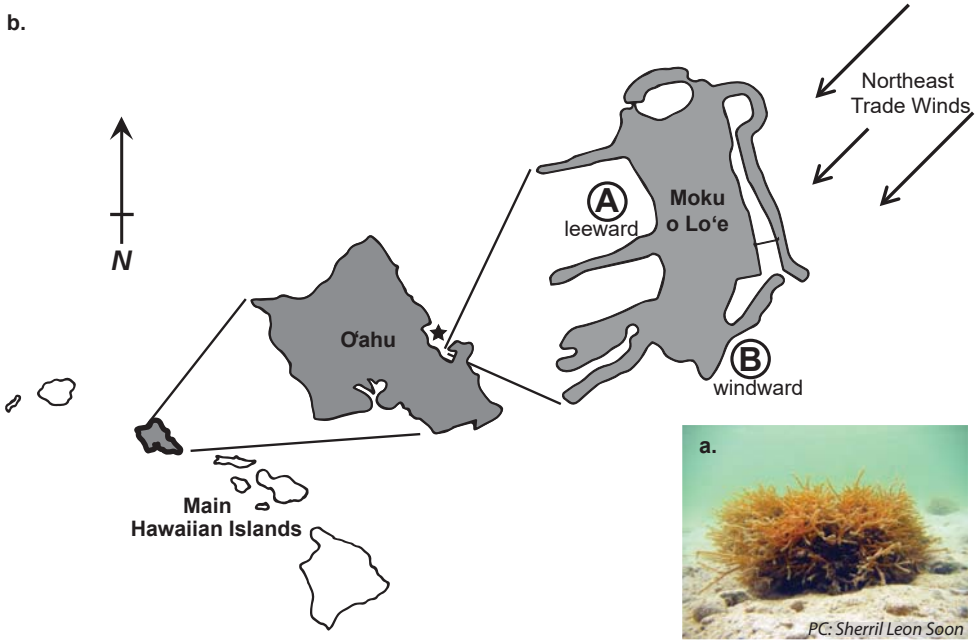

Fig. 2.1. (a) Photograph of *Gracilaria salicornia* canopy taken at Site A. Photo credit: Sherril Leon Soon. **(b) Map showing study site at Coconut Island (Moku o Lo‘e), home of the Hawai‘i Institute of Marine Biology.** The island is located in the southern portion of Kāne‘ohe Bay (★), O‘ahu, Hawai‘i. Site A (Leeward side) is located at 21° 25’ 55”N, 157° 47’ 14”W and Site B (Windward side) is located at 21° 26’ 2 N, 157° 47’ 22” W.

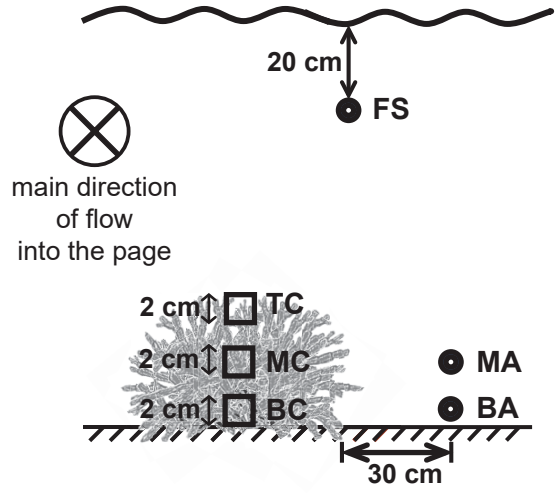

Fig. 2.2. Canopy-associated sampling locations. *FS*: freestream – 20 cm below the water's surface away from the canopy; *TC*: tip of canopy – within the top 2 cm of the algal canopy, *MC*: middle of the canopy – within the center 2 cm of the canopy; *BC*: bottom of the canopy – just above the sediment-water interface within the bottom 2 cm of the canopy understory; *MA*: adjacent to the canopy – 30 cm away in a direction perpendicular to mainstream flow at the same height as the *MC* location; *BA*: adjacent to the canopy – 30 cm away in a direction perpendicular to mainstream flow at the same height above the sediment as the *BC* location. Hydrodynamic parameters were assessed at the *MC*, *MA*, and *FS* locations and nutrient samples were taken at the *TC*, *BC*, *BA*, and *FS* locations. Algal tissue samples were taken at the *TC*, *MC*, and *BC* locations.

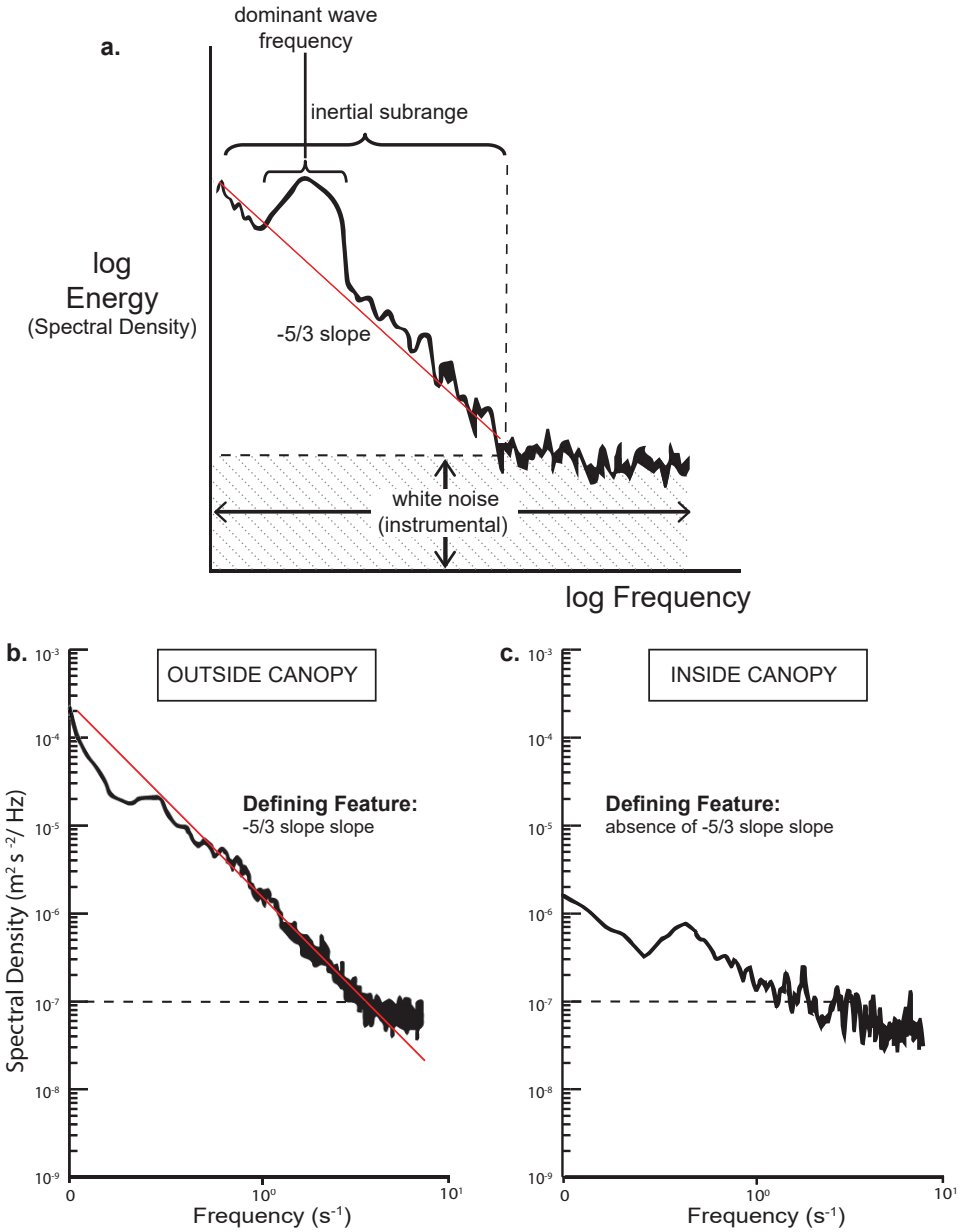

Fig. 2.3. A velocity signal can be decomposed into its constitutive components – a mean velocity, an oscillatory component, a turbulent component, and an instrumental white noise component – which can be identified on an energy density spectrum. **(a) Conceptual figure of a typical energy density spectrum generated from acoustic Doppler velocimeter (ADV) data.** Contribution of energy to the system from wave activity presents as an energy "bump" (located at the dominant wave frequency), while the -5⁄3 slope indicates the presence of turbulence and reflects its natural decay. The contributions of these various components to the total signal are obtained by integrating under their respective regions of the curve. **(b) Example of an energy density spectrum generated from data collected in this study outside the algal canopy.** These spectra all show energy decay along a -5/3 slope (red line) indicating turbulent flow. **(c) Example of an energy density spectrum generated from data collected in this study within the canopy understory.** None of the sub-canopy spectra displayed a -5/3 slope nor did they display any notable spike in energy density. The absence of these features indicates a suppression of both turbulence and wave activity, respectively.
The dashed line in panels b. and c. represents the noise floor that defines the upper limit of instrumental white noise, as determined from the 'no flow' Bucket Test results.

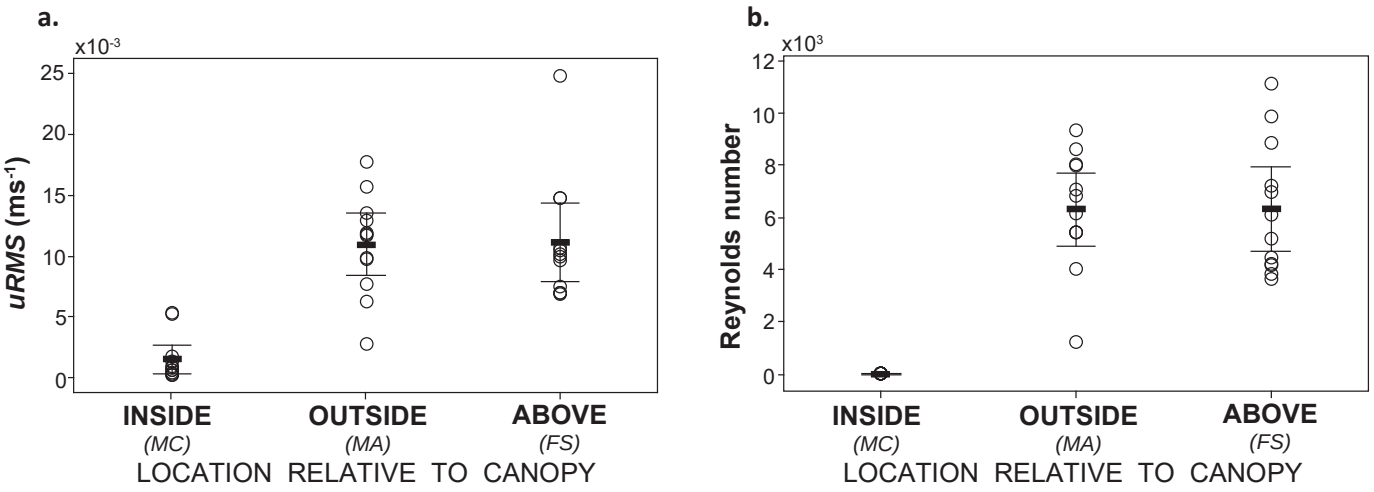

Fig. 2.4. (a) Distribution of Root Mean Square (*uRMS)* values and (b) Reynolds numbers (Re) at the canopy sampling locations. Values were calculated for the *MC* (middle of the canopy; INSIDE), *MA* (adjacent of the canopy at the same height as MC; OUTSIDE), and *FS* (freestream; ABOVE) sampling locations. For both *uRMS* and Reynolds number, the INSIDE (*MC*) location was significantly lower than the outside (*MA)* and above (*FS)* locations ($F_{2,22}$ = 33.63; p <0.0005 and $F_{2,22}$ = 34.96; p <0.0005, respectively). Black horizontal bars indicate mean values and interval bars show the 95% Confidence Interval about the mean. Note: All (12) data points are plotted for each location; some points overlap because they are so similar in value.

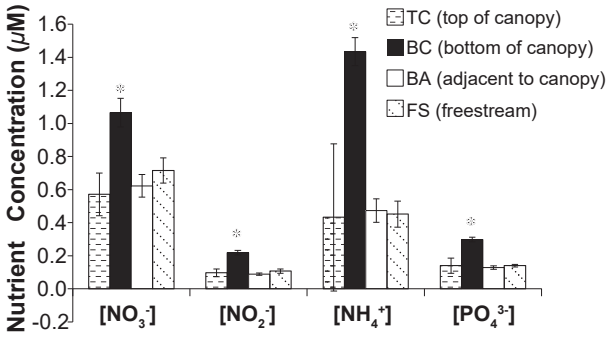

Fig. 2.5. Mean nutrient concentrations at canopy sampling locations. Data shown for TC (tip of the canopy;⊟), BC (bottom of the canopy;■), BA (adjacent to the canopy at the same height above the sediment as BC;□), and FS (freestream;⬚) sampling locations. Error bars represent standard error. Asterisks (*) indicate sample locations that were significantly different. There was no significant difference between means at sample locations for silicate (data not shown) ($F_{3,33}$ = 2.39, p = 0.086).

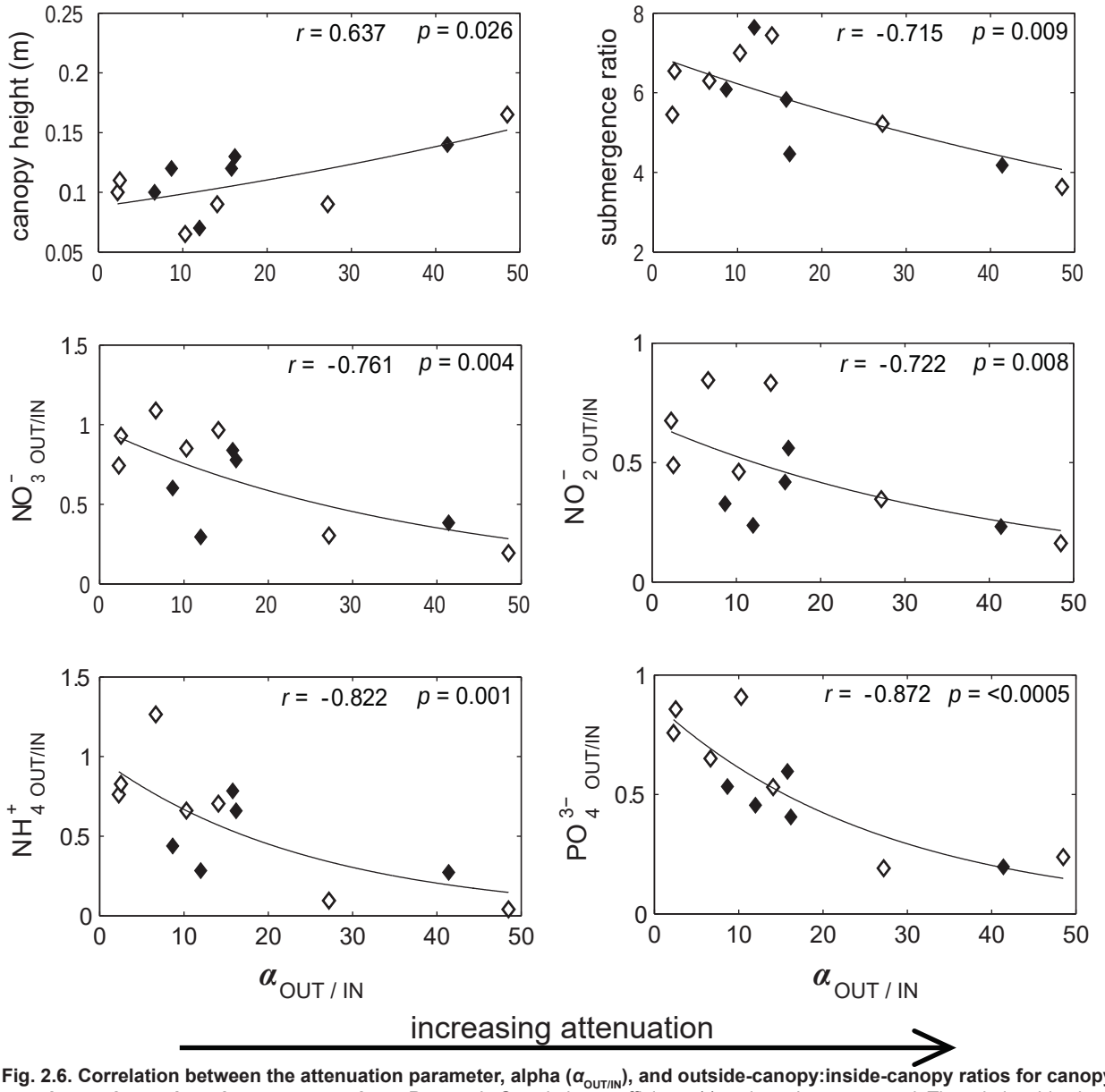

Fig. 2.6. Correlation between the attenuation parameter, alpha ($\alpha_{OUT/IN}$), and outside-canopy:inside-canopy ratios for canopy morphometrics and nutrient concentrations. Pearson's Correlation coefficients (*r*) and p-values are noted. The relationships between the hydrodynamics of the canopies and the various inorganic nutrients measured are clearly illustrated by the statistics. For example, alpha was high at low submergence ratios, indicating a progressively stronger attenuation of flow as the height of the canopy increases relative to water depth. A decreasing OUT:IN ratio for the nutrients suggests a relative build-up within the canopy. There was no significant relationship between silicate OUT:IN concentration ratios and alpha (r = -0.122, p = 0.706; data not shown). Solid markers correspond to algal canopies where the range of data quality parameters fell entirely within the validation test ranges. Data quality ranges for canopies represented by the open markers substantially overlap, but did not fall entirely within validation test parameter ranges.

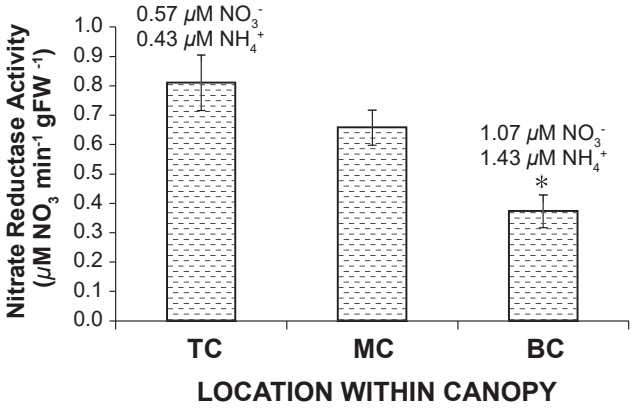

Fig. 2.7. Mean Nitrate Reductase (NR) enzyme activity in μM NO_3^- min^{-1} gFW^{-1} at canopy sampling locations. Samples were taken at *TC* (tip of the canopy), *MC* (middle of the canopy), and *BC* (bottom of the canopy) locations. Error bars represent standard error. Asterisks (*) indicate sample locations that were significantly different ($F_{2,22}$ = 12.64; p <0.0005). Nutrient concentration labels show the geochemical environment of the tissue expressing the measured nitrate reductase (NR) activity (nutrient data unavailable for MC).

Table 2.1.
Site descriptors for the Leeward (Site A) and Windward (Site B) sides of Coconut Island during the sampling period. See Figure 1 for site locations. A p-value $\leq$ 0.05 indicates a significant difference between sites. For all descriptors and at each site, *n* = 6. N/A: not applicable.

Site Descriptor	Site A (Leeward)	Site B (Windward)	P-value
tidal phase	incoming	incoming	N/A
water temperature (°C ± SD)	25.995 ± 0.834	24.802 ± 1.341	0.101
canopy height (m ± SD)	0.105 ± 0.040	0.112 ± 0.015	0.708
water depth (m ± SD)	0.532 ± 0.059	0.672 ± 0.058	0.002
submergence ratio (± SD)	5.522 ± 1.558	6.111 ± 0.980	0.451
***uRMS* (ms^{-1} ± SD)**	0.015 ± 0.015	0.017 ± 0.023	N/A

Table 2.2.a.
Mean nutrient concentrations ± standard deviation (in μM) at sample locations. For all nutrients, except silicate, concentration was significantly higher at the bottom of the canopy (*BC*) than at all other sampling locations, as shown by the p-values and F-statistics listed in the last two columns of the table. A p-value $\leq$ 0.05 indicates a significant difference between sampling locations.

Nutrient	***Mean Concentration ± Standard deviation (µM)***				***P-value***	***F statistic ($F_{3,33}$)***
	BC	***BA***	***TC***	***FS***		
nitrate	1.07 ± 0.45	0.62 ± 0.24	0.57 ± 0.30	0.72 ± 0.26	<0.0005	10.73
nitrite	0.22 ± 0.08	0.09 ± 0.03	0.10 ± 0.05	0.11 ± 0.04	< 0.0005	23.76
ammonium	1.43 ± 1.54	0.47 ± 0.25	0.43 ± 0.29	0.45 ± 0.27	0.011	4.34
phosphate	0.30 ± 0.16	0.13 ± 0.03	0.14 ± 0.05	0.14 ± 0.03	< 0.0005	13.20
silicate	6.71 ± 2.60	6.62 ± 0.72	6.17 ± 0.93	7.60 ± 1.50	0.086	2.39

Table 2.2.b.
Percent increase in nutrient concentration at the *BC* (bottom of the canopy) location relative to other canopy sampling locations. Percent increase at *BC* relative to *BA* = (([*BC*] – [*BA*]) / [*BA*]) x 100, where [*BC*] = nutrient concentration at the bottom of the canopy and [*BA*] = nutrient concentration at the sediment-water interface (SWI) adjacent to the canopy. Percentages were calculated in the same way for all sampling locations.

BC: bottom of the canopy, **BA: adjacent to the canopy, **TC**: tip of canopy, **FS**: freestream*

Nutrient	***% concentration increase at BC location relative to other sampling locations***		
	BA	***TC***	***FS***
nitrate	71	86	49
nitrite	147	127	105
ammonium	203	232	217
phosphate	131	114	113
silicate	1	9	-12

CHAPTER 3 – MARINE EPIPHYTE COMMUNITY RESPONSE TO VARIABLE NITRATE FLUXES IN A TROPICAL SHALLOW REEF FLAT SYSTEM

1. Introduction

Marine epiphytes, a group which includes “algae (micro and macro), bacteria, fungi, sponges, bryozoans, ascidians, protozoa, hydroids, crustaceans and mollusks” (Larkum et al. 2006), colonize the surfaces of seagrasses and macroalgae. They have been studied extensively in ecological systems in some areas of the world, and are known to respond rapidly to environmental perturbations. Even though epiphyte biomass is small compared to the biomass of their hosts, epiphytes play a crucial role in ecosystem functioning, as they modify the abiotic environment and can directly and indirectly influence both host and grazer activities.

Epiphyte community structure is determined by multiple biotic and abiotic influences, including host leaf age, (Marino et al. 1995, Prado et al. 2007, Mabrouk et al. 2011), grazing pressure by herbivores (Gambi et al. 1992), light, temperature, nutrients, and water motion (Lavery et al. 2007, Lee et al. 2007, Mabrouk et al. 2012). As summarized in Mabrouk et al. (2014), epiphyte distribution and abundance can correlate with seagrass leaf and stem age, as well as shoot morphology, as these characteristics determine the surface area available for epiphyte settlement. The shading effect of a dense seagrass canopy can also control epiphyte biomass via light limitation. Epiphyte distribution within a system is inherently dependent upon their host distribution, which is often ephemeral (van Montfrans et al. 1984) and, as such, their impact on the ecosystem is tied to the seasonality and success of their living substrates.

Epiphytes on marine macrophytes can play a significant role in overall community nutrient uptake and nutrient cycling compared to their seagrass (Cornelisen & Thomas 2002, 2006) or macroalgae hosts. For

example, epiphyte nitrate uptake rates can be up to 39-fold higher than that of their host organism (Cornelisen & Thomas 2006). Observed nitrate reductase enzyme activity displayed by epiphytes on *Padina thivye* in southern Kāneʻohe Bay was 1.8-fold (i.e., 2.8 times) and 2.3-fold higher than the macroalgal host in manipulated flume experiments and field samples, respectively (unpublished data; Appendix IV). In addition, highly variable responses to nutrient loading and other environmental perturbations can be observed within an epiphyte community due to the rich variety of epiphyte physiology and morphology present.

Epiphyte production can represent a significant proportion of total system productivity (Nelson 1997, Cornelisen & Thomas 2002); they may display high levels of productivity, often higher than their algal and seagrass hosts (unpublished data; Appendix IV). Cornelisen and Thomas (2002) demonstrated, using stable isotopes, that the proportion of total community (assemblage) ammonium uptake by the epiphyte community increased linearly with ammonium concentration, while ammonium uptake by the seagrass host was independent of ammonium concentration. The differential response to ammonium concentration suggests that, even though algal and seagrass hosts typically account for a higher biomass than their epiphyte complement, epiphytes have the potential to respond more quickly to nutrient input than their host organisms. Thus, epiphytes may be more responsive to storm-pulse nutrient input than their host organism. Epiphytes thus have the potential to affect the size of the inorganic nutrient reservoir, and thus the availability of nutrients to other organisms. Additionally, epiphytes may play unique roles in the function of the ecosystems within which they are found, making their high metabolic rates even more consequential. For example, Goering and Parker (1972) found that blue-green algae growing epiphytically on *Thalassia testudinum* (seagrass) was the only important nitrogen-fixer in the

seagrass community. Further, even after the seagrass leaves had sloughed off, N-fixation activity by the epiphytes on the floating blade continued.

Epiphytes can be an important source of food for heterotrophs (Yamamuro 1999, Moncreiff & Sullivan 2001). Isotopic analyses by Yamamuro (1999) suggest that heterotrophs preferentially consume epiphytic material on *Syringodium isoetifolium*, rather than either the seagrass itself or detrital material. Karez et al. (2000) observed preference by mesograzers for macroepiphytes over host plants in field studies conducted at the Norwegian Institute for Water Research. Since epiphytes cover the host surface, however, the grazing process has been assessed as beneficial to the host. Removal of epiphytes exposes more of the host surface area to light and relieves some competition between the epiphyte and the host itself. Conversely, Karez et al. (2000) also report an increase in host consumption in the presence of the epiphyte versus without. The same study also reports observation of changes in the behavior (rejection) by a mesograzer species in the presence of a particular epiphyte. Thus, in addition to competing with their host for light and nutrients, epiphyte cover may serve to increase grazing of the host (via co-consumption), in some cases, or may act as a protective coating for the alga in other cases.

Epiphyte grazers function as a top-down control on the epiphyte community. As such, these grazers effectively reduce competition for light and nutrients between the host and its epiphytes, resulting in improved host fitness (Nelson 1997) and, by extension, affecting ecosystem function as well. Different grazers target specific epiphytes, with the result that the presence/absence of certain epiphyte species will affect grazing pressure, which in turn affects the ecology of the system. These behaviors are not generally described for all grazers, and interaction patterns can be complex. The precise complement of epiphytes at a given time and the relative proportions of members of the assemblage can, therefore,

play a critical role in ecology, nutrient cycling, and system function. Because of the potential of epiphytes to impact the ecology of systems in crucial ways, as just described, it is of interest to gain an improved understanding of how epiphytes respond to environmental change such as increased nutrient loading, increased sedimentation, and shifts from coral-dominated to algal-dominated reefs.

The number of studies focused on characterizing the macrophitic epiphyte community in Hawai‘i are few. Full characterization would include a description of the structure of the epiphyte community, its diversity, function, variability, and patterns of response to changing environmental parameters. The lack of focus on epiphytes is striking given their impact on host organisms, as well as the ecology of organisms that graze upon epiphytes, and the potential for epiphytes to influence nutrient cycling and distribution. Existing evidence that epiphyte cover can be influenced by multiple factors (Larkum et al. 2006, Prado et al. 2008) indicates that full characterization of the ecology of epiphytes, and their impact on the larger ecology of a system, will be a complex undertaking.

Kāne‘ohe Bay presents an ideal venue to investigate the response of epiphytes to storm-derived nutrient pulses. Kāne‘ohe Bay is the receiving water body for a number of rivers and streams that pass through the characteristically short watersheds of Oahu (Hoover and Mackenzie 2009, Young 2011, Dulai et al. 2016). Under non-storm (baseline) conditions, the residence time in the southern portion of the bay is relatively long, on the order of 13 days (Smith et al. 1981). It has been proposed that post-storm flushing times are shorter, however, because flushing time is inversely proportional to stream flow (Ringuet and Mackenzie 2005). The short watershed results in a corresponding short time lag between land-based precipitation events and discharge into adjacent coastal waters. Storms therefore can have an almost immediate and intense impact on coastal nutrient loading (Ringuet & Mackenzie 2005, De Carlo et al. 2007, Young 2011). The relatively long residence time of the bay serves to retain

land-derived nutrients once they enter coastal waters and, as such, nutrients may serve as a persistent food source for primary producers, particularly during the rainy season. The degree of impact of storm-derived nutrient pulses on the primary producing community becomes clear when one considers that the doubling time of several primary-producing epiphytes are short (Prado et al. 2008), likely shorter than the residence time of water in the southern part of the bay. Elevated nutrient concentrations originating in storm runoff may therefore persist over multiple generations of epiphyte populations.

The focus of this chapter is on community-level response to changes in the environment, specifically nutrient flux. To deepen understanding of how epiphytes function in Kāneʻohe Bay, a functional gene approach was adopted to (1) determine the capability of detecting and assessing the epiphytic community structure in Kāneʻohe Bay using a custom-designed microarray chip, (2) assess the community structure and diversity of epiphytes associated with *Padina thivyae*, and (3) use the microarray to assess changes in the epiphyte community in response to variable nitrate flux (nitrate delivery to uptake surfaces). The hypothesis underlying these experiments was that physiological differences between the members of the epiphyte community would drive differential responses to variable nitrate flux, and that these differences would manifest in changes in overall community structure. Three genetic markers that encode proteins essential for uptake and assimilation of nitrogen and carbon in primary producers were employed: **rbcL**, which codes for the large subunit of the enzyme ribulose 1, 5 bisphosphate carboxylase/oxygenase (**RuBisCO**) – the enzyme involved in the first step of carbon fixation by primary producers; **NR**, which codes for Nitrate Reductase – the enzyme that catalyzes the reduction of nitrate to nitrite; and **EukNrt,** which codes for the membrane-bound nitrate transporter protein in eukaryotes. This custom suite of functional genes was printed onto a microarray

chip, henceforth called the “phytoarray”, which was used to challenge whole community samples collected throughout the experiment.

One of the primary reasons for selecting the functional gene microarray approach to evaluate the epiphyte community is the ability it affords to assess both known and unknown sequences of the primary-producing community. The added benefit of assessing the entire assemblage as a whole, while simultaneously tracking individual groups that make up the community, permits investigation of the response to environmental stimuli on a community level, as well as identification of specific community members that may be driving any observed changes.

This chapter presents data from two paired experiments run at two different nitrate concentrations: 2 µM and 10 µM, each of which was run under different flow regimes. The data presented herein provide insight into the response by the community to nutrient pulses of similar magnitude to those that may be encountered as a result of storm nutrient pulses to Kāne‘ohe Bay.

2. Methods

2.1. Background

Algal uptake of dissolved substances in the water takes place in multiple stages, the first of which is the transport (flux) of these substances to algal uptake surfaces (the external cell membrane) and the subsequent transport across cell membranes. The flux of dissolved components to uptake surfaces in water is described by:

$$J = S_i([C_i]_b - [C_i]_w) \quad (1)$$

where J is flux in g (or mol) $m^{-2}s^{-1}$, S_i is the uptake rate constant for i, $[C_i]_b$ is concentration of the component i in the bulk flow, b, and $[C_i]_w$ is concentration of i at the uptake surface, w (Cornelisen &

Thomas 2002). Flux is therefore determined by the concentration gradient of *i* at the uptake surface and by the uptake rate constant, *S*. Since *S* is related to Stanton number (St; ratio of mass transfer rates to inertial forces) by water velocity (*U*) in ms^{-1}:

$$S_i = St_i * U \quad (2)$$

and both values are also impacted by benthos geometry and the molecular diffusivity of the nutrient, flux is also related to these parameters and can therefore be approximated by:

$$flux_i = concentration_i * water\ velocity \quad (3)$$

This simplification facilitates the generation of a range of nutrient fluxes under experimental conditions by manipulating water flow rates and/or nutrient concentrations. Flumes provide an ideal platform for conducting these types of manipulation experiments. In the following sections, a brief description of the study site and flume design and set-up are given first, and then separate elements of the experimental design are described.

2.2. Study Site and Study Organism

The study site is located in a sheltered cove on the leeward side of Moku o Loʻe (Coconut Island; 21° 25' 54.8" N, 157° 47' 20.4" W) in Kāneʻohe Bay, Oʻahu (Figure 3.1A). Water depth at this site is typically relatively shallow (~1 to 1.5 m), and never exceeded 1 m during sampling periods. At the time of this study, the cove (approximately 90 m^2; 9.5 m across at the widest point by ~10 m long) was populated by a mixture of *Padina thivyae* (Phaeophyta) and *Gracilaria salicornia* (Rhodophyta), with *P. thivyae* comprising 70-80% of the algal cover, and a combination of *G. salicornia* and bare sediment covering the remaining 30-20% of the seabed. *P. thivyae* is fairly common in Hawaiʻi and is found in both intertidal and subtidal zones (Ni-Ni-Win et al. 2011). It is a native brown macroalga with thalli that have a flat

undulating blade morphology (Figure 3.1B). The blades have horizontal calcified bands, but remain soft and flexible, and they overlap to form a rose-shaped structure. These rose-like structures are discrete and, as such, individual algae are easily identifiable. Epiphytes colonize the surface of the blades, some of which are easily visible with the naked eye. The epiphytes associated with the *Padina thivyae* canopies were targeted for investigation in this study. To date, there have been few studies characterizing the epiphyte community on macroalgae in Hawai‘i.

2.3. Flume Design and Set-up

Flumes are devices used to isolate water, organisms, and any benthic structures of interest from the external environment for the purpose of conducting controlled perturbation experiments. For the experiments described here, the flumes were designed for indoor experiments. Required features of the flume for these experiments included that it be water-tight, provide easy access for repeat sampling of the alga during the course of the experiment, and allow light penetration. The flumes were constructed out of Plexiglas® and included an extension (dropbox) which encased a trolling motor used to generate and control flow during experiments. Flow straighteners were used to order the flow of water driven by the trolling motors, and UV lamps were set 0.6 m above the working area of the flume (i.e., above the algae) to keep the algae on a 12:12 light:dark cycle.

2.4. Experimental Design & Rationale

For each experiment, parallel flumes were set up side-by-side to minimize environmental variability between flumes. Four paired 10-day nitrate uptake flume experiments were conducted during the period from August to October 2011. For each experimental pair, the selected nutrient concentration was held constant over the experimental period in both flumes. Nitrate was held constant via the continuous drip-wise addition of a high concentration potassium nitrate stock solution. The

concentration of this stock solution and the drip-rate required to maintain the constant nitrate concentration within the flume were determined based upon data collected in a preliminary set of experiments. These initial experiments mimicked the final flume experimental set up and provided uptake rate constants for use in calculations. A high flow regime (15 cms^{-1}) was applied to one of the two, paired flumes, and a low flow regime (2 cms^{-1}) was applied to the other. A range of nitrate fluxes across the four experiment pairs was achieved by maintaining the two designated flow speeds for all experimental trials, and changing the nitrate concentration for each paired experiment. Thus, the organisms in each flume experienced a different nutrient flux environment. Pairing of the experiments in this manner facilitated assessment of the effect of water velocity on nutrient uptake, and any consequent effects on epiphyte community structure.

2.5. Sampling Scheme & Analysis

A multi-stage sampling frequency was employed to enable determination of epiphyte community response time to environmental perturbations. A higher sampling resolution was employed at the beginning of the experiments (every 20 minutes for the first hour), followed by a lower sampling rate for the remainder of the experiment (See Appendix III). The initial more rapid sampling rate permits assessment of short-term changes in community structure, and also captures the time-course of upregulation of protein synthesis via RNA analysis. The experimental sampling time-scales adopted were based upon advice from Dr. Bess Ward (Faculty and Geoscience Chair, Princeton University), who was a collaborator on this project. In particular, Dr. Ward provided information based upon preliminary work that showed changes in the RNA abundance, which corresponded to organismal response, on time scales on the order of one hour or less.

2.6. Field Collection and Experiment Setup

P. thivyae (along with seawater sample WC (Table A3.T1 in Appendix III)) was collected from the study site the day before the start of each experiment. Four to seven *P. thivyae* individuals were selected for harvesting from the field without design or prejudice. In the laboratory, these individuals were subdivided into 240 sections of blades, each approximately 6-cm wide (Figure 3.2A). These sections were pooled to form a stock assemblage that served as an integrated representation of the epiphyte community for the experiment that day. Using plexiglass sheets with a series of holes bored for each blade, two pavements of 60 blades each (Figure 3.2A) were constructed, one for each flume. Each 60-blade algal compliment was gently blotted dry and weighed before placement on the plexiglass pavement. The pavements of blades were left overnight in an acclimation tank containing seawater from the study site. This ordered array of algal sections on the pavement facilitated true random sampling during the experimental period. The holes were mapped and numbered, and a set of random numbers was generated from this list prior to the start of the experiment. This list was used to guide the random order of sampling during the experiment. The physical set-up just described also allowed for the maintenance of the experimental algal canopy because as blades were removed at sample timepoints, they could be readily replaced at the precise locations by inserting new blades from the stock assemblage. Replacement of sampled blades during the experiment was necessary in order to maintain the overall morphology of the algal pavement and, by extension, the hydrodynamic characteristics of the flume.

On the morning of the experiment, each flume was filled with 120 L of unfiltered seawater. Background reference samples were taken for both seawater and algal/epiphyte tissue, as follows. Before the start of the experiment, seawater reference (background) samples were taken from the flume (FBKGD,

Appendix III, Table A3.T1) and from the acclimation tank (LBKGD, Appendix III, Table A3.T1) for inorganic nutrient analysis. Triplicate algal samples were also taken from the field (study site) and the acclimation tank for nitrate reductase enzyme analysis and microarray analysis. The un-manipulated field samples were used to assess epiphyte diversity.

At the start of each experimental period, a previously-calculated volume of potassium nitrate (KNO_3) was added to each paired flume to achieve the desired experimental concentration, and allowed to mix for 20 minutes to ensure homogenization of the nutrient spike within flume water. At the end of this mixing period, the algal pavements were transferred from the acclimation tank to the flumes, and the experiment time was started.

At each time point during the course of the experiment, three *P. thivyae* blade sections were randomly subsampled from the pavement and replaced with three blades from the stock assemblage. Epiphyte tissue was carefully scraped from the three replicate samples, using a scalpel and/or microscope slide, and combined. The combined sample was assumed to be representative of the epiphyte community at that time. Samples were flash frozen using liquid nitrogen and stored at -80°C until analysis. No preservative was added (Figure 3.2B).

In order to track nutrient concentrations throughout the experiment, an integrated water sample was collected drip-wise via a tubing system over a 10-minute period at each algal sampling time point (Appendix III, Table A3.T1) into an HDPE bottle. For each flume, the 10-minute water-sampling period straddled the algal sampling time point. The sampled water was thoroughly mixed, duplicate subsamples were filtered through 0.2 µm Thermo Scientific™ Target2™ nylon syringe filters using 140 ml syringes, and stored in 30 ml HDPE bottles at -80°C until analysis. All sampling equipment and storage containers were acid-washed (10% HCl) in order to avoid contamination. Nitrate, nitrite, ammonium,

phosphate, and silicate concentrations were determined following the protocols of the WOCE Hydrographic Program using a Technicon AAII system (University of Washington Marine Chemistry Laboratory, *http://www.ocean.washington.edu/story/Marine+Chemistry+Laboratory*).

2.7. Sample Preparation and Microarray Hybridization

Community structure diversity was assessed using the phytoarray functional gene microarray. Development of this type of custom microarray is well-described in Taroncher-Oldenburg et al. (2003) following techniques outlined in Bulow et al. (2008), where the precursor to this phtotoarray was developed for the denitrification gene, *nirS*, and tested on community samples extracted from estuarine sediments. Previous application of functional gene microarrays is reported in Wu et al. (2008), Bulow et al. (2008), Ward & Van Oostende (2016). The current study was designed in collaboration with Dr. Bess Ward at Princeton University who developed and used the phytoarray on previous projects.

The functional gene microarray includes sequences for genes that code for CO_2-fixation (RuBisCO (*rbcL*)), nitrate reduction (Nitrate Reductase (*NR*)), and eukaryotic nitrate transport (*Nrt2*), printed on a glass slide. RuBisCO and NR markers include sequences that represent chromophytes, chlorophytes and cyanobacteria (Table 3.1). The phytoarray design facilitates acquisition of information about the presence/absence and activity (gene expression) of multiple organisms, simultaneously. The short glossary of terms found in Box 1 of Ward and Van Oostende (2016) is also provided in Appendix V of this paper to clarify how the phytoarray was established, and to describe the ways in which it can be used as a community structure assessment tool.

The array contains a set of “archetype” probes from species in culture as well as from environmental samples. The probe set chosen for the phytoarray employed in this study was selected from the entire database of homologous sequences available at the time of array design and development. Based on

sequences printed on the chip (microscope slide), up to 103 archetypes can be identified via the nitrate reductase (NR) gene, 107 via the RuBisCO (rbcL) gene, and 49 based on the nitrate transporter (*Nrt2*) gene. This corresponds to 19 archetype probes for chlorophyte RuBisCO, 78 for chromophyte RuBisCO, and 10 for cyanobacteria RuBisCO. For Nitrate reductase, the array contains 24 archetype probes for chlorophytes, 62 for chromophytes, and 17 for Cyanobacteria. Finally, for the nitrate transporter protein, the chip contains 49 archetype probes that represent eukaryotes in general (Table 3.1). Each archetype encompasses all sequences within 85% identity with the probe sequence, meaning that any sample sequence matching ≥ 85% of the probe sequence (i.e., with statistically significant similarity) will hybridize to the probe. The resolution of the array format is 87% +/- 3% (Taroncher-Oldenburg et al. 2003); therefore, we use a conservative 85% cutoff for probe selection. From this point forward, therefore, we use the term 'archetype' to refer to the unique identifiers printed on the array to which all community sample sequences within 85% identity will hybridize. In this regard, even though the array is targeted toward known genes, it also hybridizes with closely related sequences and, thus, facilitates acquisition of information about the activity of multiple organisms simultaneously, including unknown sequences.

DNA from whole community epiphyte samples was extracted and cleaned using the FastDNA® SPIN Kit for Soil (MP Biomedicals™). After quantitation, the genetic material was digested into smaller fragments using Hinf1 enzyme from Ambion® and linearly amplified and labeled with fluorescent dUaa in a Klenow reaction. The product was then tagged with a fluorescent cyanine dye (Cy3) and hybridized, in the dark, to the array slides for at least sixteen (16) hours. Hybridized slides were then washed and dried. cDNA was built from RNA extract, which was then quantified and processed in the same manner as the DNA. This protocol was provided by the Ward Lab, where the samples were processed (Ward & Bouskill 2011).

2.8. Data Analysis

2.1.1. Image Analysis

The dried slides were scanned immediately after washing on a GenePix 4000A scanner (Axon Instruments, Inc., Foster City, Calif.) using the GenePix Pro image analysis software provided with the scanner. The slide images were checked and aligned manually with a grid to identify each probe. Spots where the probe sequences were printed are known as features (Figure 3.3). The fluorescence of the dye in each of the features was quantified by subtracting the background fluorescence for each channel (i.e., the wavelengths of the dyes used: 532nm (Cy3) and 635 nm (Cy5)).

The direct (absolute) fluorescence intensity of the features were not used because of the variability inherent in environmental samples. Instead, relative fluorescence ratios (RFRs) were calculated, which provide an indication of the relative number of copies of the DNA segment of various members of the community in the sample. Presence-absence information can be ascertained, and it is also possible to make inferences about the relative abundances of the community members present.

Because the phytoarray chip targets functional genes, which can occur in multiple copies per organism, we cannot definitively correlate fluorescence intensities to organism abundances. Even though RFRs more accurately correspond to number of gene copies, varying fluorescence intensities provide an approximate proxy for measuring abundance. For the purposes of this investigation, we will consider these RFRs as indications of organism abundance.

2.1.2. Phylogentic Reconstruction

An unrooted phylogenetic reconstruction of the organisms present in the samples was conducted, using the probe sequences, created for each functional group, that were used to hybridize samples to the gene microarray. A model for DNA sequence evolution and the model parameters were selected using

the program jModelTest v.2.1 (Guindon & Gascuel 2003; Darriba et al. 2012). The best-fit model of nucleotide substitution was identified for each functional group by the Akaike Information Criterion and used for phylogenetic reconstructions. A maximum likelihood tree was created using the program PHYML v.3.0.1 (Guindon et al. 2010), with clade support assessed after 1000 non-parametric bootstrap replicates. Bayesian inference (BI) was conducted using the program MrBayes v.3.1.2 (Huelsenbeck et al. 2001; Ronquist 2004), and a pair of independent searches was run for 1 million generations, with trees saved every 1000 generations, with the first 250 sampled trees of each search discarded as burn-in (the initial set of trees that are generated before the model settles on the most probable values).

2.1.3. Diversity Calculations and Statistics

For each community sample, based on each sequence library (i.e., nitrate reductase, RuBisCO, and *Nrt2*), Species Richness (i.e. the number of different species present), a Shannon Diversity Entropy (*H'*), and a "true diversity" index (Jost 2006) were calculated. Shannon Entropy (*H'*) was calculated as:

$$H' = -\sum_{1}^{i=n} (p_i * \ln p_i) \quad (4)$$

where *n* is the number of species and p_i is the relative abundance of species *i*. Because of the range of diversity measures (indices) used in ecology, we also present the diversity data as "true diversity" calculations. For lack of a better term, we retain this nomenclature coined by Jost (2006); however, this "true diversity", initially presented by Hill (1973), is indeed one of the better approaches for discussing the diversity of a community. It is essentially the "effective number of species," which is the number of equally common species required to give a particular value of a diversity index. "True diversity" is a linear index and as such, it is easier to interpret and compare to other studies. It is calculated from Shannon Entropy values as:

$$e^{H'} \quad (5)$$

To describe the diversity of the entire community, mean diversity of the 4 field samples collected was calculated. In an effort to better understand the variability of the epiphyte community, and set a reference point against which to compare samples from the experiment, the coefficient of variation (CV) for these field samples was also calculated (coefficient of variance = standard deviation / mean). We selected a 10% coefficient of variance threshold for the community to establish difference between samples.

2.1.4. Rate of change of relative fluorescence ratios (RFRs)

The rate of change was simply calculated as the difference in relative abundance divided by the time over which the change took place.

2.1.5. DNA:RNA ratios

RNA:DNA ratios were used to characterize the physiological state of the epiphyte communities as a whole. The quantity of RNA per cell can vary, and is a reflection of protein synthesis, while the quantity of DNA per cell remains fairly constant (Foley et al. 2016). Increases in DNA usually indicate replication and cell division, in other words, population growth. As such, a comparison of the number of copies of RNA molecules to the number of copies of DNA permits an assessment of the metabolic activity (protein-synthesizing potential) of the community and its response to its external environment (Chícharo & Chícharo 2008). The nucleic acid-derived index (RNA:DNA), alongside environmental data and community descriptors such as abundance, is commonly used in marine ecology to make evaluations of the eco-physiological status of organisms and communities, in order to describe processes such a growth and reproduction.

For each sampling time point, and for each gene, RNA relative abundance is plotted against DNA relative abundance. A comparison of the slopes of these relationships allows us to compare the levels of gene expression between samples.

3. Results

3.1. Results of Hybridization

Across all the samples discussed here, 51 to 100% of the printed probes were hybridized – i.e., 132 to 259 of the 259 possible probes displayed positive hybridization with sequences found in environmental samples.

3.2. Diversity of Naturally Occurring Epiphyte Community (i.e. non-treatment assemblages)

Phylogenetic reconstruction of the sample data from the T0 samples resolved various numbers of clades, depending upon the gene. Nitrate Reductase and RuBisCO each resolved eight clades (Figures 3.4A and 3.4B), whereas *Nrt2* resolved seven (Figure 3.4C). Each clade was organized by specific archetypes, illustrating the ability of microarray probes to resolve phylogenetic relationships for specific archetypical groups.

When the community was grouped by class, organisms fell out into twenty-seven (27) classes for rbcL (Figure 3.5), eighteen (18) classes for NR (Figure 3.6), and five (5) classes for *Nrt2* (Figure 3.7). There were eight (8) classes common to both NR and *rbcL* probe sets. The relative contribution to community composition of these common classes were, however, different between NR and *rbcL* (Figure 3.8).

The *Padina thivyae* epiphyte community sampled for the experiments described were dominated by diatoms. There were 60 distinctive community members, with Bacillariophyceae being the dominant class, compared to the 17 discrete Cyanobacteria members. Based upon the printed NR sequences, community members with highest abundances were fairly consistent from sample to sample, with the

most abundant member being exactly the same: a very close relative to the Raphidophyte *Heterosigma akashiwo*. Not only did relative abundance of community members vary from sample to sample, but so too did absolute abundance. This variability was exemplified based on all loci (Figures 3.5 to 3.7).

Based on NR, with a maximum number of identifiable archetypes of 103, Species Richness (S) ranged from 80 to 100. Based on rbcL (maximum identifiable archetypes = 107), S ranged from 37 to 82, and based on *Nrt2* (maximum identifiable archetypes = 48), S ranged from 41 to 48. While Species Richness was fairly consistent between samples based on the *Nrt2* (nitrate transporter protein) gene (6.84% coefficient of variance), Nitrate Reductase (*NR*) and RuBisCO (*rbcL*) indicated higher variability between community samples (10.49% and 34.57% coefficient of variance respectively) (Table 3.2).

Mean community diversity was generally high across the four T0 samples (Shannon Entropy, $H' = 3.83 \pm 0.18$ SD based on nitrate reductase marker) compared to other epiphyte community diversities, with Shannon Diversities and "true diversities" ranging from 3.18 to 4.04 and 26.15 to 56.77, respectively, across all loci and samples (Tables 3.2 – 3.4). For the three targeted genes (*NR*, *rbcL*, and *Nrt2*), these ranges correspond to coefficients of variability of 4.70, 11.30, and 3.46, respectively, for Shannon Entropy, and 17.56, 40.07, and 11.93, respectively, for "true diversity" (Tables 3.3 and 3.4). Additionally, due to the different sizes of the gene libraries, choice of gene marker can result in varied measures for Diversity (Figure 3.9).

3.3. Flume Experiment Results

3.3.1. Nitrate Drawdown

For the 2 µM paired experiments, in both high (0.15 ms^{-1}) and low (0.02 ms^{-1}) flow regimes, nitrate was drawn down to the level of the initial concentration by 3 hours, and drawn down to levels below

detection by 6 hours. For the 10 µM experiments, nitrate was drawn down to initial concentrations by 6 hours, and to levels below detection by 12 hours (Figure 3.10).

3.3.2. Time series of Epiphyte Community Structure

Epiphyte community structure changed during the course of the 10-day experiment. Diversity indices indicate that not only were the two T0 samples different from each other, but that between T0 and Day 2 of the 10 µM at 0.15 ms^{-1} experiment, the community also changed structure. Relative abundances of the various community members changed throughout the experiment (Figure 3.11). For each sample, the Richness (S), Shannon Diversity (H'), and "true diversity" are reported to enable comparison.

Day 2 is characterized by a lower overall diversity than Day 0 and a different dominant organism. *Thalassiosira weissflogii* is dominant at Day 0 while, by Day 2, an unidentified diatom is dominant.

3.3.3. Effect of Nitrate Concentration on Epiphyte Community Structure

A comparison of the 2 µM and 10 µM experiments for a given flow speed reveals that the epiphyte community in the 2 µM experiment (i.e., lower nitrate flux) was less responsive, displaying smaller changes in relative abundances, or no change at all, relative to the 10 µM experiment (i.e., higher nitrate flux). Results for two organisms that were common to both experimental assemblages (*Thalassiosira weissflogii* (*T. Weiss*) and an unidentified diatom) highlight this differential response (Figure 3.12). Based on the NR reductase gene, for the 0.15 ms^{-1} flow speed under 10 µM conditions, the relative abundance of *T. Weiss*, a ubiquitous diatom, decreased from 14% to 2% by Day 2. Over this same time period, another diatom in the assemblage underwent an increase in its relative abundance from 3% to 16%. Under 2 µM conditions and the same 0.15 ms^{-1} flow speed, however, neither of these two organisms exhibited much change, with *T. Weiss* shifting from 2% to 6% on day 5, down to 4% by day 10, and the relative abundance of the unidentified diatom remaining unchanged at 8%.

3.3.4. Effect of Water Flow Rate on Epiphyte Community Structure

Focusing on *T. weiss* and the unidentified diatom again for the 10 µM experiment, the hybridization data from the chromophyte NR gene permits us to discern an effect of water flow rate on community composition (Figure 3.13). Under lower nitrate flux conditions, i.e. 10 µM at 2 ms^{-1}, the response by the community is 'muted' compared to that under the higher flux conditions (10 µM at 15 ms^{-1}). Other members of the assemblage display the opposite trend, however, with a larger change in relative abundance observed under the low flux condition compared to the high flux condition. Relative abundance of the Cryptophyte *Rhodomonas salina* increased from 2% to 13% under low flux conditions, while it maintained a 1% relative abundance under high flux conditions 24 hours after initiation of the experiment (Figure 3.13). *R. salina* is either absent from the assemblage on Day 2, or it exists below the detection threshold. Due to sample processing complications, equivalent time points for the two experiments could not be compared.

3.3.5. Daily Rate of Change

The daily rates of change of the relative fluorescence ratio (RFR/day) provide an additional quantitative assessment of the data. Given that the epiphyte communities seem to be responsive to the high flux experiments, it seems reasonable to assume that the rate of change will be greater in the high flux experiments relative to the low flux experiments. Individual value plots support this; however, a more interesting pattern is also revealed. Under high flux (10 µM at 0.15 ms^{-1} and 0.02 ms^{-1}) conditions, a greater spread in the response time by the various community members is observed (Figures 3.14 and 3.15). The data can clearly be binned into groups based upon the two concentrations, indicating that there is an effect of concentration on the rate of change of RFR. The same trend is observed for both the chromophyte NR and chromophyte rbcL genes. The disparity in rates of change was, however, far more apparent for RuBisCO (rbcL) (Figure 3.15).

3.3.6. RNA:DNA Ratios

RNA:DNA ratios function as an indicator of metabolic activity. All Day 0 samples (i.e. epiphyte communities at the very start of the experiments) show the community at "rest" with respect to NR activity. The number of transcripts per gene copy is less than 1 (all slopes are <1).

For the 2 µM nitrate treatment under 0.02 ms^{-1} flow speed, the relationship between RNA and DNA changes throughout the experiment. In fact, for chromo NR, the slope of the relationship increased between day 0 and day 5, and again between day 5 and day 10 (Figure 3.16). For chloroNR (Figure 3.17), cyanoNR (Figure 3.18), and *Nrt2* (Figure 3.19), the pattern across the time points is not as straightforward, but all three of these gene markers show the same characteristic increase between 0 and 5 days, followed by a decrease from 5 to 10 days. For RuBisCO, no pattern was observed between time points (Figure 3.20).

4. Discussion

As a consequence of the relatively long residence time that characterizes southern Kaneohe Bay, elevated nutrient concentrations can be maintained in the water column for several days following intense rain events. For example, nitrate can become elevated by as much as 61 to 124 times mean background levels after rain events (Ringuet & Mackenzie 2005, De Carlo et al. 2007). After storm events, both Ringuet and Mackenzie (2005) and Young (2011) observed fairly rapid drawdown of nutrients, from the elevated post-storm nutrients levels down to baseline levels. Thus, the conditions of experiments described here, in which constant nitrate levels are maintained over an experimental time course of 10 days, is a reasonable approximation of the type of nutrient environment that resident algae in Kāneʻohe Bay might be expected to experience.

4.1. Diversity of Naturally Occurring Epiphyte Community (i.e. non-treatment assemblages)

Diversity indices, such as Shannon Entropy and "true diversity," take into account the relative proportions of the organisms present in a community. While useful in some ways, other indices such as Richness are insufficient to describe communities. For example, based on Species Richness alone, a community consisting of 5 species, with four individuals of each species, will be indistinguishable from a community of 5 species, with six individuals of species 1, five individuals of species 2, four individuals of species 3, three individuals of species 2, and two individuals of species 1, despite the obvious differences in complexity of their community structure. Richness on its own does not offer any indication that these two communities are structured differently. In addition, for all loci, other measures of diversity (Shannon Entropy and True Diversity) highlight the true variable nature of the distribution of the organisms due to differences in their relative abundances, compared to simply looking at Richness (Tables 3.1 – 3.3; Figure 3.8).

For the eukaryotic nitrate transporter protein (*Nrt2*), *S* ranged from 41 to 48, which seems small compared to the Species Richness determination that was based on nitrate reductase. These *Nrt2* Richness values correspond to 84 to 98% of the total possible transporter protein hybridizations on the phytoarray chip. The lower Richness values based on *Nrt2*, therefore, are not a reflection of a lack of the ability of the chip to identify organisms based on *Nrt2*, but a reflection of the small library available for *Nrt2*. Even though the choice of gene marker can result in very varied measures for Diversity (Figure 3.9) due to the size of the library, the pattern of diversity values between samples is the same for each marker. The results just described for *Nrt2* highlight the need for multiple measures of diversity in order to confidently describe the diversity of organisms present in a given sample. The use of methods such as high-throughput sequencing of an entire sample is an approach that is well suited to capturing all organisms present.

4.2. Flume Experiment Results

4.2.1. Nitrate Drawdown

The design and intent of the 10-day flume experiments was to maintain an elevated (constant) nitrate level throughout the experiment period in order to simulate the post-storm nutrient environment experienced by algae in the southern portion of Kāneʻohe Bay. The objective of maintaining a constant nitrate level was not achieved, however, as evidenced by the nitrate drawdown curves shown in Figure 3.10. The mechanism by which constant nitrate level was to be maintained, by regularly introducing small-volume aliquots of a high concentration nitrate solution into the larger flume volume, proved unsuccessful. Options that might prove more effective include: (1) use of a large enough volume of flume water such that drawdown during the experimental period will be insignificant, or (2) periodic exchange of larger volumes of seawater, made up to the desired concentration, with flume water. Of these, the second option seems more practical as it would not require the massive volume of seawater that the first option necessitates. However, the second option is potentially far more disruptive to the experimental set-up than the first. Despite the fact that the intended high nitrate levels (2 and 10 µM) were not maintained, we are able to interpret the results of the experiments as a response to a shorter nutrient pulse.

The increase in nitrate observed at the beginning of each experiment (Figure 3.10) may be a consequence of incomplete mixing of water within the flume or, more likely, an artifact of sampling (sampling error). Water was collected over a 10-minute period, drip-wise, through a tubing system located in the well-mixed dropbox area of the flume. The intent of this sampling method was to obtain an integrated water sample. However, if the sampling assembly was not sufficiently purged prior to sample collection, initial samples may have been diluted by water not containing the nitrate spike, causing an artificially low measure of nitrate concentration.

The sharp decrease in nitrate concentration in the flumes over the course of each 10-day experiment, independent of water flow rate, indicates that the epiphyte and/or the host alga are able to respond quickly to changes in their nutrient environment. The fact that nitrate was drawn down to levels below detection under both high and low flow conditions suggests that, even at the high flow rate, uptake sites on the algae were not saturated. Consequently, we can conclude that the organisms in the flume were mass transfer limited.

4.2.2. Time series of Epiphyte Community Structure

A measure of the natural variability of epiphyte community structure as a function of time is unavailable. As a consequence, we are unable to confidently determine whether the observed changes are significantly different from those typically seen in the community, *in situ*. Thus, we cannot definitively attribute observed changes to the nutrient treatment. Given these uncertainties, we instead describe observed general trends in diversity of individual organisms, and any notable features of the timeseries.

In retrospect, it is unfortunate that an insufficient number of environmental samples were collected to provide a robust reference for each paired experiment. In future experiments, it would be extremely beneficial to collect multiple environmental samples with high enough temporal and spatial resolution to offer confident reference points against which the results of experimental perturbations could be measured. In other words, it is important to establish what the baseline characteristics of the epiphyte community are. Such things as defining the 'normal' or mean state of the epiphyte community, the natural degree of variability that can exist in the community, are pre-requisites to confidently interpreting experimental data such as those generated for this work. Further, it would be important to establish whether natural variability is more important in time or in space, and the scale over which such

variability is observed. It would also be of interest to determine how consistent natural community variability is throughout the year. For a case in which community variability is minimal, it may be possible to use a single well-selected species as an adequate indicator of response to environmental changes. Because epiphytes can play an important role in ecosystem function, as described earlier, these questions are relevant for understanding how ecosystem function is restored and maintained subsequent to perturbations.

The two T0 samples associated with the 10 µM paired experiment, taken right at the beginning of the experiments, had very different community structures despite being drawn from the same acclimation tank. This difference highlights the inherent variability of the epiphyte community and the importance of assessing this baseline condition in order to achieve successful outcomes of comparative studies (Figure 3.11). A shift in the identity of the dominant species occurred between the T0 and Day 2 epiphyte communities, and 9 species were present in the Day 0 sample that were absent from the Day 2 sample. Given the possibility that any one of these unique and/or dominant species could play a crucial role in ecosystem functioning, these characteristics of the community structure are potentially significant.

4.2.3. Effect of Nitrate Concentration on Epiphyte Community Structure

Observed changes in two members of the epiphyte assemblage over the course of the experiments indicate that these organisms respond to modifications in nutrient flux by changes in abundance. Further, the responses observed were not the same for the two organisms analyzed, suggesting, not surprisingly, that all members of the community do not respond identically to a given environmental perturbation. Specifically, while the relative abundance of *T. weiss* decreased under the 10 µM treatment, the relative abundance of the unidentified diatom increased (Figure 3.12). One explanation

for this differential response could be that the unidentified diatom is physiologically better equipped than *T. weiss* to respond positively to high nutrient concentrations, and is able to exploit this difference. Our inability to directly compare equivalent time points for the two experiments hinders our ability to comprehensively contrast the behavior of the community, or individual components of the community, over the course of the experiments. For example, it is possible that that between the 2nd and 10th day of the experiment multiple changes in community composition may have taken place. Given the experimental design, such high-resolution changes in community structure are not resolvable for our data set.

4.2.4. Effect of Water Flow Rate on Epiphyte Community Structure

The patterns observed in these experiments reinforce the notion that the epiphyte community is responding to changes nitrate flux. That is, for the 10 µM experiment under the higher flow conditions, *T. Weiss* and the unknown diatom display larger changes in their relative abundance compared to the response observed under the low flow conditions. It is striking that *Rhodomonas salina* (*R. salina*) displays the opposite pattern, with larger changes in its relative abundance under lower flow conditions. These contrasting results underscore the fact that the physiology of different organisms plays a profound role in the response of the community as a whole. *R. salina* is a very interesting alga. It is a member of the cryptomonad group, and can form cysts to survive unfavorable conditions, or alternatively can use its flagella to escape attachments such a mucus membranes, allowing it to exist as a free-living flagellate (Throndsen 1997). The fact this this algal microbe is motile, and that it acutely senses its environment, can be a determining factor in whether it is found as part of an epiphytic community or not.

R. salina was not present in the Day 2 sample of the 0.15 ms^{-1} experiment. Two possible explanations for its absence are (i) that it was out-competed and died out of the community, or (ii) that it is in such low abundance in the natural environment (evidenced by its 1% relative abundance at the beginning of the experiment) that it may not be captured in small sample sizes. Because we do not have a robust estimate of the natural variability of the epiphyte community, we cannot say with any certainty which explanation is more likely.

4.2.5. RNA:DNA Ratios

Changes in RNA:DNA ratios with time reflect community response to the experimental treatment, in this case increased nitrate flux. Specifically, the change in the RNA:DNA ratio observed in Figures 3.16 to 3.18 correspond to a change in the expression of the nitrate reductase enzyme. Considering the ratios for the entire assemblage, an assessment of the status of the community as a whole can be made. For chromophyte nitrate reductase, the increase in slope from Day 0 to Day 10 indicates that RNA increased relative to DNA over time. The existence of a temporal trend in the slopes indicates that not only is there a change in activity between time points, but that these differences are non-random, which suggests that the observed changes represent a response to the experimental treatment.

Additionally, confirmation that observed changes in NR activity are in response to the nutrient flux suggests that the differences in relative abundance observed are not solely related to random or typical mortality and/or growth of one organism versus another. Rather, the uptick in gene expression suggests that differential responses of members of the epiphyte assemblage to the nitrate stimulus imposed upon the community are being translated into measurable changes in community structure (i.e., changes in relative abundance). The different responses observed likely relate to different abilities, or

capacities, to respond to the environmental variability. Such a differential response may underpin one mechanism of competition that is operant among different components of the community.

For chlorophyte NR, cyanobacteria NR, and *Nrt2* under the same treatment, no clear trend in slope over time was observed. However, these three genes all display the same pattern, in which the slope increases from day 0 to day 5, but then decreases from day 5 to day 10, seemingly returning to "rest". Since these ratios are an indicator of activity, it is possible that the observed shifts in RNA:DNA ratios are representative of upregulation and downregulation of these genes within the 10-day experimental period.

The coherent response of chlorophyte NR, cyanobacteria NR, and *Nrt2* suggests that groups of organisms may have similar behaviors (e.g. chromophytes vs chlorophytes vs cyanobacteria), and also that all of the genes involved in nitrate uptake and assimilation do not respond on the same time scales. For example, since *Nrt2* is a membrane transport protein, it is reasonable to expect that an organism may downregulate expression of this protein in response to a decrease in available nitrate in the water column. By contrast, expression of nitrate reductase may remain high, despite changes in external nitrate concentrations, in order to continue processing the nitrate that was taken up by the cells. The reduction in the RNA:DNA ratios in Day 10 samples is not entirely surprising considering that nitrate concentration within the flume was not maintained at elevated levels throughout the experiment. Instead, nitrate was drawn down within 3 to 6 hours of the start of the experiment. It is not unreasonable to conclude, based on the Day 10 RNA:DNA ratios, that some members/groups of the community are able to respond equally as fast to changes in nutrient flux in the positive or negative direction.

The fact that there is no observable temporal change in RuBisCO activity throughout the experimental time course is consistent with the fact that it was not anticipated that this gene, involved in carbon fixation, would respond directly to changes in nitrate availability. It is important to note that carbon fixation is a light-mediated process, and samples were collected at the same time of day by design, precisely to eliminate light as a factor that might inject variability at sample points. Organisms may exhibit cyclical differences in RNA:DNA ratios and, as such, the time of day of sampling is integral to maintaining the integrity of a dataset and the ability to directly compare sample data to each other. Time of day influences which metabolic functions are operant, as well as the intensity of metabolic functions. This variability was avoided by sampling at the same time of day for the daily sampling. Thus, if a similar experiment were to be sampled under variable light conditions, it may be that RuBisCO would display changes in activity due to variable light intensity.

Comparisons such as RNA:DNA ratios are more informative when they are considered together with abundance information, which puts the data into perspective, and contributes to a fuller interpretation of the microarray data output.

4.2.6. Daily Rate of Change

Information about rates of change of community composition can be particularly useful from a managerial standpoint. Knowledge such as this may provide a basis for making predictions about how long it will take a system to recover after a given perturbation. For example, the current dataset shows low daily rates of change in epiphyte community composition in the 2 µM treatments. From this result, one might predict that after a smaller storm event, the overall effect on the epiphyte assemblage would be minimal. The slow rate of change also means that, under these conditions, should there be a

significant change in community structure, that recovery time from that change and return to a pre-storm state, may be on the longer side.

4.2.7. Advantages and Limitations of Microarray Analysis

Microarray analysis is a high-throughput tool that allows characterization of several genomic sequences simultaneously. The simultaneous collection of genomic data permits evaluation of multiple processes being carried out by organisms within an assemblage by looking at functional genes. Application to a study such as the one described here, in which our objective was to analyze sequential snapshots of the epiphyte community at various time points, is very apt. The method is efficient, as it simultaneously can produce valuable information about abundance, expression, and interactions between organisms.

The archetype approach of the phytoarray facilitates investigation of unknown species because the probes printed on the slide will hybridize not only to its specific match, but also to organisms within 85% identity of its sequence. This is particularly useful for investigating whole community samples that have not previously been described, because the contribution of even unidentified organisms can be taken into account. This attribute does have a down side, however, in that it also means that we may not be able to resolve closely-related (but distinct) organisms (i.e., sequence homologues).

Hybridization intensity correlates both to the abundance of the sequence and also to the strength/level of identity. This means that a sequence having 87% identity and a low abundance may have the same hybridization signal intensity as another that has 100% identity; both will be interpreted as having the same abundance based on absolute fluorescence intensity. As such, assemblage structure is viewed in terms of relative abundances in the form of relative fluorescence ratios (RFR). For a given increase in RFR, we cannot conclusively determine whether or a particular species has actually increased the

number of gene copies, or whether the number of copies of the other species decreased. The fact that the final fluorescence data used in the analysis are relative, as opposed to absolute values, does not hinder our ability to draw informative conclusions. We are able to extract information from these comparisons because it is, in fact, the relationships between different members of the community that are of interest.

An important caveat that accompanies use of the microarray for diversity assessment is that the microarray can only provide information about the genes printed onto the chip. This fact results in an inherent bias in the data generated from the microarray. One consequence of a bias such as this is that an active, or even dominant member of assemblage may escape detection, and thus not be included in the final analysis.

5. Conclusions

Despite the fact that the initial intention to expose the epiphyte community to elevated nitrate levels for an extended time was not realized, a number of interesting patterns in the behavior of the epiphyte community were observed. Namely, the community seems to respond to changes in nitrate flux, as evidenced by the change in RNA:DNA ratios over time. Community structure also shifts in response to the flow rate, or the nutrient level to which the assemblage is exposed. Some members of the assemblage are able to respond more rapidly than others, likely due to differences in their physiology.

The results of these experiments raise several questions for future exploration, some of which are enumerated here. Are the epiphyte assemblages that form in response to environmental stimuli persistent? Is a pulse of duration similar to the one delivered in this experiment sufficient to shift community structure? Are there distinct seasonal differences in the epiphyte community, for example

during the Dry versus Wet Seasons? Can we identify epiphyte communities that are specific to certain algae? Given the ephemeral nature of macroalgal cover, and thus epiphyte presence, how does the system compensate for loss of function due to a reduction in epiphytes? When a particular organism or group of organisms become dominant, can specific physiological features be distinguished that set them apart from other, non-dominant members of the community? And finally, given the potential for epiphytes to significantly impact nitrate availability, what is the net effect that epiphytes have on the ecology of the system as a whole, and its ability to respond to and recover from perturbations? These questions await further experimental work, as they are beyond the scope of the present study.

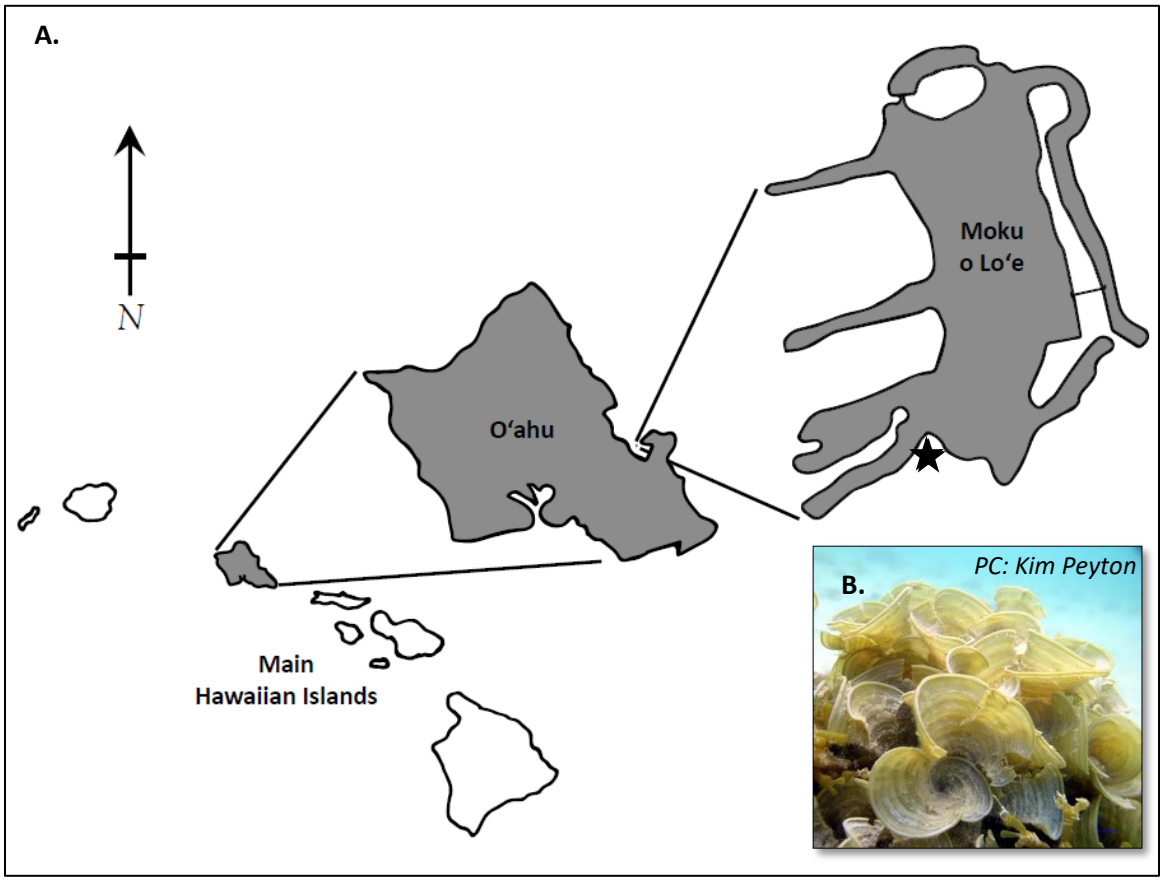

Figure 3.1 A. Map showing study site at Coconut Island (Moku o Lo‘e), home of the Hawai‘i Institute of Marine Biology. The island is in the southern portion of Kāne‘ohe Bay, O‘ahu, Hawai‘i. The collection site is located at 21° 25’ 54.8”N, 157° 47’ 20.4”W (★). **B.** Photograph of *Padina thivyae*. Photo credit: Kim Peyton.

A.

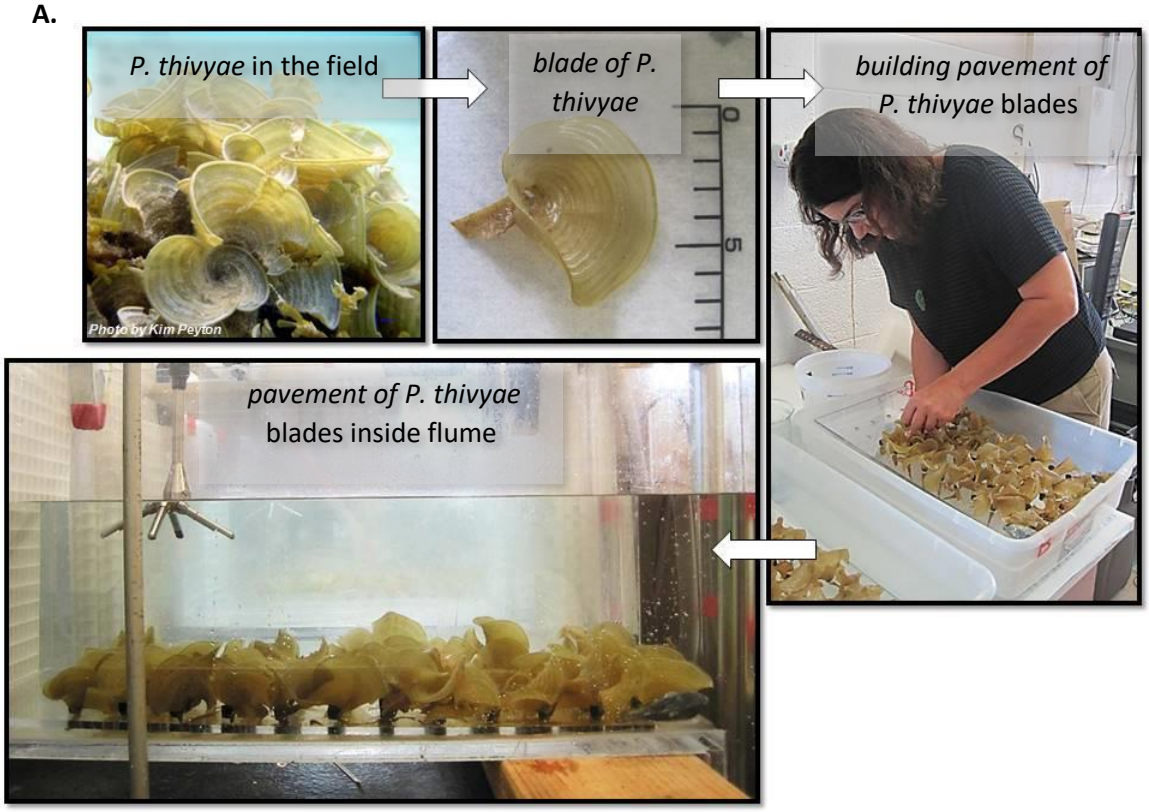

B.

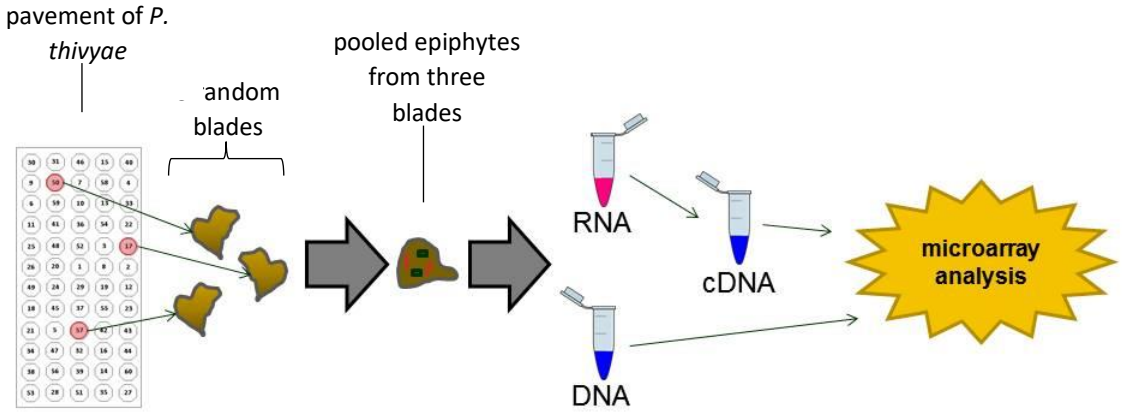

Figure 3.2 A. Padina thivyae collection and preparation for flume experiments **B.** Flow chart illustrating experiment sample collection and processing.

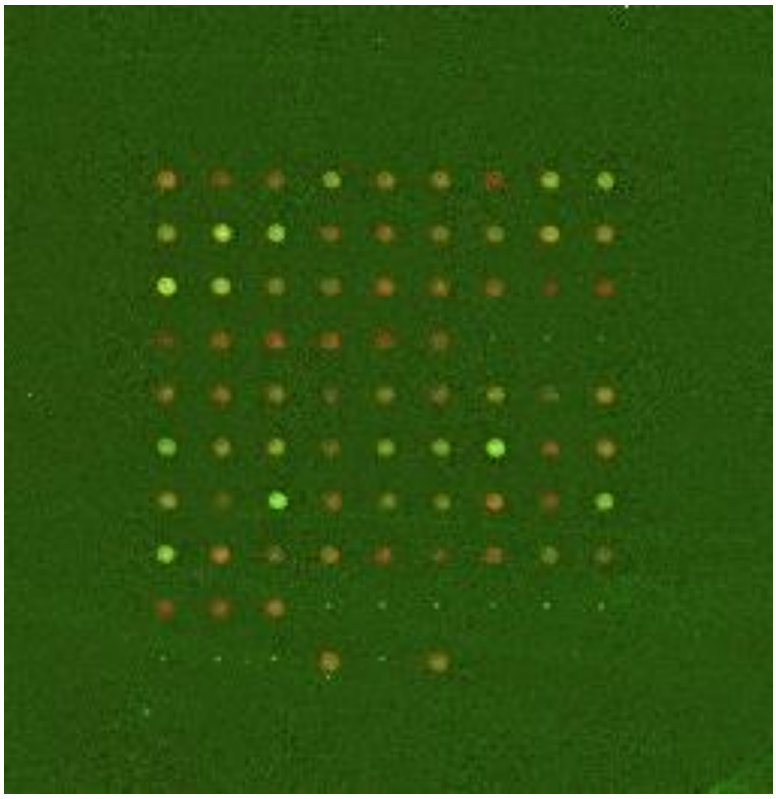

Figure 3.3 Section of scanned hybridized slide. Each circle (feature) represents the location of a unique probe printed on the slide. Cy3 and Cy5 fluorescent dyes used appear green and red, respetively, once excited during the scanning process.

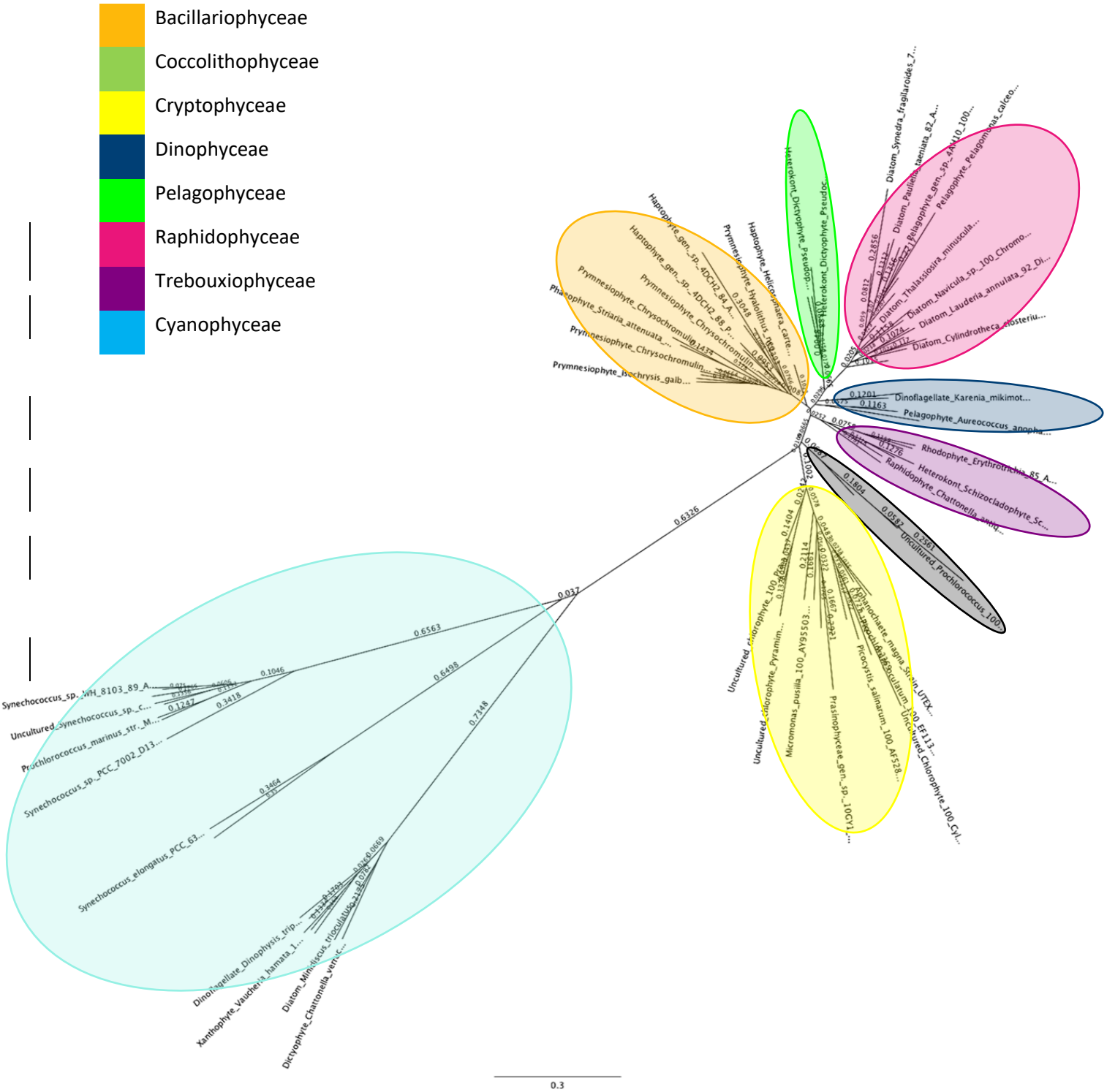
Bacillariophyceae
Coccolithophyceae
Cryptophyceae
Dinophyceae
Pelagophyceae
Raphidophyceae
Trebouxiophyceae
Cyanophyceae
Diatom_Synedra_fragilaroides_7...
Diatom_Pauliella_taeniata_82_A...
Pelagophyte_gen._sp._4DCH10_100...
Pelagophyte_Pelagomonas_calceo...
Heterokont_Dictyophyte_Pseudop...
Heterokont_Dictyophyte_Pseudoc...
Haptophyte_gen._sp._4DCH2_84_A...
Haptophyte_gen._sp._4DCH2_88_P...
Prymnesiophyte_Hyalolithus_neol...
Haptophyte_Helicosphaera_carte...
Prymnesiophyte_Chrysochromulin...
Prymnesiophyte_Chrysochromulin...
Phaeophyte_Striaria_attenuata_...
Prymnesiophyte_Chrysochromulin...
Prymnesiophyte_Isochrysis_galb...
Diatom_Thalassiosira_minuscula...
Diatom_Navicula_sp._100_Chromo...
Diatom_Lauderia_annulata_92_Di...
Diatom_Cylindrotheca_closteriu...
Dinoflagellate_Karenia_mikimot...
Pelagophyte_Aureococcus_anopha...
Rhodophyte_Erythrotrichia_85_A...
Heterokont_Schizocladophyte_Sc...
Raphidophyte_Chattonella_anti...
Uncultured_Prochlorococcus_100...
Uncultured_Chlorophyte_100_Cyl...
Picocystis_salinarum_100_AF526...
Prasinophyceae_gen._sp._10CY1...
Micromonas_pusilla_100_AY955503...
Uncultured_Chlorophyte_Pyramim...
Uncultured_Chlorophyte_100_Pseu...
Synechococcus_sp._WH_8103_89_A...
Uncultured_Synechococcus_sp._c...
Prochlorococcus_marinus_str._M...
Synechococcus_sp._PCC_7002_D13...
Synechococcus_elongatus_PCC_63...
Dinoflagellate_Dinophysis_trip...
Xanthophyte_Vaucheria_hamata_1...
Diatom_Minidiscus_trioculatus_1...
Dictyophyte_Chattonella_veri...c...
0.6326
0.037
0.6563
0.6498
0.7348
0.1046
0.1247
0.3418
0.3464
0.0669
0.3
Figure 3.4A Phylogenetic tree of epiphyte community based on gene sequences coding for Rubisco (rbcL)

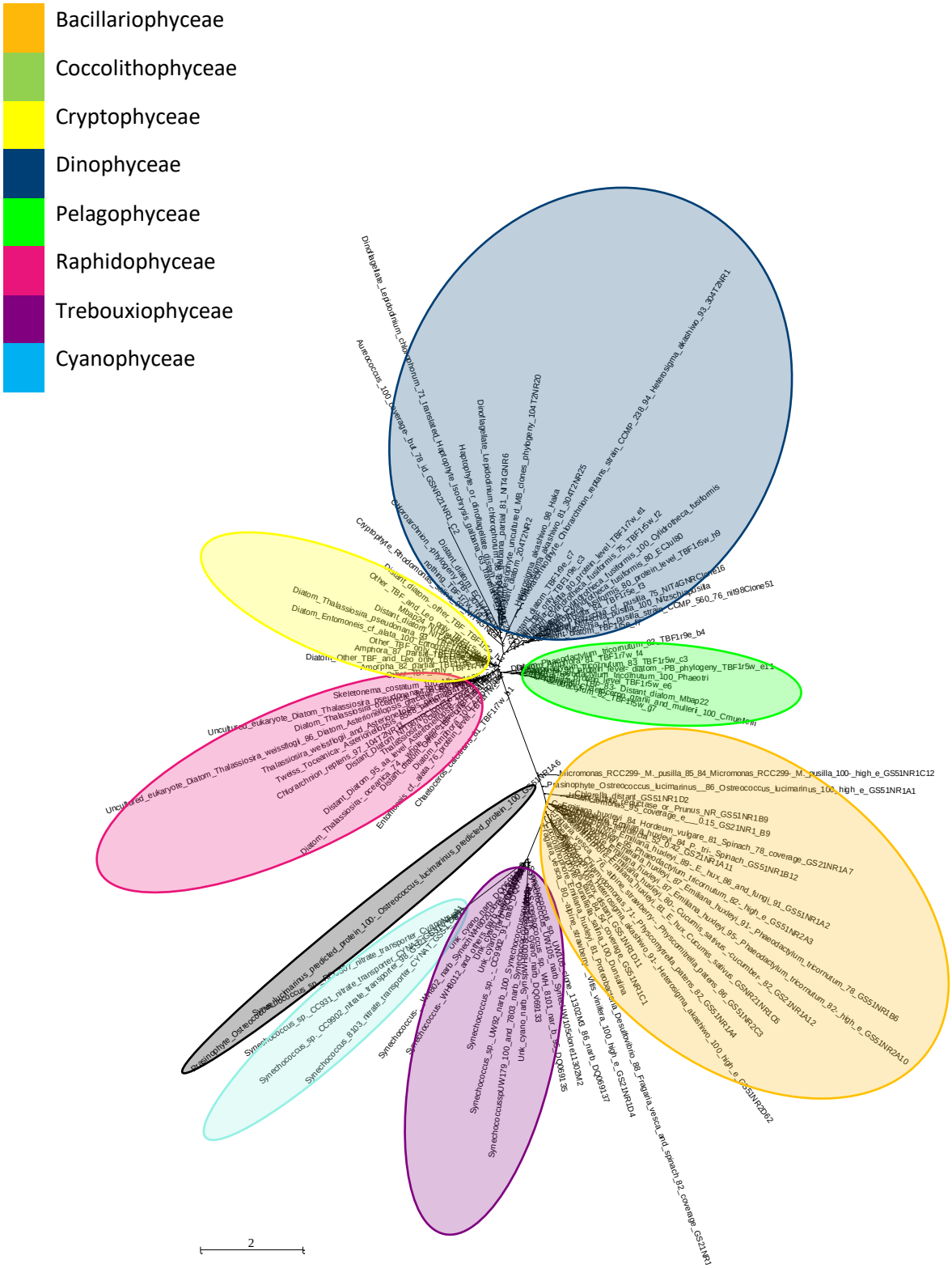

Figure 3.4B Phylogenetic tree of epiphyte community based on gene sequences coding for Nitrate Reductase (NR) enzyme

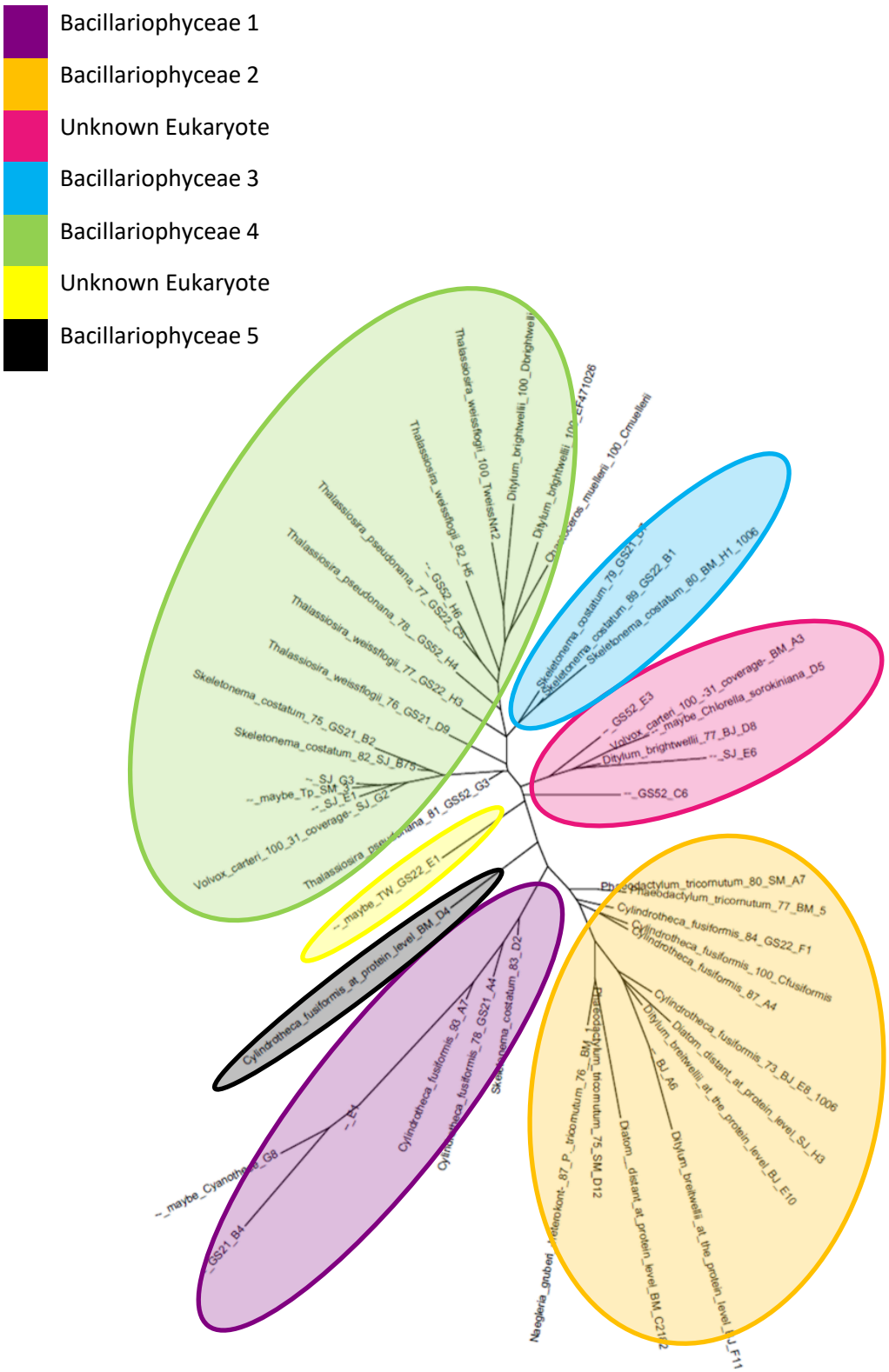

Figure 3.4C Phylogenetic tree of epiphyte community based on gene sequences coding for a eukaryotic membrane-bound nitrate transporter protein (*Nrt2*)

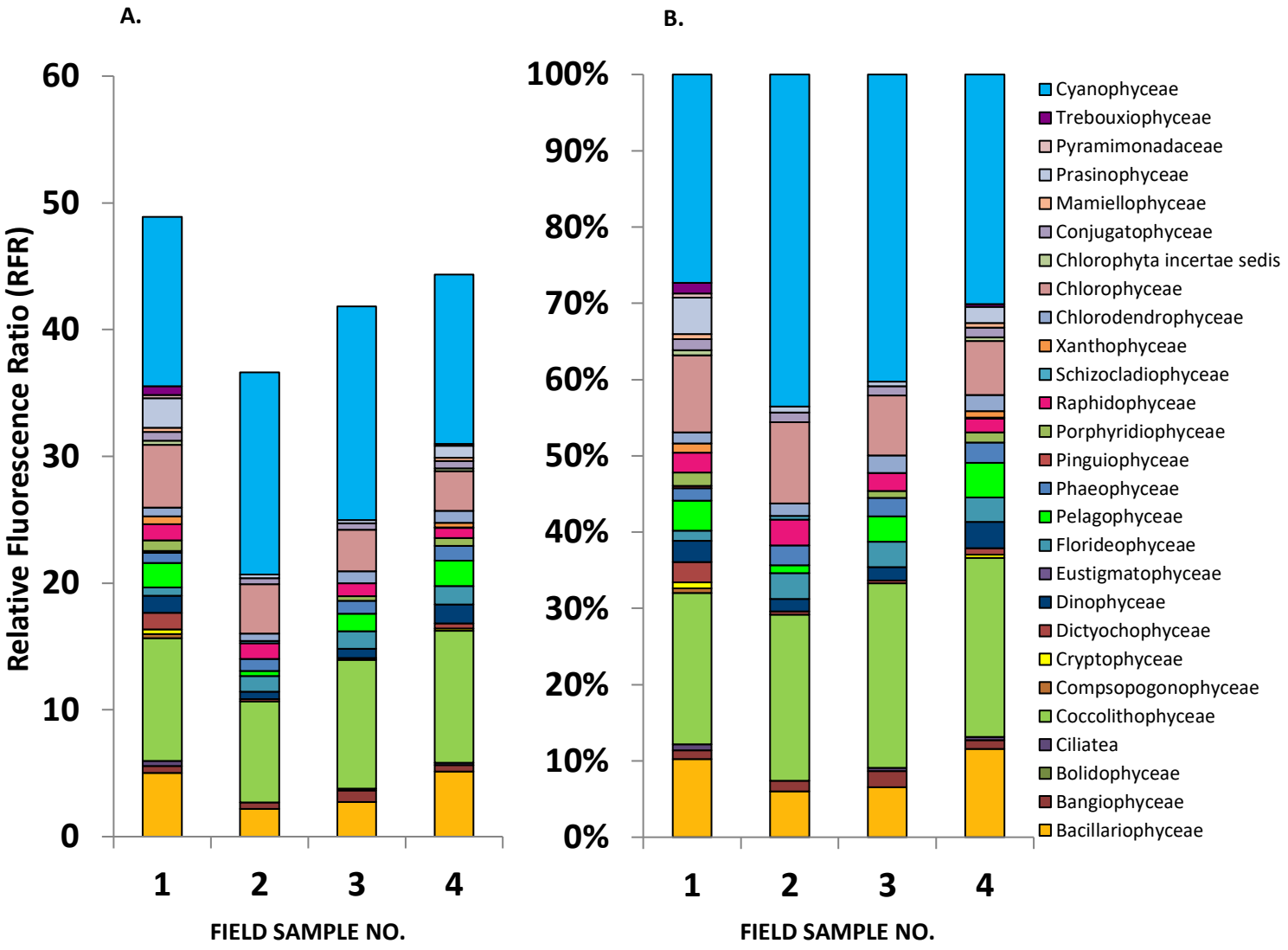

Figure 3.5 Barcharts showing community structure based on the rbcL gene marker. Panel A illustrates absolute RFRs, while Panel B illustrates the proportion of the total community represented by each class.

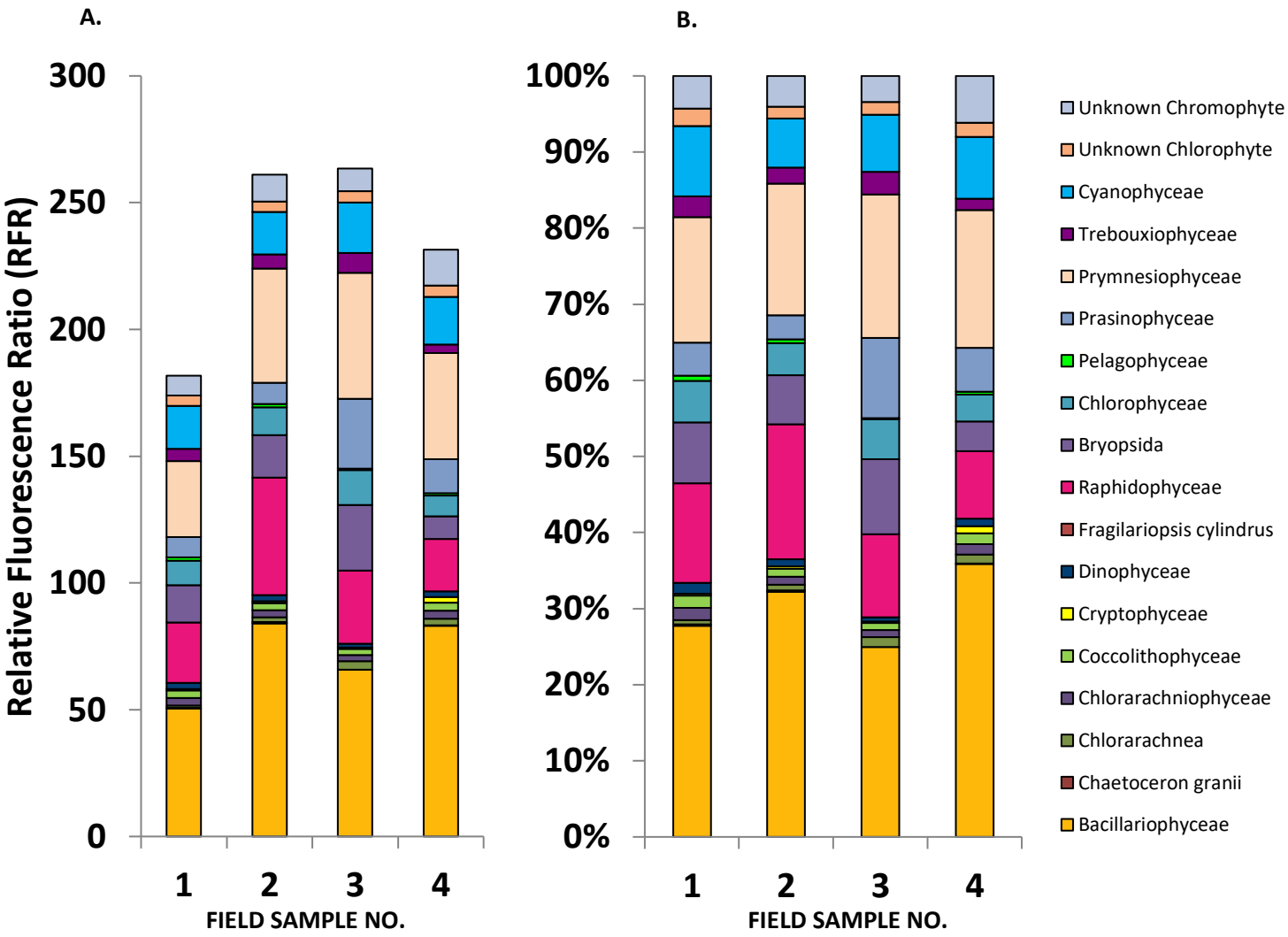

Figure 3.6 Barcharts showing community structure based on the NR gene marker. Panel A illustrates absolute RFRs, while Panel B illustrates the proportion of the total community represented by each class

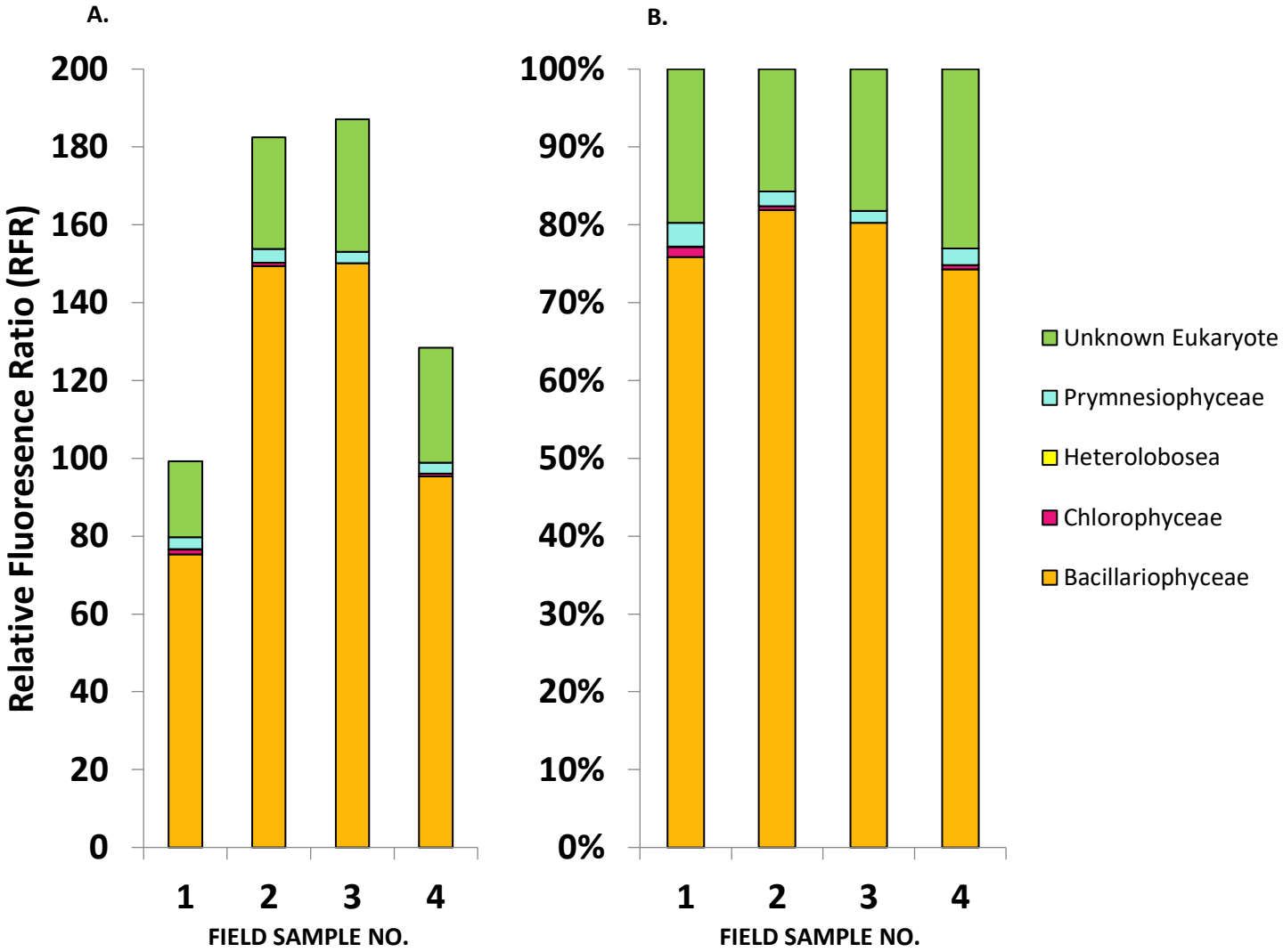

Figure 3.7 Barcharts showing community structure based on the *Nrt2* gene marker. Panel A illustrates absolute RFRs, while Panel B illustrates the proportion of the total community represented by each class

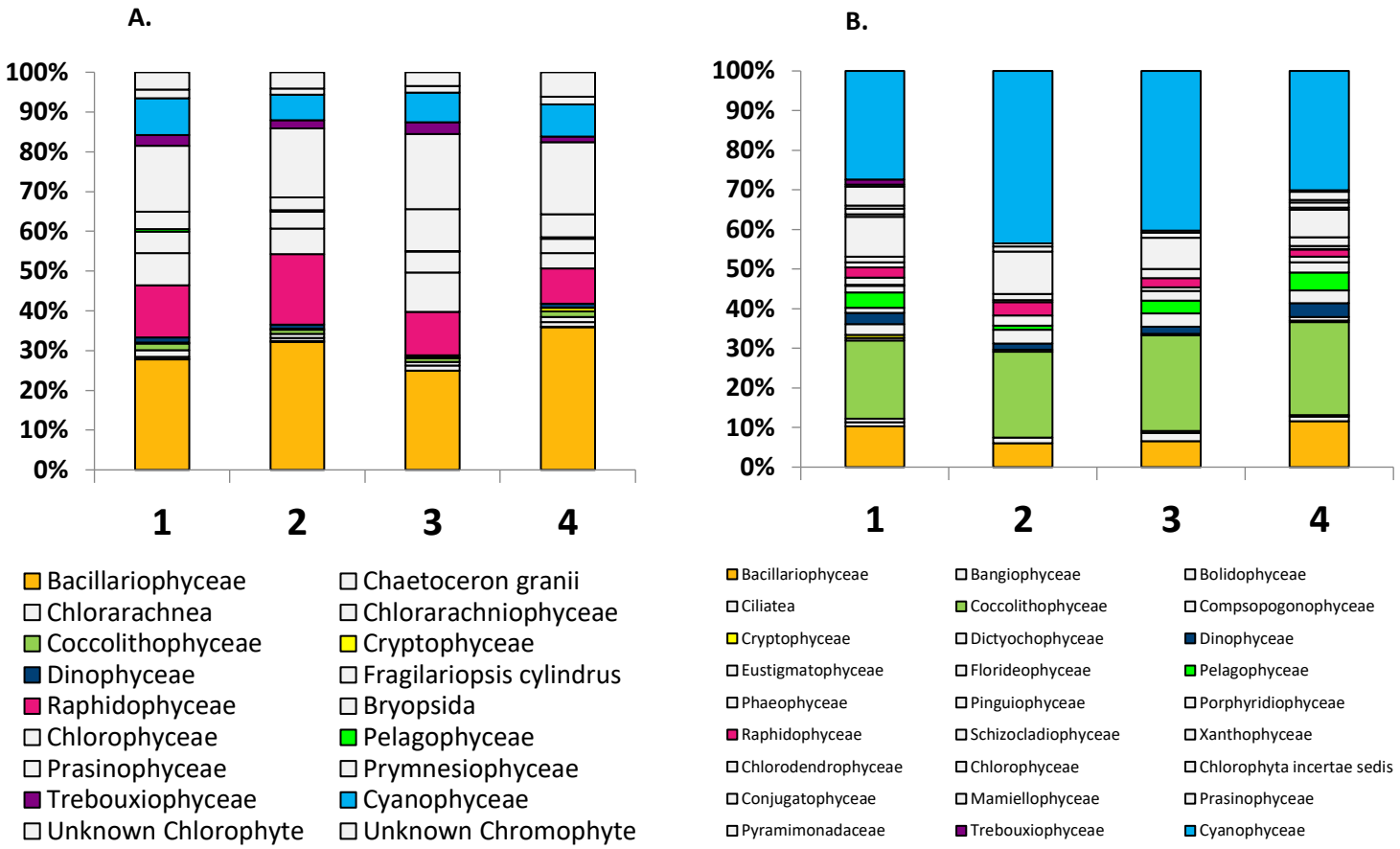

Figure 3.8 Barcharts illustrating how the representation of Classes in a community sample can change depending upon choice of gene marker. Panel **A** shows community structure based on NR, while Panel **B** shows community structure based on rbcL. Colored bars represent Classes in common between the NR and rbcL libraries.

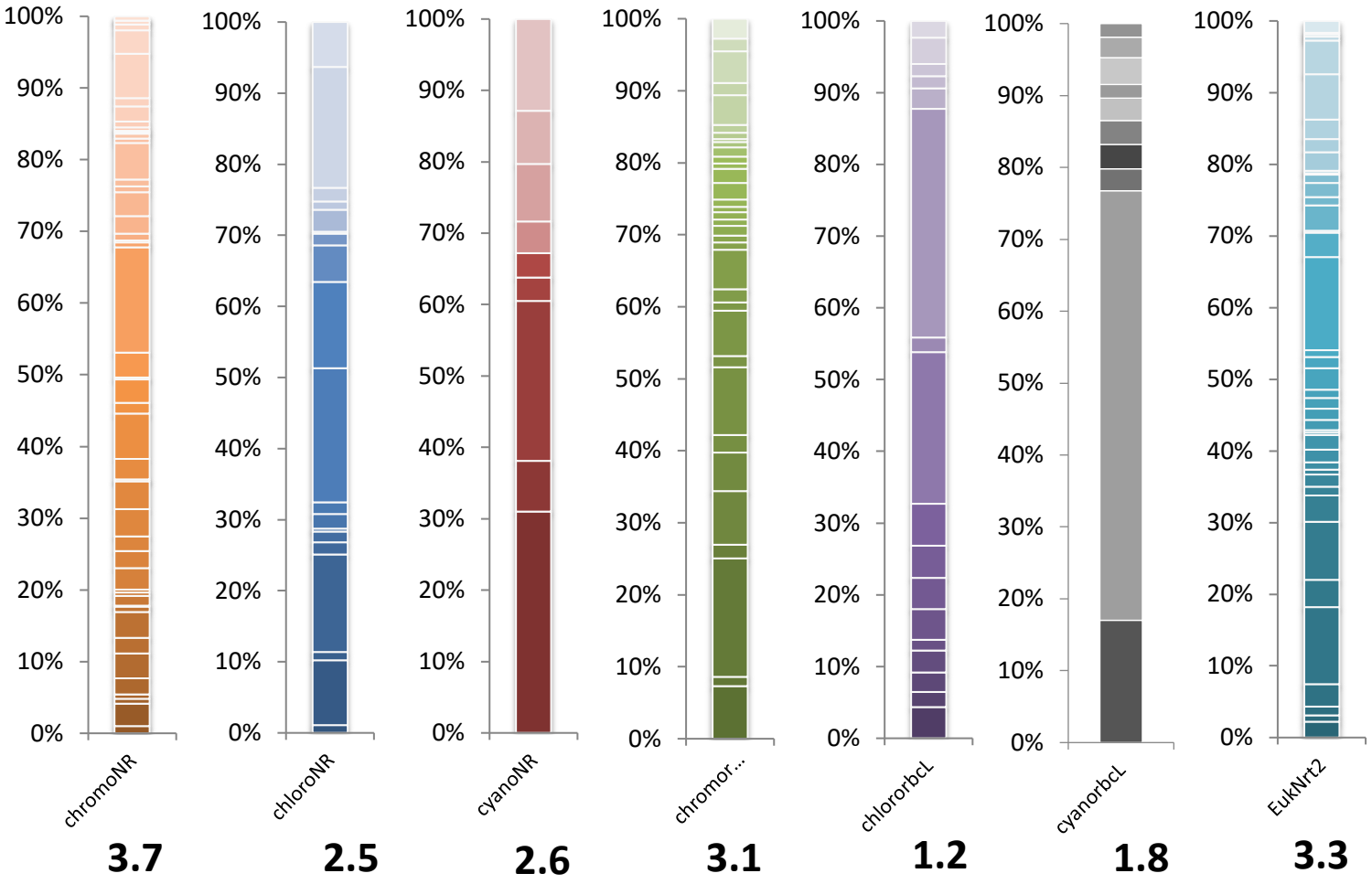

Figure 3.9 Barcharts showing the range of Shannon diversity indices across multiple genes and treatments. Shannon diversity indices ranged from 1.2 to 3.7 across multiple genes (*NR*, *rbcL*, and *Nrt2*) and experiment treatments (high and low flow, and both 2µM and 10µM nirate concentration).

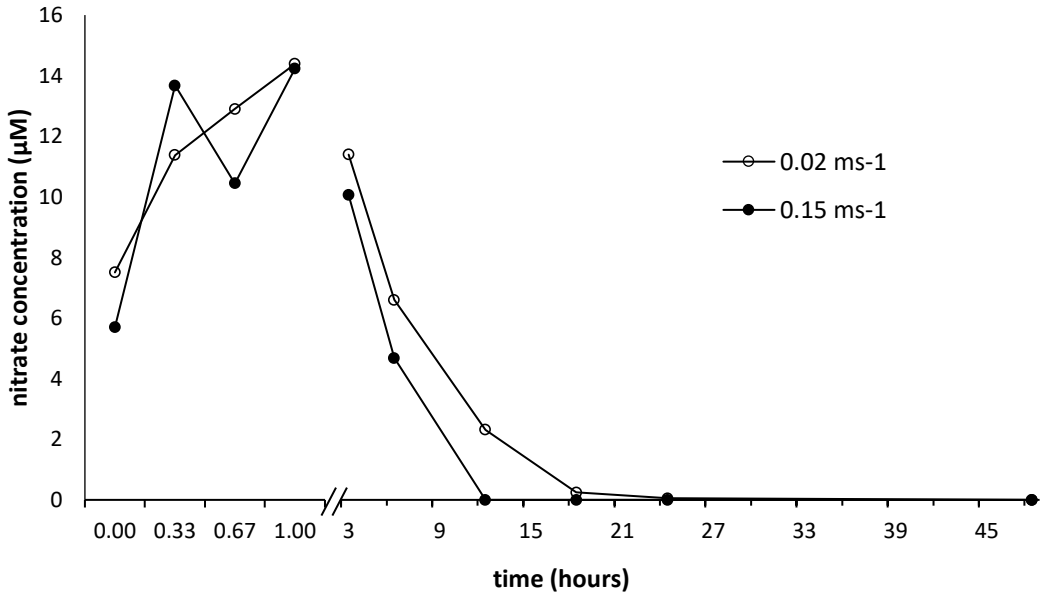

Figure 3.10 Timeseries of nitrate concentration of the flume water in the 10 µM experiment. Nitrate is drawn down to near zero by 12 hours. Initial nitrate concentration at the beginning of the experiment suggests that flume water was not sufficiently homogenized to achieve the target concentration of 10 µM.

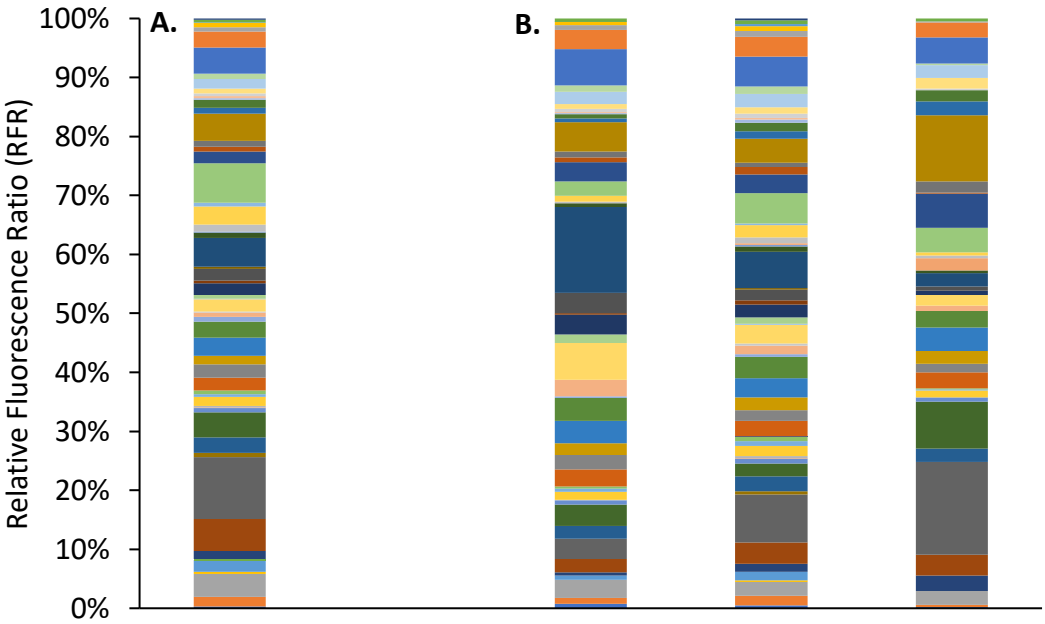

	10µM 0.02 ms-1 DAY 0	DAY 0	DAY 1	DAY 2
Richness	59	49	60	41
Shannon Entropy	3.6	3.4	3.7	3.18
"true diversity"	36.6	30.1	40.6	24.0

Figure 3.11 Barcharts showing **A.** Day 0 sample epiphyte community structure, assessed for the 10 µM at 0.02 ms^{-1} based on chromophyte NR and **B.** a timeseries of epiphyte community structure over the experimental period for the 10 µM at 0.15 ms^{-1} experiment.

Richness (*S*), Shannon Diversity (*H'*), and "true diversity" are reported for comparison.

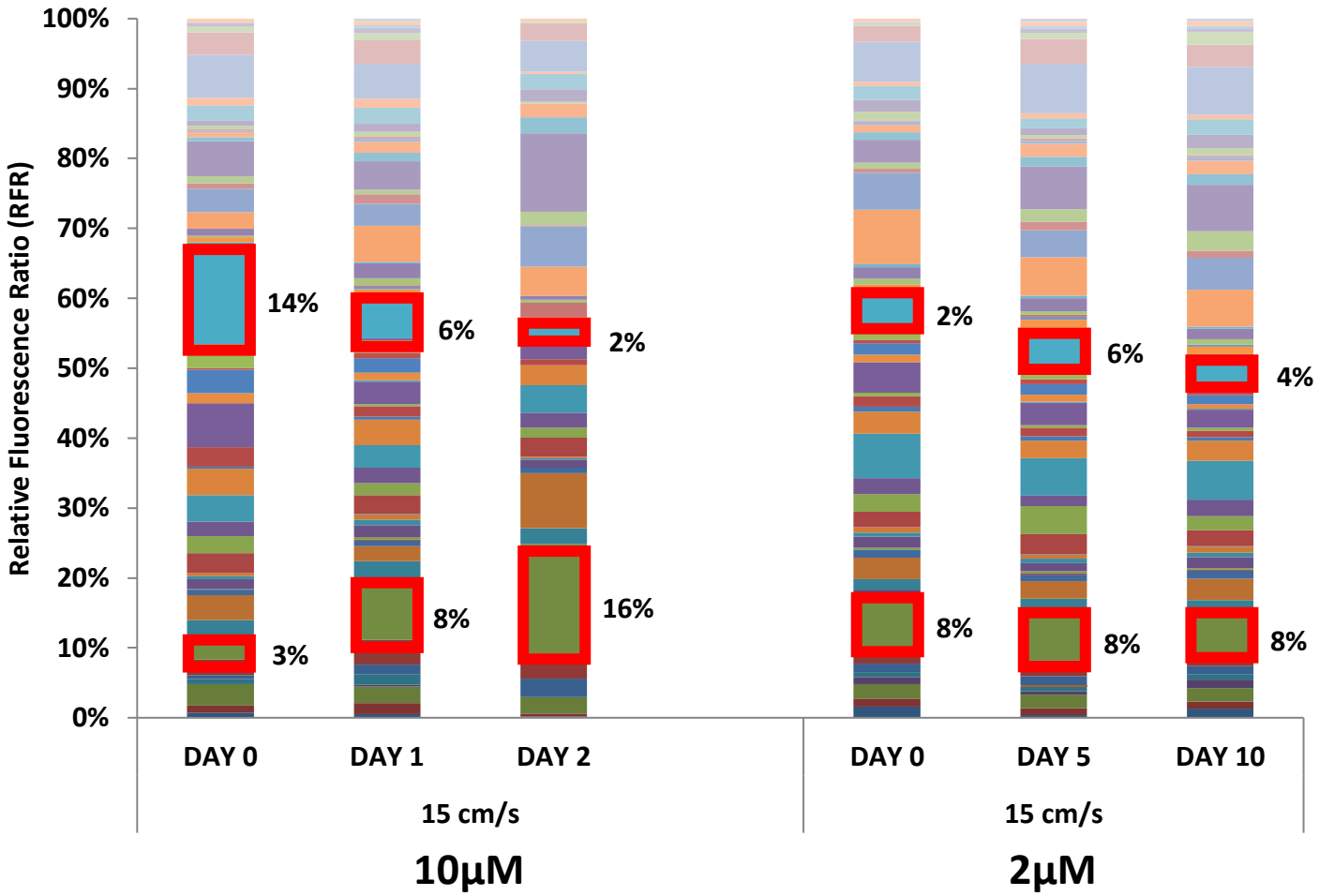

Figure 3.12 Barcharts showing variations in epiphyte community structure based upon hybridization of the chromophyte nitrate reductase (NR) gene over the experimental time course for 10 µM and 2 µM nitrate treatments. Both data sets were subject to 0.15ms^{-1} of water flow conditions.

Relative abundance of *Thalassiosira weissflogii* shown as the highighted blue blocks, decreased from 14% on Day 0 to 2% by Day 2 under the 10 µM treatment while it only underwent a 2% change under the 2 µM treatment. Relative abundance of an unnidentified diatom, shown as the highlighted green block, increased from 3% on Day 0 to 16% on Day 2 under the 10 µM treatment, but maintained an 8% relative abundance under the 2 µM treatment.

Differences in community structure illustrate response to a perturbation in nitrate concentration – the community in the 2 µM treatment was less responsive to nitrate flux than it was in the 10 µM treatment.

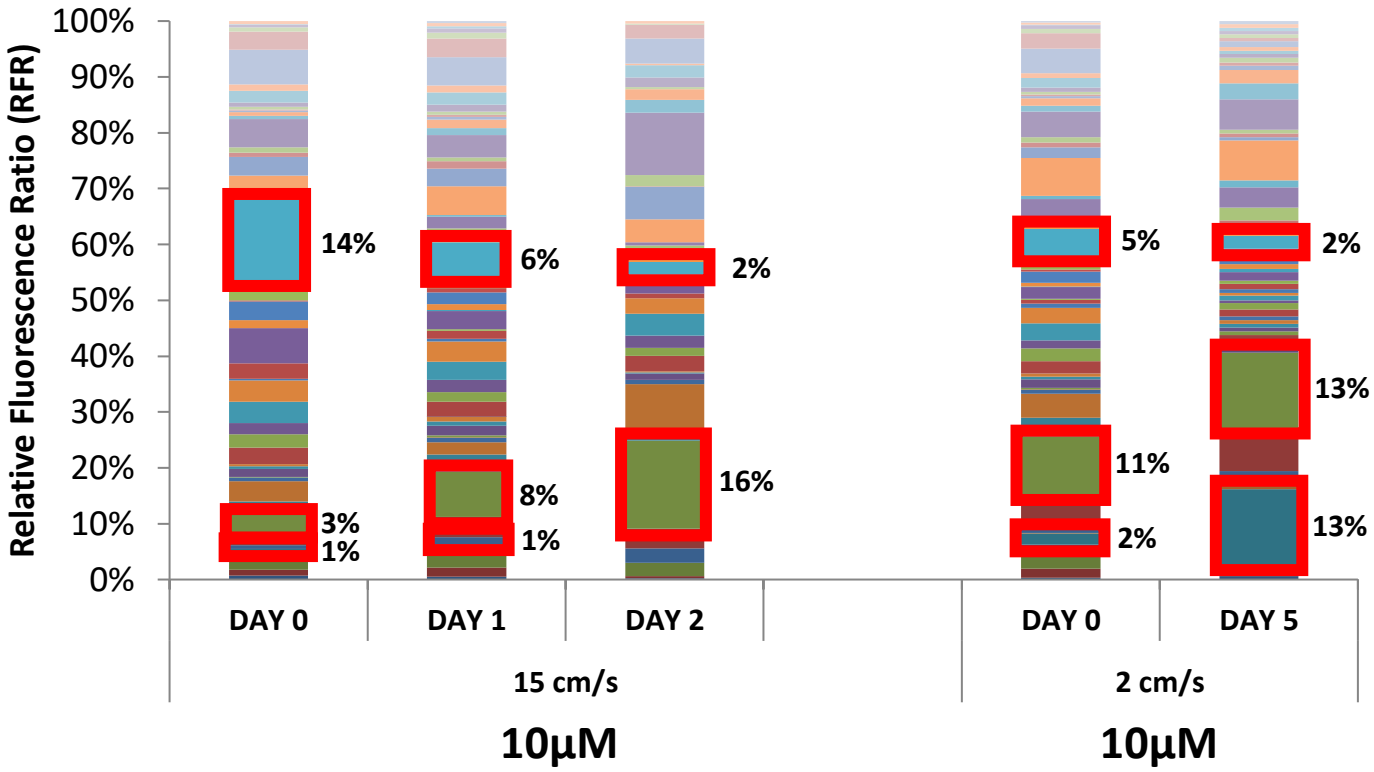

Figure 3.13 Epiphyte community structure based on hybridization of the chromophyte nitrate reductase (NR) gene at sampling timepoints for paired 10 µM experiments. Relative abundance of *Thalassiosira weissflogii* shown as the highighted light blue blocks, decreased from 14% on Day 0 to 2% by Day 2 under the 0.15 ms^{-1} treatment while it underwent only a 3% change under the 0.02 ms^{-1} treatment. Relative abundance of an unnidentified diatom, shown as the highlighted green block, increased from 3% on Day 0 to 16% on Day 2 under the 0.15 ms^{-1}, while its relative abundance underwent a 2 % increase under the 0.02 ms^{-1} treatment.

Differences in community structure illustrate an effect of water flow rate: the community in the 0.02 ms^{-1} treatment was less responsive to nitrate flux than it was in the 0.15 ms^{-1}treatment.

Cryptophyte *Rhodomonas salina* displays the opposite pattern – its relative abundance underwent a more dramatic shift under the lower flux (0.02 ms^{-1}) treatment as compared to its response under the 0.15 ms^{-1} treatment.

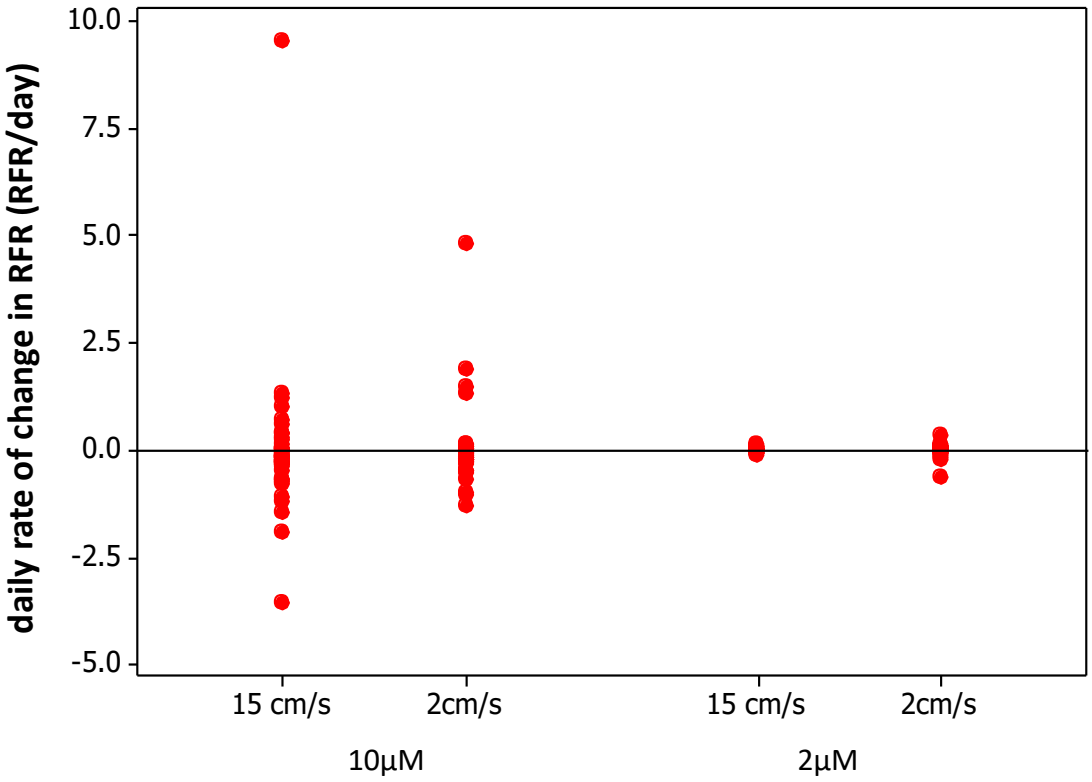

Figure 3.14 Daily rate of change of relative abundance based on hybridization of the chromophyte nitrate reductase (NR) gene. 10µM treatments show a wider range in rate of change than the 2µM treatments.

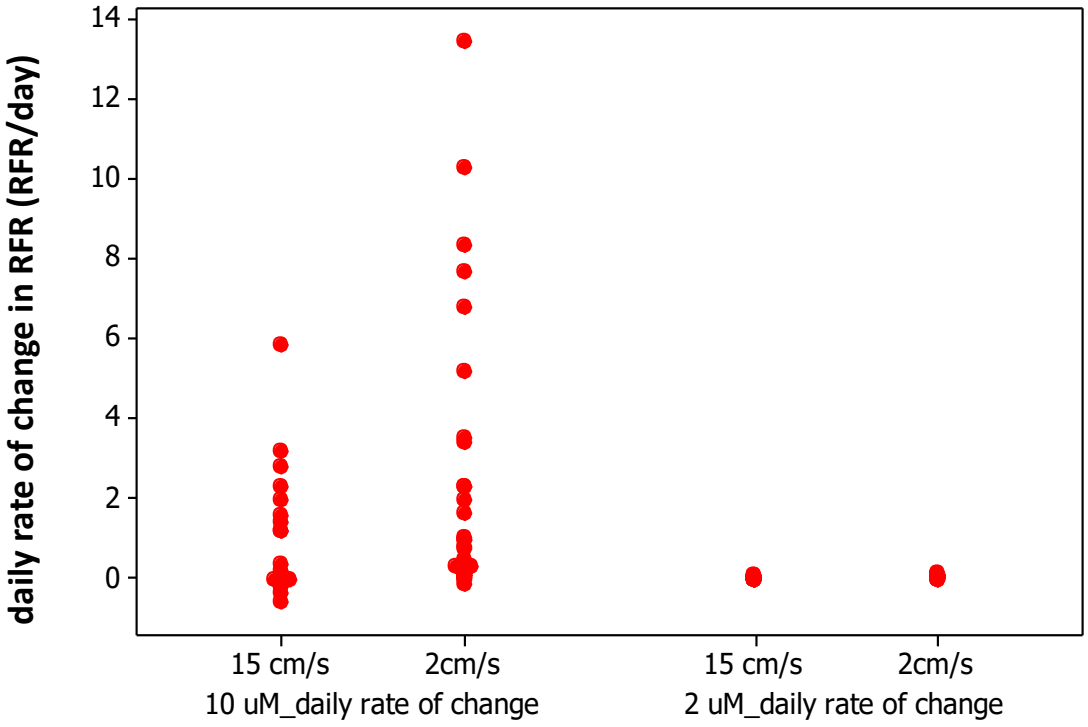

Figure 3.15 Daily rate of change of relative abundance based on hybridization of the chromophyte RuBisCO (rbcL) gene. 10µM treatments show a wider range in rate of change than the 2µM treatments.

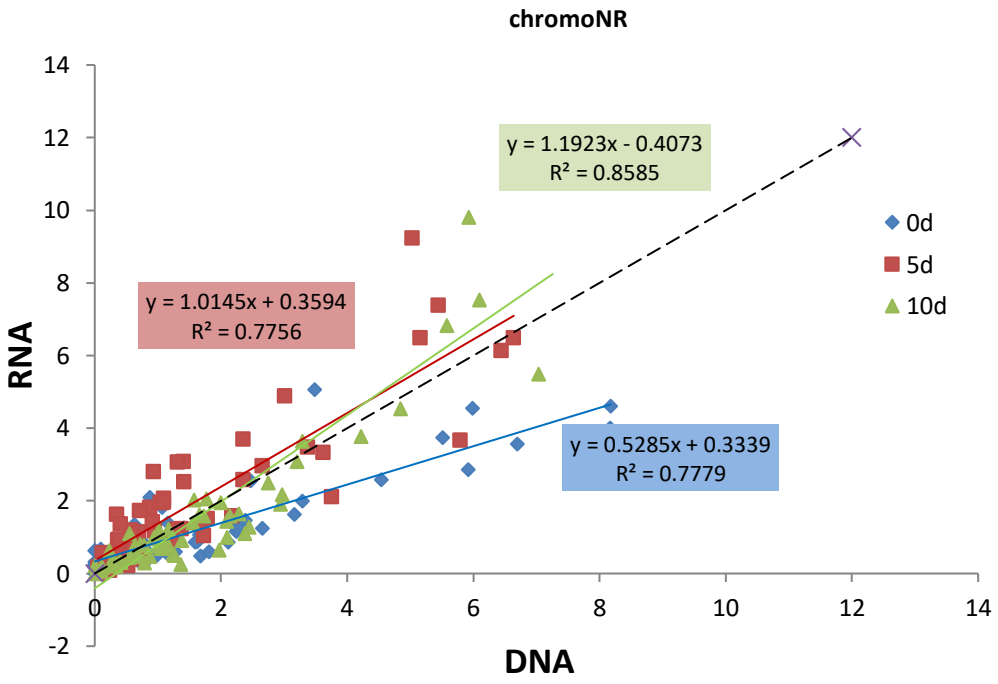

Figure 3.16 Scatterplot showing RNA:DNA ratios based on chromophyte nitrate reductase (NR) for Day 0 (blue diamonds), Day 5 (red squares), and Day 10 (green trianges) of the 2 µM at 0.02 ms^{-1} treatment experiment.

Dashed black line illustrates an RNA:DNA ratio of 1:1. Slopes increased as experiment time elapsed from Day 0 to Day 10, indicating an increase in RNA relative to DNA.

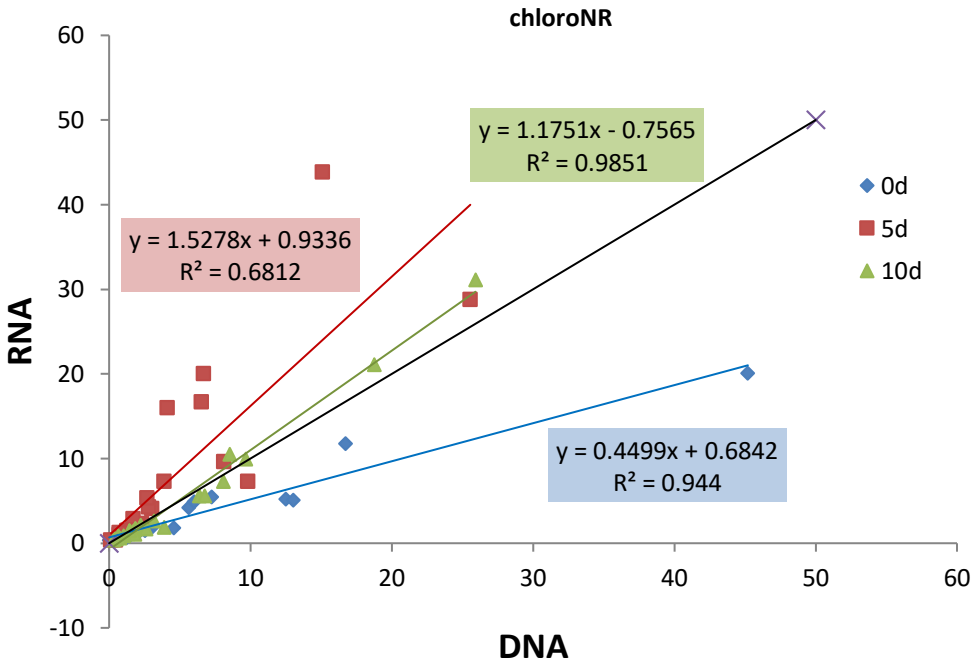

Figure 3.17 Scatterplot showing RNA:DNA ratios based on chlorohyte nitrate reductase (NR) for Day 0 (blue diamonds), Day 5 (red squares), and Day 10 (green triangles) of the 2 µM at 0.02 ms^{-1} treatment experiment.

Dashed black line illustrates an RNA:DNA ratio of 1:1. Slope increased from Day 0 to Day 5, indicating an increase in RNA, however slope decreased from Day 5 to Day 10, indicating a decrease in RNA relative to DNA.

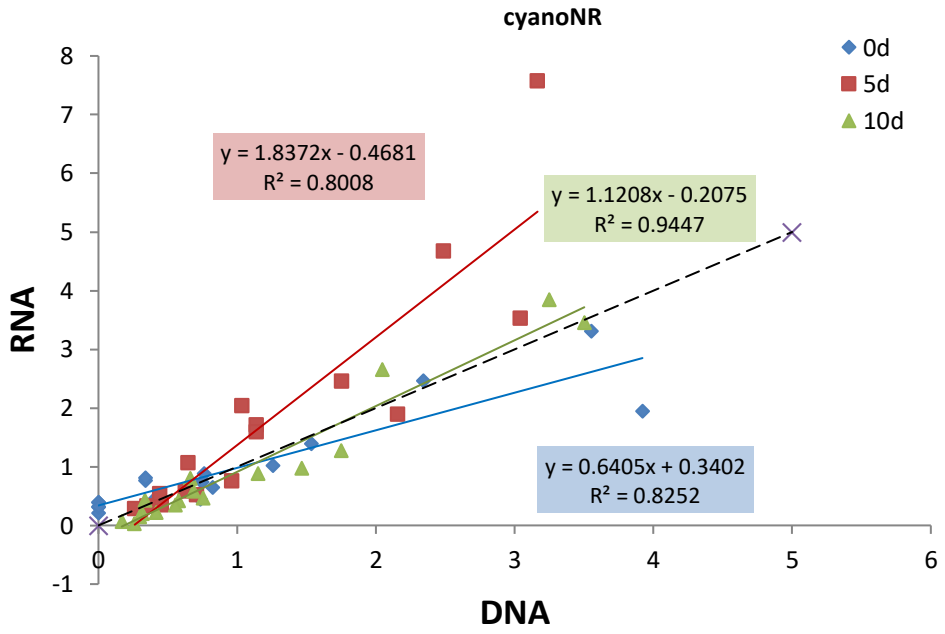

Figure 3.18 Scatterplot showing RNA:DNA ratios based on cyanobacteria nitrate reductase (NR) for Day 0 (blue diamonds), Day 5 (red squares), and Day 10 (green triangles) of the 2 µM at 0.02 ms^{-1} treatment experiment. Dashed black line illustrates an RNA:DNA ratio of 1:1. Slope increased from Day 0 to Day 5, indicating an increase in RNA, however slope decreased from Day 5 to Day 10, indicating a decrease in RNA relative to DNA.

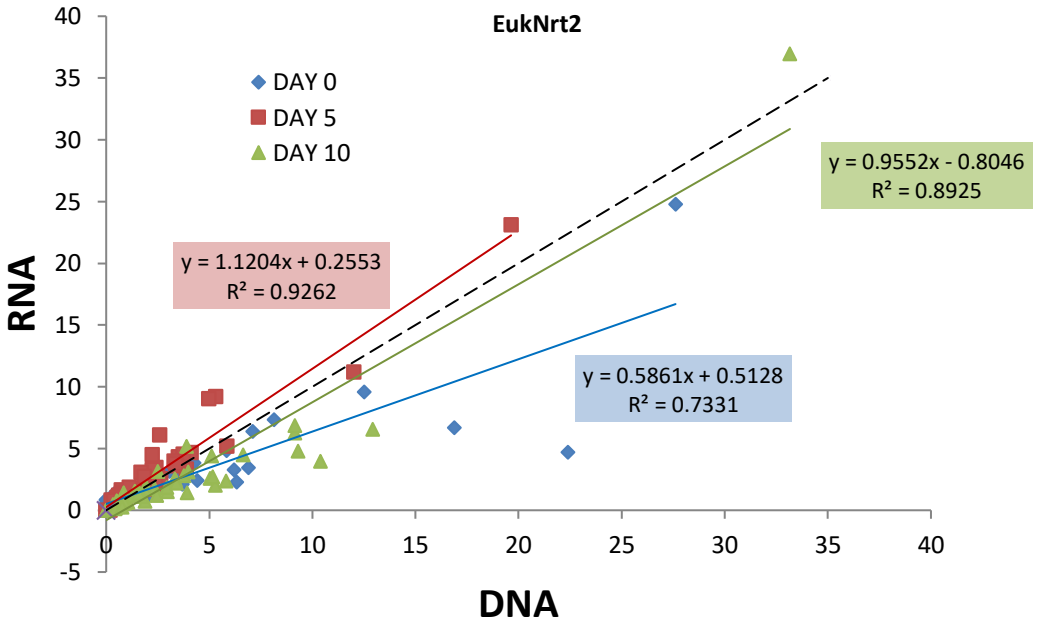

Figure 3.19 Scatterplot showing RNA:DNA ratios based on eukaryotic membrane transport protein (*Nrt2*) for Day 0 (blue diamonds), Day 5 (red squares), and Day 10 (green triangles) of the 2 µM at 0.02 ms^{-1} treatment experiment. Dashed black line illustrates an RNA:DNA ratio of 1:1. Slope increased from Day 0 to Day 5, indicating an increase in RNA, however slope decreased from Day 5 to Day 10, indicating a decrease in RNA relative to DNA.

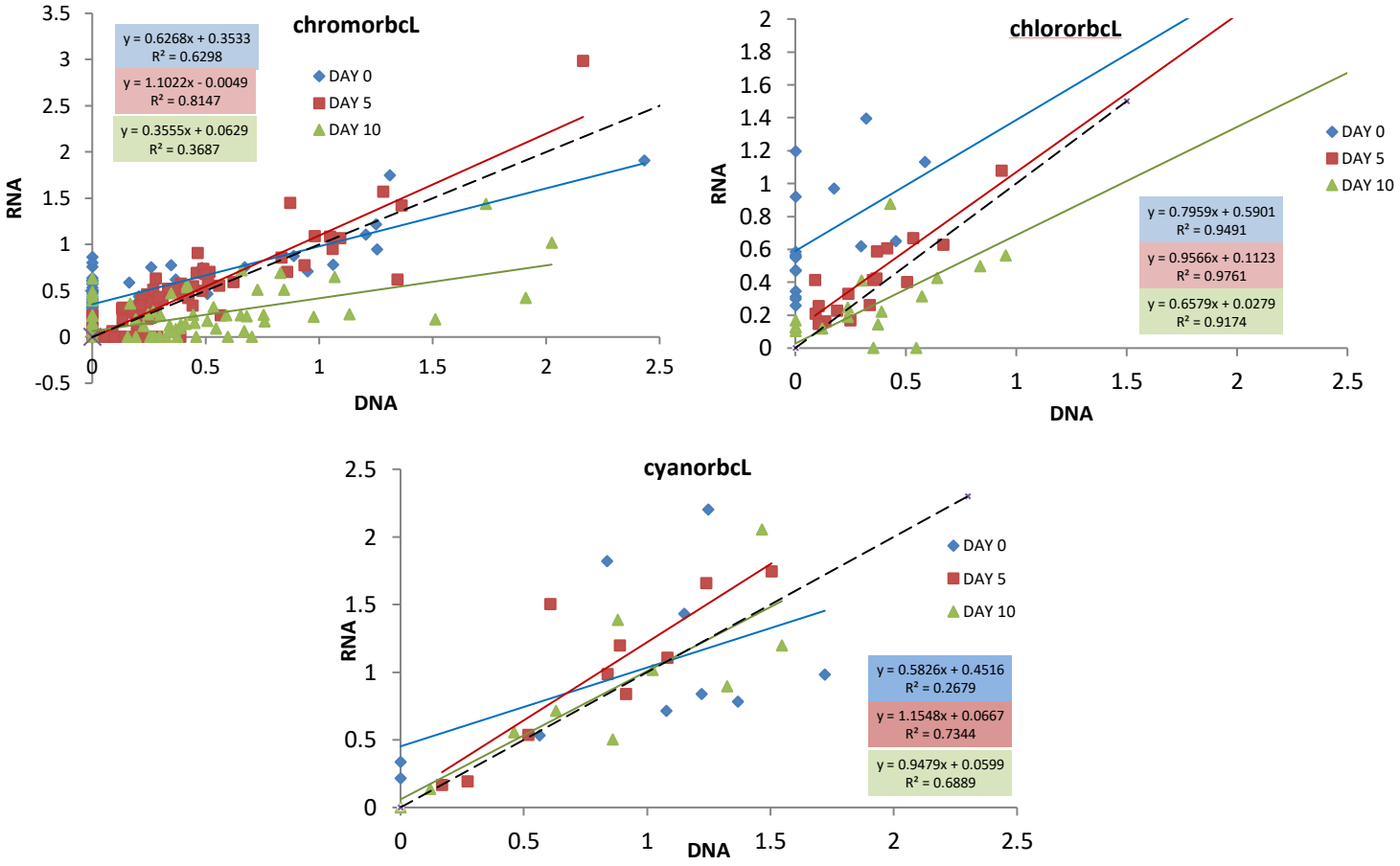

Figure 3.20 Scatterplot showing RNA:DNA ratios based on RuBisCO (rbcL) for Day 0 (blue diamonds), Day 5 (red squares), and Day 10 (green triangles) of the 2 µM at 0.02 ms^{-1} treatment experiment. Dashed black line illustrates an RNA:DNA ratio of 1:1. RuBisCO displayed no systematic pattern either with respect to time or amongst the algal groups.

Table 3.1 Phytoarray description. Archetype refers to the unique identifiers printed on the microarray chip to which all community sample sequences within 85% identity will hybridize.

	Gene Marker	Classes	No. of Archetypes	no. of base pairs
RuBisCO (*rbcL*)	Chlorophyte (green algae)	Chlorodendrophyceae	1	70
		Chlorophyceae	4	
		Chlorophyta incertae sedis	1	
		Conjugatophyceae	1	
		Mamiellophyceae	1	
		Prasinophyceae	6	
		Pyramimonadaceae	1	
		Trebouxiophyceae	1	
		Cyanophyceae	3	
	Chromophyte (brown algae)	Bacillariophyceae	22	
		Bangiophyceae	1	
		Bolidophyceae	2	
		Ciliatea	1	
		Coccolithophyceae	20	
		Compsopogonophyceae	1	
		Cryptophyceae	1	
		Dictyochophyceae	3	
		Dinophyceae	5	
		Eustigmatophyceae	1	
		Florideophyceae	2	
		Pelagophyceae	9	
		Phaeophyceae	1	
		Pinguiophyceae	1	
		Porphyridiophyceae	1	
		Raphidophyceae	3	
		Schizocladiophyceae	1	
		Xanthophyceae	3	
	Cyanobacteria (photosynthetic bacteria)	Cyanophyceae	10	
Nitrate Reductase (*NR*)	Chlorophyte (green algae)	Raphidophyceae	1	
		Bryopsida	1	
		Chlorophyceae	4	
		Pelagophyceae	1	
		Prasinophyceae	5	
		Prymnesiophyceae	9	
	Chromophyte (brown algae)	Bacillariophyceae	43	
		Chaetoceron granii	1	
		Chlorarachnea	2	
		Chlorarachniophyceae	1	
		Coccolithophyceae	2	
		Cryptophyceae	1	
		Dinophyceae	2	
		Fragilariopsis cylindrus	1	
		Raphidophyceae	2	
	Cyanobacteria (photosynthetic bacteria)	Cyanophyceae	17	
Nitrate transporter protein (*Nrt2*)		Bacillariophyceae	31	
		Chlorophyceae	2	
		Heterolobosea	1	
		Prymnesiophyceae	1	

Table 3.2

Species Richness, *S*

gene	Sample IDs				coefficient of variance, %
	1	2	3	4	
Nrt2	48	45	41	47	6.84
NR	100	89	80	100	10.49
rbcL	82	37	50	75	34.57

Table 3.3

Shannon Entropy, *H'*

gene	Sample IDs				coefficient of variance, %
	1	2	3	4	
Nrt2	3.41	3.26	3.33	3.54	3.46
NR	3.95	3.75	3.61	4.00	4.70
rbcL	4.04	3.18	3.31	3.80	11.30

Table 3.4

"True Diversity"

gene	Sample IDs				coefficient of variance, %
	1	2	3	4	
Nrt2	30.20	26.15	28.01	34.38	11.93
NR	52.07	42.41	37.13	54.56	17.56
rbcL	56.77	24.10	27.35	44.75	40.07

CHAPTER 4 – BIOPHYSICAL INTERACTIONS ON THE ECOSYSTEM LEVEL: INVESTIGATING NITRATE DISTRIBUTION IN A SHALLOW COASTAL REEF FLAT SYSTEM USING A NUMERICAL MODEL

1. Introduction

As the global human population continues to increase, so too does the pressure on our natural resources. This pressure has been acutely felt in coastal areas, where increased nutrient loading associated with over-fertilization to meet resource demand (e.g., Mississippi River, Rabalais et al. 1996; the North Sea, "Eutrophication in Europe's coastal waters Topic report 7/2001" 2001) not only results in algal blooms within hours to days (Lapointe & O'Connell 1989), but also in a decadal doubling in the number of "dead zones" since the 1960s (Diaz & Rosenberg 2008). Other biogeochemical effects of anthropogenic perturbations include the development of harmful algal blooms (HABs), such as in southeast Florida, where these blooms are linked to increasing anthropogenic activities such as land-based sewage input (Lapointe et al. 2005b), and the introduction of non-native species either deliberately (Allen 1998, Siple & Donahue 2013: mangroves in Hawai'i) or unintentionally (Jacoby et al. 2004). Shoreline features and, consequently, water flow patterns, are often reshaped due to dredging, coastal urbanization, and tourism-related development. As exhaustive use of coastal resources takes place within the context of the effects of climate change, understanding how coastal communities respond to nutrient perturbations becomes increasingly important in order to implement improved coastal management strategies that mitigate the harmful environmental effects of our activities.

It is well known that changes in nutrient availability impact the growth of marine primary producers, and can thus alter the composition of the primary producer community (e.g., Cembella et al. 1982; Young 2011). Since primary producers form the base of the aquatic foodweb, impacts of changes in their community structure can be observed at higher trophic levels. For example, harmful algal blooms (HABs)

often are linked to mass mortality of fish (Anderson et al. 2002). As another example, grazing damselfish have been reported to exhibit preference for particular algae and subsequent behavioral changes in response to shifts in their food source (Ormond et al. 1996). Consequently, abundance and distribution of the food source preferred by damselfish can be critically important to damselfish population stability. Particularly relevant to the present study is the effect of nutrient concentration and distribution on the primary producer community. Shifts in nutrient source may provide conditions in which invasive (often opportunistic) species thrive preferentially over native ones. As argued by Lapointe & Bedford (2011), non-native species may be better suited to take advantage of enriched sources of nutrients, such as stormwater (sewerage) discharge, than native species.

The state of Hawai‘i recognizes the importance of dynamic management practices in maintaining the health of water resources. In the face of Climate Change, the stated goal of Hawai‘i policy makers is to improve “adaptive capacity”, which is defined as the laws and policies that require water management to be forward-looking, flexible, integrated, and iterative (Wallsgrove & Penn 2012). Understanding and predicting how organisms and systems respond to, and recover from changes in nutrient loading is essential for optimal management of coastal resources, particularly within the framework of future environmental change. Keeping pace with, and getting ahead of rapidly changing environmental conditions mandates the use of adaptive tools and management strategies in monitoring, assessing, and managing resources. An important pathway to the formulation and development of such tools is to take advantage of the predictive power of numerical models.

Here, we describe the development of a one-dimensional numerical model for nitrate uptake by the primary producer community in He‘eia Fishpond. In this study, we investigate the nutrient uptake capacity and distribution of a community consisting of phytoplankton, microphytobenthos (MPB), and

two invasive benthic algal species common in Hawai‘i (*Gracilaria salicornia* and *Acanthophora spicifera*). We focused on nitrate, an essential nutrient for biochemical building blocks of all primary producers, including amino acids, proteins, nucleic acids, and chlorophyll (Chow & de Oliveira 2008). Although other nutrients may play an important role in shaping primary producer communities (e.g., Rabalais et al. 1996, Ringuet & Mackenzie 2005, Young 2011) , nitrate has been identified as the dominant limiting nutrient in many coastal areas (Chow & de Oliveira 2008).

He‘eia Fishpond is an ancient Hawaiian, man-made structure built for aquaculture. The semi-enclosed nature of the fishpond provides a well-defined study area within which nutrient inputs and outputs can be measured at established permanent exchange points. The fishpond is enclosed by a rock wall (kuapā), which has deliberate breaks in its continuity (mākāhā or sluice gates) that serve as exchange points or connections between fishpond water and external water sources (rivers and the ocean). The fishpond lies at the interface between tributaries of He‘eia Stream and Kāne‘ohe Bay, thus serving as an estuarine (brackish water) link between the two. At the time of project development, an existing, and growing body of high quality environmental data was available that describe the dynamics of the system during both ‘baseline’ and storm conditions (Young 2011). These data were utilized to define many of the model parameters in this study.

The study described here consists of three parts: (i) assessment of algal cover during the dry and wet seasons, (ii) evaluation of the flow-dependent specific nitrate uptake rates of the phytoplankton community, the microphytobenthos community, and the two main (invasive) benthic macroalgal species found at the site – *Gracilaria salicornia* and *Acanthophora spicifera*, and (iii) development of a one-dimensional numerical model of nitrate distribution within He‘eia Fishpond. The data collected in (i) and (ii) were used along with data previously collected at the site by Young (2011) to characterize the

anticipated differential responses in nitrate uptake amongst the three main categories of the primary-producing community (phytoplankton, microphytobenthos, and macroalgae). Due to its complement of algae, He‘eia Fishpond potentially serves as a sink for inorganic nutrients as water is transferred from upland freshwater systems, through the fishpond, before it reaches the coral reef offshore of the fishpond. The relative proportions of the algal categories and their flow-mediated and/or physiologically-mediated differential responses in nitrate uptake may therefore exert strong influence on this ‘sink’ capacity. The model allows us to assess how differences in algal cover may dictate the partitioning of inorganic nutrients between different biological components and the water column, and thus to determine what fraction of land-derived nutrients may be available for transfer out of the fishpond and onto the adjacent reef.

He‘eia Fishpond is actively managed and is currently undergoing restoration by the non-profit organization Paepae o He‘eia (POH). Their goal is to restore the loko i‘a (fishpond) to its former functionality not only as a viable food resource for the immediate community, but also as a gathering place for learning and exchange. Experiences and knowledge are shared between community members and passed on from kupuna (elders) to youth, and cultural practices are kept alive as they too are passed on to younger generations. Restoration efforts include removal of invasive species such as mangroves and *G. salicornia* (one of the target macroalgal species in this study), repair of a 50-m break in the fishpond wall, and addition of a new mākāhā. These modifications directly influence the ecology of the fishpond and its water circulation, which both have effects on nitrogen cycling at the site. For example, changes to the fishpond wall have altered the pattern and magnitude of exchange of water between the fishpond and the adjacent ocean; mangrove removal reduces shading and increases water flow in the regions closest to the kuapā, as well as flow through a previously obstructed river mākāhā,

while invasive benthic macroalgae removal potentially reveals more surface area for native species to occupy. An important goal of our work is to create a simple tool that can assist managers in determining optimal remediation practices with regard to invasive macroalgae. The marked and measured efforts to rehabilitate the fishpond landscape provide an opportunity to employ the model to analyze both the 'before' and 'after' of specific restoration events.

2. Materials & Methods

2.1. Study Site

He'eia Fishpond is located in the southern part of Kāne'ohe Bay, O'ahu, Hawai'i (21° 26' 10.07"N, 157° 48' 27.94"W) (Figure 4.1). It is a semi-enclosed estuarine (brackish water) system with a dry-stacked rock wall that defines its boundaries. There are six (6) structured openings in the wall (mākāhā) that function like sluice gates – three (3) that exchange fishpond water with the ocean and three (3) that facilitate freshwater river inputs into the fishpond. At the time of the study, there was a 50-m break in the wall (ocean break – OB), remnant of a 60+ m break created during the Keapuka Flood of 1965 (The Fishpond, http://paepaeoheeia.org/thefishpond/) (Fig. 3A). Repairs on this break to reduce the gap and form a seventh mākāhā (2.5m wide) were completed in December 2012.

Water depth across the fishpond ranges from less than 0.3 m to 1.5 m depending on bathymetry and tidal cycle (Young 2011). Mean fishpond-wide baseline salinity is 31.00 ± 0.27 S.E. PSU (n = 186), based on data from Young (2011) who designated baseline salinity conditions as those occurring during time periods characterized by rainfall less than a storm threshold of 5.08 cm rain/24 hr. Rainfall in the greater Kāne'ohe Bay watershed has been as low as 85 cm (unusually dry) to 365 cm (wettest) per year (Giambelluca et al. 1986, Ringuet & Mackenzie 2005). The fishpond is exposed to prevailing north-east trade winds. Fishpond water temperatures range from lows of below 20°C in winter months to highs up

to 34°C in summer months (Young 2011, McCoy et al. 2017). Bottom sediment type ranges from soft and silty (and thicker/deeper) near the regions receiving riverine input, to pebbly and/or sandy, with coral rubble, nearer to the ocean mākāhā (Briggs 2011, Table 1 in Briggs et al. 2013).

The dominant macroalgal species found in the fishpond are *Gracilaria salicornia* and *Acanthophora spicifera*, which are both invasive Rhodophytes (Rodgers & Cox 1999). These macroalgae grow in monospecific stands as well as in mixed-canopy patches.

2.2. Primary Producer Distribution

Primary producers were grouped into three categories, defined as (1) phytoplankton (water column), (2) macroalgae (benthic), and (3) microphytobenthos (MPB; benthic). These category designations are based upon their location relative to the water column and/or their relative size. By extension, these three categories also reflect anticipated differences in their interaction with flowing water.

For sampling purposes, the 88-acre fishpond was subdivided using a grid with 50 m x 50 m cells, and a stratified random sampling method was used to identify cells within which measurements and samples were to be taken (Figure 4.2). Biomass samples of each component were taken monthly over the course of 3 years at 8 locations, and at 32 locations once each during the Wet and Dry Seasons (Figure 4.2) as defined by Price (1983), where the Dry Season runs from May to October and the Wet Season runs from October to April.

Phytoplankton abundance was assessed using chlorophyll concentration as a proxy. One-liter water samples were taken within the top 20 cm of the water column and filtered on site through 0.7um GF/F filters. Filters were stored in the dark at -20°C until analysis. Chlorophyll a (Chl a) content of samples was

determined by acetone extraction and fluorometry following the protocols outlined by Strickland (1972) and Environmental Protection Agency Method 446.0 (1997).

Macroalgal cover (area) and biomass (gm^{-2}) were assessed using a 0.25 m^2 quadrat subdivided into twenty-five 10 cm x 10 cm blocks. The percent cover for each species was calculated based on the number of quadrat blocks occupied by the species of interest (out of the total 25 blocks). Canopy heights and substrate type (bare sediment, silty, sandy etc.) were recorded. For a given macroalgal species, samples for algal biomass were collected by carefully removing all of the algal tissue within one representative block of the quadrat. The total biomass of that species within the 0.25 m^2 quadrat was then estimated by scaling this biomass value up to correspond to the total number of blocks occupied by that species.

Microphytobenthos (MPB) distribution was assessed by sampling triplicate 5 cm^2 sediment cores within the 0.25 m^2 sampling quadrat. The top 2 cm of the cores were immediately separated using a thin plastic slicer and subsampled into separate brown (light-excluding) centrifuge tubes for storage and later chlorophyll analysis. This relatively small area was used due to preliminary sampling that revealed very high chlorophyll concentrations, requiring multiple dilutions during analysis. MPB Chl a was assessed using the same techniques for the phytoplankton with some adaptations. For example, sediment samples were sonicated to improve efficiency of chlorophyll extraction from the organism cells attached to the sediment grains. The mean chlorophyll concentration over triplicate sediment cores was taken as the representative surface sediment value for that sampling location. All samples were stored at -20°C until analysis.

2.3. Nitrate Uptake Assessments

2.3.1. Field Flume Description & Experimental Design

Six 45-minute long flume experiments were conducted across the fishpond to assess the biological response of a naturally occurring community of primary producers to various nitrate flux regimes. A stratified random sampling method was employed to select experiment locations (Figure 4.3A). The flume, constructed of clear plexiglass® to allow light penetration, extends about 5 cm into the sediment and encloses a 2.6 m^2 area of the natural benthic community and the overlying water column. When sealed at its base, the flume facilitates control of both nutrient concentration and water flow, and thus nutrient flux, using a trolling motor (Figure 4.3B). A 12V battery was used to power the trolling motor. Experiments were conducted under unidirectional flow. The motor was connected to a flow controller (Linear Power Systems, Clearwater, Florida USA), its propeller set at mid-water column height. Flow straighteners (egg crate lighting panels) were used to organize the turbulent flow, particularly at the bends in the flume, such that there was ordered flow across the 'working section' of the flume (See Figure 4.3B). The working section is the designated area of the flume within which consistent ordered flow is established. It is within this working section that tissue and sediment samples were taken. Following Cornelisen & Thomas (2004), experiments were run using a 50% ^{15}N-nitrate labeled 3 µM nitrate nutrient spike under unidirectional flow rates ranging from 0.016 to 0.265 ms^{-1}. This range of water flow was selected to represent flow at quiescent regions of the fishpond as well as at higher flow areas in the vicinity of the mākāhā.

2.3.2. Hydrodynamic Characterization

Hydrodynamic parameters were measured using a Nortek Vectrino acoustic Doppler Velocimeter (ADV) fitted with a field probe. The ADV probe was oriented down-looking, affixed to a stationary arm whose height could be adjusted to facilitate data collection at multiple heights and develop a vertical velocity

profile. Profiles were measured at the center of the flume working area, and extended from the surface of the water column down through the algal canopy to within no less than 2 cm of the sediment-water interface (SWI).

At each height, data were acquired for five (5) minutes at a sampling rate of 25 Hz in the stream-wise (*u*), cross stream (*v*), and vertical (*w*) directions. Sampling volume and transmit length were set to 7 mm and 1.8 mm, respectively, and data was collected for five (5) minutes at each profile height. Due to the relatively short duration of the experiments, and our decision to have a longer sampling period in order to capture more information about the turbulent structure, vertical profile resolution was limited to 3 to 10 heights depending upon water depth and canopy height.

ADV output was processed using MATLAB (R2011b; The MathWorks, Inc.®; Matlab code developed by Oscar Guadayol o Roig (O. Guadayol o Roig pers. comm.)). Spikes (anomalous peaks in the data) were removed using the 3D phase-space thresholding technique outlined by Goring & Nikora (2002) and Wahl (2003), and as applied by Kregting et al. (2013). Velocity components with beam correlations of <60%, or below a threshold signal-to-noise (SNR) of 15 dB, were removed (McLelland & Nicholas 2000). The number of spurious data points excluded was small (0.04%), and linear interpolations were made to bridge the gaps left by excluded data points.

To ensure that the data accurately represented flow along the stream-wise/cross-stream axes, empirical orthogonal function (EOF) analysis was used to correct slight misalignments of the probe during data collection. In this analysis, horizontal dimensions are re-oriented such that they are orthogonal to the dominant current. This treatment assumes that no changes in the orientation of the probe occurred during data collection. All calculations from this point forward utilized parameters in the stream-wise (*u*) direction only, as this was defined as the principal axis of the horizontal current.

Flow parameters were calculated following methods in Stiansen & Sundby (2001) and Kregting et al. (2013). The velocity signal was decomposed into a low frequency mean velocity (*U*), a wave component (u_w), a turbulent component (u'), and an instrumental white noise component (u_{noise}):

$$u = U + u_w + u' + u_{noise} \quad \text{Eq. 1}$$

The various components of the total signal were estimated by integrating different regions of the power density spectra of the signals. The white noise component of the signal was identified using the flat segment at the highest frequencies in the spectra, while the inertial subrange was identified as the segment of the density spectrum that followed a - $^5/_3$ slope, after subtraction of white noise (Kregting et al. 2013; Chapter 2, this dissertation). By integrating under the inertial subrange region of the spectrum, the turbulent component of the signal was determined. The wave component was estimated by integrating the peak (spike in energy density) that appears in the wave frequency. Bulk velocity (U_b) was estimated as the depth-averaged velocity in the dominant direction of flow ($\bar{U}$).

2.3.3. Nitrate Uptake Rates

For each experiment run, the base of the flume was sealed to prevent exchange with ambient water and dilution of the nutrient spike within the flume, thus facilitating a more accurate measure of the impact of the biological community enclosed within. To achieve the experimental 3 µM ^{15}N-lableled target nitrate (NO_3^-) concentration in the flume, a pre-determined volume of a 50% ^{15}N 2.0 x10^4 µM working solution of sodium nitrate ($Na^{15}NO_3$) was added. This volume was calculated on site based on the total volume of water within the flume and, once added, the trolling motor was started at a low speed and allowed to run for five minutes to ensure a final well-mixed solution before initiating sample collection. The beginning nitrate concentrations fluctuated between 2.9 to 3.7 µM due to mixing and background nitrate concentrations.

Total community nitrate uptake rates were determined from the decline in nitrate concentration of the water within the flume over the experiment period (Cornelisen & Thomas 2002). Water samples for nutrient analysis were taken every five (5) minutes over the 45-minute experimental run. Duplicate samples were filtered through a 0.2 µm nylon syringe filter into 30 ml HDPE bottles. Samples were stored at -80°C until analysis. Nitrate concentrations were determined by the SOEST Laboratory for Analytical Biogeochemistry (S-LAB) at the University of Hawai'i, following the protocols outlined by Seal Analytical (*http://www.soest.hawaii.edu/S-LAB/*).

A first-order rate constant (*k*), which describes the decline in nitrate concentration in the flume over time, was determined from the slope of the least-square regression of the natural log of concentration (*C*) versus time (*t*) for each experiment:

$$C = -k \frac{dC}{dt} \quad (1)$$

This analysis is consistent with prior work (Bilger & Atkinson 1995, Thomas & Atkinson 1997, Cornelisen & Thomas 2002). Tissue samples for isotopic analysis were taken 15 minutes after initiation of the experiment. We used the regression of the decrease in concentration over the entire experiment period (45 minutes), and assumed that the rate of uptake within the first 15 minutes is equivalent to that which occurred over the 45-minute experimental time course.

An estimate of the total nitrate taken up by the community over the experimental period was also calculated using the change in concentration over time. An uptake rate constant for each experimental run was determined using the equation

$$S = k \times \frac{Vol}{A} \quad (2)$$

where *S* is the uptake rate constant (in units of ms^{-1}) for the entire algal community enclosed within the flume. Following Cornelisen & Thomas (2002), the first order rate constant, *k,* is normalized to the volume of water in the flume (*Vol*) and the area of exposed benthos within the flume (*A*). S can then be multiplied by concentration of the nutrient to obtain specific nutrient uptake rates (in moles NO_3 m^{-2} s^{-1}).

Uptake rates for the various algal components of the primary producing community were determined by tracking incorporation of the ^{15}N-labeled nitrate from the water column into the algal tissues. Representative samples from each component were taken prior to experiments, to determine the ambient (background) isotopic ratios. Samples for experimental isotope analysis were collected at the 0-minute and 15-minute timepoints of each experimental run. Previous work by Cornelisen and Thomas (personal communication) has shown that 15 minutes is ample time for sufficient labeled nitrogen to be incorporated into the tissues to assess nitrogen uptake rates. Phytoplankton were retrieved by filtering a 250 ml aliquot of flume water through combusted and pre-weighed 25 mm GF/F filters (pore size 0.7 µm), and MPB collection was as previously described for algal surveys – using syringe push cores and sub-sampling the top 2 cm of the core. Samples of each macroalgal species present within the working section of the flume were also taken. For each species, samples were combined from at least three locations within the working section of the flume. At each of these locations, the entire height of the alga was collected to ensure that the sample captured the net effect of an anticipated gradient in nitrate uptake along the height of the alga (i.e., a vertically integrated measure of uptake activity). Collecting at multiple locations within the working section of the flume also ensures that the samples were representative of the enclosed population of each algal component. All samples were dried at 60°C until a constant weight was achieved, then stored in a desiccator until analysis. Both macroalgal tissue and sediment (MPB) samples were ground to a fine powder and homogenized using an amalgamator (Wig-L-

Bug by Dentsply®). Sediment samples were acidified to remove carbonates from the sample. Isotope analysis was carried out by the SOEST Biogeochemical Stable Isotope Facility (*http://www.soest.hawaii.edu/GG/isotope_biogeochem/*).

Specific uptake rates (V) for each component of the community, in units of (g N removed) (g N tissue)$^{-1}$, were calculated as

$$V = \left(\frac{da_s}{dt}\right) / \left(a_w - a_s\right) \quad (4)$$

where a_s is the atom% ^{15}N in the component tissue, a_w is the atom% ^{15}N in the enriched substrate (i.e. the water), and dt is the time over which uptake took place (Cornelisen & Thomas 2006). Atom% ^{15}N of the enriched water (a_w) was based on the amount of 50 atom% $^{15}NO_3^-$ added and background DIN concentrations. da_s is the difference in atom% ^{15}N between the enriched sample at the experimental sampling point and the ambient sample collected prior to the start of the experiment. This equation for V assumes that the atom% ^{15}N source pool did not change over the course of the experiment. A possible source of error is dilution of ^{15}N in the source pool, which would result in an underestimation of nitrate uptake rates (Laws et al. 1984). Since these experiments are relatively short, the concentration of the nitrate spike is high, and atom% ^{15}N 50%, any dilution that occurs is likely minimal.

A series of normalizations of V were made to account for nitrogen content of tissues and cell abundance, in order to get more accurate uptake rates, ρ, that could be compared between experiments. For all three primary producer categories (macroalgae, phytoplankton, and MPB), V was normalized to the nitrogen concentration (%N) of the tissue. For phytoplankton, additional normalizations to Chl *a* concentration were made (to account for the fraction of the material actually participating in nitrate uptake), resulting in a further updated uptake rate ($\rho_{Chl} = \rho$ / [Chl *a*]) in units of (g

N removed) (µg Chl *a*)$^{-1}$ s^{-1}. Finally, to account for any change in uptake rate due to the first-order decline in nutrient concentration in the water column within the flume, *ρ* was adjusted by applying a correction term, alpha (α):

$$\alpha = e^{-kt} \quad (5)$$

where *k* and *t* are the first-order rate constant for decline in nitrate concentration and time, respectively. The normalized and adjusted final uptake rates represent those for the water column at the beginning of the experiments, and are the values used to assess the effect of water flow on nitrate uptake by the individual algal components.

The relative contribution of the three algal categories to total nutrient uptake over the course of each experiment was assessed by multiplying the normalized uptake rate (*ρ*) by its total biomass in the flume (*ρ x g dry wt)*, yielding a measure of total nitrate removed by each component (in *g N s^{-1}*). For phytoplankton, the total amount of ***N*** removed was based on *ρ*, the concentration of plankton (*Chl a*), and the volume of water in the flume. Biomass (measured in grams) was used to track macroalgal abundance.

2.4. Nitrate Distribution Model

2.4.1. Model Goals/Objectives

The goal of the model developed for this project was to simulate and predict nitrate distribution in He'eia fishpond, using empirical data including algal cover, nitrate concentration ranges, water flow rates, and specific nitrate uptake rates to inform and parameterize the model. The response of the naturally occurring primary producer community to changes in nitrate flux was evaluated through model simulations initialized with varying suites of conditions that were selected and parameterized based upon known environmental conditions (e.g., Dry vs. Wet Season algal cover). Changes over time in the

relative size of the nitrate reservoirs (e.g., nitrate in the water column, nitrate bound in primary-producer biological tissues) was assessed under different starting conditions – Dry Season, Wet Season, 100% microphytobenthos cover, and storm-induced nitrate pulses.

2.4.2. Model Schematic

Nitrate-nitrogen in the fishpond exists in multiple reservoirs which are here defined as: nitrate-nitrogen in the water column (***N***), phytoplankton-bound nitrate-nitrogen (***P***), *Gracilaria salicornia*-bound nitrate-nitrogen (***G***), *Acanthophora spicifera*-bound nitrate nitrogen (***A***), and microphytobenthos-bound nitrate-nitrogen (***M***) (Table 4.1). This is consistent with the primary producer categorization in the previously described algal cover (Section 2.2) and field flume nitrate uptake assessments (Section 2.3). The nitrate-nitrogen content of the reservoirs is quantified in units of μg N m^{-3}.

Nitrogen is transferred between the biotic reservoirs and the water column via nitrate uptake and mortality (Figure 4.4). Uptake refers to the removal of inorganic nitrogen (in the form of NO_3^-) from the water column and incorporation into algal tissues. Uptake rates are modulated by the time of day, such that uptake only takes place during daylight hours. In addition, because the benthic algae exhibit flow-mediated nitrate uptake, nitrate uptake for the benthic algae is also modified by water flow speeds. Mortality rates describe the decrease in algal abundance and the transfer of nitrate-nitrogen from the biological components back to the inorganic nitrogen water column reservoir (***N***). Mortality encompasses natural death, disease or viral death, grazing, and sloppy feeding via grazing. We combine these various processes into a single general mortality term because data to parameterize these individual loss (or sink) processes in the fishpond are unavailable.

2.4.3. Governing Equations

Based on the factors, described above, that regulate nitrate uptake, the following Governing Equations were developed. These equations describe how the value for each parameter at a given point in time (*t*) was calculated for each model cell. The nomenclature used in the governing equations is defined in the following list:

β: 'growth' rate (s^{-1})

γ: mortality rate (s^{-1})

ρ: nitrate uptake rate (s^{-1})

k: half saturation constant (µg N m^{-3})

$\overline{N}$: mean nitrate concentration (µg N m^{-3})

U_b: bulk flow (ms^{-1})

The following subscripts identify the four nitrogen reservoirs included in the model:

p: phytoplankton (***P***)

g: *Gracilaria salicornia* (***G***)

a: *Acanthophora spicifera* (***A***)

m: microphytobenthos (***M***)

For phytoplankton (***P***):

$$P(t) + P_{advected} = P_{existing} + P_{added\ via\ growth} - P_{removed\ via\ mortality} + P_{diffused} \quad (1)$$

$$\frac{dP}{dt} + U_b \nabla P(t) = \beta_p * P(t) - \gamma_p * P(t) + \nabla^2 P(t) \quad (1.1)$$

$$\beta_p = \frac{\rho_p * N(t)}{k_p + N(t)} \quad (1.2)$$

$$\gamma_p = -\frac{\rho_p * \overline{N}}{k_p + \overline{N}} P(t) \quad (1.3)$$

$$\frac{dP}{dt} + U_b \nabla P(t) = \frac{\rho_p * N(t)}{k_p + N(t)} P(t) - \frac{\rho_p * \overline{N}}{k_p + \overline{N}} P(t) + \nabla^2 P(t) \quad (1.4)$$

For *Gracilaria salicornia* (***G***):

$$G(t) = G_{existing} + G_{added\ via\ growth} \quad (2)$$

$$\frac{dG}{dt} = \beta_g * G(t) \quad (2.1)$$

$$\beta_g = \frac{\rho_g * N(t)}{k_g + N(t)} \quad (2.2)$$

$$\frac{dG}{dt} = \frac{\rho_g * N(t)}{k_g + N(t)} G(t) \quad (2.3)$$

For *Acanthophora spicifera* (***A***):

$$A(t) = A_{existing} + A_{added\ via\ growth} \quad (3)$$

$$\frac{dA}{dt} = \beta_a * A(t) \quad (3.1)$$

$$\beta_a = \frac{\rho_a * N(t)}{k_a + N(t)} \quad (3.2)$$

$$\frac{dA}{dt} = \frac{\rho_a * N(t)}{k_a + N(t)} A(t) \quad (3.3)$$

For microphytobenthos (***M***):

$$M(t) = M_{existing} + M_{added\ via\ growth} \quad (4)$$

$$\frac{dM}{dt} = \beta_m * M(t) \quad (4.1)$$

$$\beta_m = \frac{\rho_m * N(t)}{k_m + N(t)} \quad (4.2)$$

$$\frac{dM}{dt} = \frac{\rho_m * N(t)}{k_m + N(t)} M(t) \quad (4.3)$$

Finally, the overall reaction for nitrate in the water column (N) is given by:

$$N(t) + N_{advected} = N_{existing} + N_{added\ via\ algal\ mortality} - N_{removed\ via\ algal\ uptake} + N_{diffused} \quad (5)$$

$$\frac{dN}{dt} = -\frac{dP}{dt} - \frac{dG}{dt} - \frac{dA}{dt} - \frac{dM}{dt} \quad (5.1)$$

2.4.4. Variables and Parameters

The variables and parameters used in this model were bounded by empirical data collected both in the current study and by other studies in the same and/or similar systems. This information is summarized in Appendix VI.

Dry and Wet Season algal distributions were based upon algal cover surveys completed in the first part of this investigation (Section 2.2), and nitrate concentration ranges were set based upon mean non-storm and post-storm conditions assessed by Young (2011). Storm events were defined, following Ringuet & Mackenzie (2005), Fagan & Mackenzie (2007), and Ostrander et al. (2008), as periods with rainfall ≥ 5.1 cm over the watershed within in a 24-hour period.

Expressions for nitrate uptake are structured to mirror Monod kinetics (which describe the growth of microorganisms) and describe the relationship between nitrate uptake rate and substrate availability. Monod kinetics was selected to model algal 'growth' (as ***N*** removal from water column) because it defines an upper bound to growth, and also limits production at constrained/low substrate concentrations. The Monod equation is:

$$\mu = \mu_{max} \frac{X}{K_X + S} \quad (6)$$

where μ is the specific growth rate, μ_{max} is the maximum growth rate, X is the substrate concentration and K_X is the half-saturation constant (substrate concentration at which $\mu = ½\ \mu_{max}$). Nitrate uptake rates for the algal components in this study have not previously been described and, as such, we use growth

as a proxy for nitrate uptake. For each algal component, we determined the half-saturation constant by substituting typical algal growth rates for μ and maximum nitrate uptake rates for μ_{max}. For these calculations, *X* was set as the mean (non-storm) nitrate concentration for the fishpond. Typical phytoplankton growth rates were obtained from studies conducted in Kāne'ohe Bay (Redalje & Laws 1981, Landry et al. 1984, Laws et al. 1984, Selph et al. 2016), while typical macroalgal growth rates were obtained from various field and laboratory studies (Larned 1998, Smith et al. 2002, 2004). Microphytobenthos (***M***) was the exception for which a literature value of growth rates could not be found. In lieu of published values, typical ***M*** growth rate was assumed to have a doubling rate related to that of phytoplankton in the system. Maximum growth rates were determined from the field flume experiments and were calculated for a mean flow rate.

Once the half-saturation constants were defined, one more modification to the Monod equation was required to yield the final expressions used for nitrate uptake in the model. For ***P***, the isotope-determined nitrate uptake rate was used *as is* for μ_{max}. For the benthic components (***G***, ***A***, and ***M***), however, nitrate uptake is additionally modulated by water flow rates. As such, the normalized flow-mediated nitrate uptake expression, rho (ρ), scaled by estimates of the typical growth rates based on data obtained from the literature, was substituted for μ_{max}. Nitrate uptake is measured in units of (μg N removed) (μg tissue)$^{-1}$ s^{-1} (or just s^{-1}).

It is important to consider several mitigating factors concerning the published growth rate data used, as described above, to obtain estimates of ***N***-uptake. Phytoplankton growth studies conducted in the region (Kāne'ohe bay) took place over only a few hours during daylight, and therefore do not provide an integrated representation of growth. For this reason, and because of the high growth rates that phytoplankton may exhibit, and also because the model simulation run time spans several days (8 days),

it was important to include a 'mortality' term for phytoplankton. The mortality term is applied based on Monod kinetics, using typical per day mortality rates (Obayashi & Tanoue 2002). ***P*** mortality serves to adjust ***P*** uptake rates during the nighttime hours, such that the net effect mimics processes such as grazing of phytoplankton at night. Similar adjustments for ***G***, ***A***, and ***M*** were not put in place. Exclusion of a mortality term for ***G***, ***A***, and ***M*** is justified because in the studies from which typical growth rates were obtained, macroalgal growth was assessed over several days in the natural environment under conditions that did not exclude grazers. These growth rates thus incorporated various loss processes (senescence, grazing, breakage) resulting in net measures of growth, and by extension nitrate uptake.

N input and removal at the points of water exchange between the fishpond and external sources (i.e., at the mākāhā) were defined as follows. Nitrate concentrations of sources of N-input at the river and the ocean mākāhā were modeled as a constant low-level background input (0.21 µM and 0.16 µM, respectively). To simulate increased runoff, and thus increased nitrate input after a storm (i.e., a nitrate pulse), river mākāhā input was increased to 40.19 µM nitrate for a 0.5-day period. The nitrate level during the applied storm pulse is based on measurements taken over the year-long monitoring study in He'eia Fishpond by Young (2011), as well as similar data collected for storm input into Kāne'ohe Bay by De Carlo et al. (2007).

Water velocity in He'eia fishpond has been assessed at the mākāhā and other sites within the fishpond wall as part of multiple studies (Young 2011; Timmerman et al., in prep; Jerolman, personal communication). While a full circulation model is unavailable, by using these existing point location velocity data and applying wind forcing, we developed a circulation scheme for the site. Once applied, these velocity fields were used to model advection and diffusion of both ***N*** and ***P***. Speeds calculated from velocity values were used to modify nitrate uptake rates of ***G***, ***A***, and ***M***.

2.4.5. Model Validation

'Null' simulations, in which algal cover was absent, were run to validate the model. Under these conditions, the only loss of ***N*** would be due to diffusion at the model boundaries (i.e. the fishpond wall). Null simulations were run for both baseline ***N*** inputs and ***N*** inputs under storm conditions.

The model is sensitive to the size of the time step (*dt*) and to diffusivity (*At*). As such, a semi-implicit integration was used to facilitate an increase in *dt*, to improve model efficiency, while maintaining the stability of the model. This means that the values of model variables were calculated and updated based both on their current values and their values at the next point in time.

Certain features of He'eia fishpond, such as nutrient concentrations and distribution (Young 2011) and discharge at the mākāhā (Young 2011, Timmerman et al. in prep) have been extensively studied, while other features, including algal cover and circulation, remain undocumented. Given the gaps in the available knowledge base about this site, it was necessary to make a number of assumptions about various parameters. Critical assumptions made in order to parameterize the model are described here, as are some of the limitations implicit in application of these assumptions. The hydrodynamic regime applied in the model was developed using tidal forcing to spin up to a steady state pattern of flow. The data used to inform the spin-up, however, was of low spatial resolution, and data points were clustered at the mākāhā. A more evenly distributed sampling of water velocity at higher resolution would facilitate a more accurate re-creation of the flow patterns within the fishpond than the one achieved here. The seasonal algal cover used in the simulations was measured at single points in time during the Dry and Wet Seasons, essentially providing snapshots of algal cover. It was subsequently determined that differences between the two seasons can be variable and, as such, the distinction between the two is not always clear. Higher resolution year-round sampling would provide a better description of algal

coverage and any seasonal patterns that may exist. Additionally, the two snapshots of algal cover were taken at timepoints close to each other, and so may not represent fully developed algal communities that are representative of each season. Finally, while the model calculates changes in biomass of the algal components, it does not model any increases or decreases in algal coverage area. The intersection of flow rate and algal biomass determines nitrate uptake, and so changes in algal cover as model time progresses could have an impact on model output.

2.4.6. Simulations and Rationale

Model simulations were curated based upon existing knowledge about environmental conditions of the fishpond, our interest in nutrient cycling as it pertains to projected nutrient conditions and climate change, and also based upon the future management goals of the caretakers of the *loko* (fishpond). The simulations explored in this investigation are summarized in Table 4.2. The simulations are categorized as either Dry or Wet Season simulations, which refer to their respective 'typical' algal cover complements of ***P***, ***G***, ***A***, and ***M***. The algal cover makeup is then exposed to two nitrate regimes: baseline (background mean nitrate concentration of 0.18 µM) and pulse (40.19 µM nitrate point source introduction at the river mākāhā). The Dry Season (DS) and Wet Season (WS) simulations are intended to establish how nitrate is cycled within the fishpond under average algal cover conditions represented by these two characteristic seasons.

The managers of He'eia Fishpond, Paepae o He'eia, seek to return the fishpond to the ecology that existed prior to non-native algal invasion. According to historical texts and verbal communication from elders in the area, the original ecology of the fishpond did not include macroalgal species. Instead, herbivorous fish kept in the fishpond fed on microalgae, keeping levels low. This historical information

about the pre-invasion algal ecology is the rationale for including 100% microphytobenthos (***M***) cover simulations, both for the Dry and Wet Seasons.

The four algal cover scenarios (DS, WS, 100% M dry, and 100% M wet) were run under baseline nitrate conditions and under a nitrate pulse regime that mimics a post-storm nutrient pulse from land-based sources. The nitrate concentration selected for the storm nutrient pulse is based upon data from Young (2011), and was applied for 0.5 days.

Null simulations (simulation #0 and 0P) were used to determine the loss of ***N*** at the fishpond boundaries due to diffusion. This value was then used to adjust the ***N*** biomass at the end of the model run, to prevent overestimation of ***N*** uptake by the algae, and to accurately assess the effect of the algae present on nitrate drawdown. The effects of the four algal complements on the total drawdown of nitrate over the model 8-day run time (simulations #1-4) were compared, and the ability of these algal complements to process sustained high nutrient concentrations, such as those after a rain or storm event (simulations #1P-4P) was assessed.

3. Results

3.1. Primary Producer Distribution

Distinct differences in overall algal cover (area, m^2) were observed between the Dry and Wet Season. These seasonal shifts emerged as a result of the different responses of the individual algal components to the change in season (Figure 4.5; Table 4.3). For example, *G. salicornia* (***G***) coverage area was greater in the Wet Season relative to the Dry Season, while areal coverage of *A. spicifera* (***A***) and microphytobenthos (***M***) was lower in the Wet Season relative to the Dry Season. Of all four algal components, ***M*** underwent the largest seasonal change in % cover (-78%). Considering first the monospecific stands of the algae (i.e. where either ***G***, ***A***, or ***M*** is the dominant entity), the extent of ***G***

coverage increases from Dry Season to Wet Season by 68%, while minimal decrease in the extent of ***A*** coverage is observed from Dry Season to Wet Season (3%).

In contrast, when ***G*** located within regions of mixed algal coverage ($\boldsymbol{G_{mixed}}$) is included into the analysis, while total ***G*** coverage, $\boldsymbol{G_{total}}$ (i.e., $\boldsymbol{G_{monospecific}}$ + $\boldsymbol{G_{mixed}}$) still increases; it does so by a much smaller margin (1.7%); 40 times less than for ***G*** stands. For ***A,*** however, the total coverage area, $\boldsymbol{A_{total}}$ (i.e., $\boldsymbol{A_{monospecific}}$ + $\boldsymbol{A_{mixed}}$) decreases by a larger margin (24%) than for $\boldsymbol{A_{monospecific}}$; ~ 8 times more than for the monospecific ***A*** stands.

3.2. Nitrate Uptake Assessments

3.2.1. Hydrodynamic Characterization

Vertical profiles of velocity confirmed that flow within the working area of the flume was highly unidirectional and that flow velocity was dampened within the algal canopies (Figure 4.6; see also Chapter 2). Bulk flow, U_b, ranged from 0.016 to 0.265 ms^{-1} for the six flume experiments (Table 4.4).

3.2.2. Nitrate Uptake Rates

For all 6 experiments, nitrate concentration decreased by 0.41 µM, on average, over the course of the 45-minute flume experiment. For all but one experiment, this reduction in nitrate concentration represents a significant first-order decline in nitrate concentration of the flume water (Figure 4.7, Table 4.4).

A general trend of increasing uptake rate constant, *S*, was observed with increasing bulk flow, U_b (Figure 4.8A). This correlation is strengthened (R^2 = 0.3299) when the uptake rate constant is normalized to the percent area covered by the macroalgae (Figure 4.8B). The positive relationship between nitrate uptake and water flow rate is consistent with our expectations based upon the current literature in the field (Thomas & Atkinson 1997, Falter & Sansone 2000, Hurd 2000, Cornelisen & Thomas 2006).

All three benthic primary producer components exhibited flow-mediated nitrate uptake, with uptake rates increasing with bulk flow (Figure 4.9A-C). As anticipated, phytoplankton nitrate uptake did not demonstrate any relationship with water flow rates (Figure 4.9D). Of the three benthic algal components, *A. spicifera* had the steepest slope and thus the highest flow-mediated uptake rate, followed by *G. salicornia* and then microphytobenthos, which exhibited the weakest response to flow (Figure 4.9E). The relative strengths of uptake response to flow translate into differences in nitrate uptake capacity, with *A. spicifera* accounting for at least 75% of NO_3^- uptake capacity (Figure 4.10). Results of the flume experiments, the corresponding enclosed algal cover, and water flow rates are summarized in Table 4.4. Additional details about individual experiment outcomes are available in Appendix V!.

3.3. Nitrate Distribution Model

3.3.1. Overall Water Column Nitrate (N) Drawdown

For all model simulations, total nitrate across the fishpond was drawn down by at least 74% (Figure 4.11). Under each model-specified nutrient regime, significantly more drawdown was observed for Wet Season distributions of algae than for Dry Season distributions (T-Value = -15.42; P-Value = 0.001). By pooling the responses to nutrient treatments (i.e. baseline nitrate conditions and pulse nitrate conditions) and comparing cover type (100% M cover versus 3-benthic algae combinations), it became clear that algal type had an impact on ***N*** drawdown. When fishpond algal cover is restricted to microphytobenthos exclusively, regardless of season, ***N*** drawdown was significantly lower than that observed for the typical Dry or Wet Season (multi-species) algal cover (T-Value = 264.56, P-Value < 0.0005).

3.3.2. Dry Season Baseline vs. Wet Season Baseline

Considering typical Dry and Wet Season algal cover under the baseline nutrient (nitrate) regime, even though mean ***P*** uptake rates throughout the 8-day experiment period are orders of magnitude higher than that of ***G***, ***G*** is responsible for the largest proportion of nitrate removed from the water column (Figure 4.12). This holds true for both Dry and Wet Season cover (92% and 87% respectively). Despite the fact that ***G*** biomass in the Wet Season is higher than in the Dry Season, ***N*** drawdown by ***G*** during the Wet Season is lower than during the Dry Season. While not readily resolved from the bar charts (see associated table for values), the disconnect between biomass coverage and uptake rate is also observed for ***A***. Additionally, while mean ***A*** nitrate uptake rates are only marginally lower than those observed for ***G***, ***A*** has negligible impact (1.52%) on the total ***N*** removed from the water column compared to ***G*** (92%) for the Dry Season; a similar pattern is observed for the Wet Season. During the Wet Season, ***G*** and ***A*** uptake account for 87% and 3%, respectively, of the total ***N*** removed. ***M*** remains a minor player with respect to both biomass and total ***N*** removed (Figure 4.12).

3.3.3. 100% Dry Season M Baseline vs. 100% Wet Season M Baseline

In the absence of macroalgae, when microphytobenthos (***M***) is the sole benthic primary producer in the fishpond (Figure 4.13), mean ***P*** and ***M*** biomass across the fishpond was higher during the Wet Season than the Dry Season. Within each season, only small differences between ***P*** and ***M*** mean biomass were observed: ***M*** is 4% higher than ***P*** during the Dry Season and 3% lower than ***P*** during the Wet Season. These differences are small enough that the mean biomass for each season can be considered as similar. During the Dry Season, however, even though mean nitrate uptake rate for ***P*** was 5 orders of magnitude higher than that of ***M***, ***M*** removed 48% more ***N*** from the water column than ***P***. For the Wet Season simulation, mean ***M*** uptake remains orders of magnitude lower than that of ***P***, however, ***M*** removed

14% less ***N*** from the water column than ***P***. The mean ***N*** uptake rate for the Wet Season ***M*** was lower than the mean ***N*** uptake rate during the Dry Season.

3.3.4. Dry Season Baseline vs. 100% M Dry Baseline

Under baseline nitrate conditions, the quantity of ***N*** drawn down by 100% ***M*** cover was 2% less than that drawn down by the typical Dry Season algal cover, which includes ***G*** and ***A*** as well as ***M***. Overall nitrate drawdown under these two conditions, ***M***-only versus the 3-component benthic algal cover, resulted in a 74% and 76% decrease, respectively, from the starting nitrate load (Figure 4.14(i)). The same pattern is observed for the Wet season (Figure 4.14(ii)).

3.3.5. Dry Season Baseline vs. Dry Season Pulse

Under nitrate pulse conditions, ***P*** was the only algal component to exhibit a substantial response to the increased nutrient input (Figure 4.15). Mean ***P*** biomass increased almost 1.6-fold, while mean ***G*** biomass remained unchanged, ***A*** increased by <1%, and ***M*** decreased by <1% (Figure 4.15). The increase in ***P*** biomass corresponds to an 8.2-fold increase in the amount of nitrogen removed by ***P***. Despite the fact that total ***N*** removed by ***G*** exceeded that of ***P*** under nutrient pulse conditions by 83%, the quantity of ***N*** removed by ***G*** was unaltered by the nutrient pulse, and was indistinguishable from the quantity of ***N***-drawdown by ***G*** under the baseline nutrient regime. While ***A*** underwent only a marginal increase in both mean biomass (<1%) and mean uptake rate (< 1%) between the two nutrient regimes, under the nitrate pulse regime, ***A*** removed 83% more ***N*** from the water column than under baseline nitrate conditions. Despite the observed increase in ***N***-removal, however, the quantity of ***N*** removed by ***A*** remains only a fraction of the amount of ***N*** removed by ***P*** and ***G*** (5% and 3% respectively). It is interesting, to speculate how the model output might change, specifically with respect to the total ***N*** removed by ***G***, if velocity at

the mākāhā was increased to simulate the often-elevated discharge associated with post-storm river discharge.

Note: The pattern observed for Wet Season algal cover was similar to that observed for the Dry Season. Mean ***G*** biomass and the amount of ***N*** removed by ***G*** remained unchanged in response to the nutrient pulse, while mean ***A*** biomass increased by <1%, and mean ***M*** biomass decreased by <1%.

3.3.6. 100% Dry Season M Pulse vs. 100% Wet Season M Pulse

Under nitrate pulse conditions, mean Wet Season ***P*** and ***M*** biomass are higher than mean Dry Season biomass (Figure 4.16). This seasonal pattern is consistent with that observed under baseline conditions (Figure 4.13), however overall biomass is higher under pulse treatments. Unlike the baseline treatment, the difference in mean biomass between the Dry and Wet Seasons does not correspond to higher ***N*** removed under Wet Season pulse conditions. In fact, ***P*** removes 11% less during the Wet Season pulse conditions compared to the quantity removed under Dry Season pulse conditions, while ***M*** removes almost 5% more during the Wet Season pulse regime than during the Dry Season pulse regime.

3.3.7. Dry Season – 0.5-day pulse vs. 1-day pulse vs. 2-day pulse

All algal components of the system (***P***, ***G***, ***A***, and ***M***) displayed a response in both mean biomass and ***N***-removal as a function of the length of the nitrate pulse (Figure 4.17). The quantity of nitrate introduced into the fishpond due to a pulse lasting 24 hours compared to one lasting 12 hours corresponded to increases in mean biomass and total ***N*** removed by all components. No additional effect was observed when pulse duration was increased to 48 hours relative to the effect observed for a pulse of duration 24 hours.

The time series data (Figure 4.18) reveal that even before a nitrate pulse was introduced, ***N*** was already substantially drawn down from its initial value to a level of about 1.4 $x10^{-6}$ µg N, by t = 0.594 days. Once the nitrate pulse was introduced at t = 1 day, the algae responded by increasing biomass, and ***N*** was again rapidly drawn down to a new low (1.825 $x10^{-6}$ µg N) by t = 1.5 days, and ultimately drawn down to a level of 1.5 $x10^{-6}$ µg N (comparable to the pre-pulse minimum). After 1.5 days, the level of N cycles about this low value. The time taken to reduce the pulsed nutrient input is approximately equal to the temporal duration of the pulse itself.

4. Discussion

4.1. Primary Producer Distribution

Coverage area as a function of seasonal variation is not coherent across all benthic components. In other words, there is not a consistent unidirectional change in percent (%) algal coverage of the three benthic algal components as a function of season. The lack of coherence suggests that morphological and/or physiological differences between the algae may be more important than their common habitat (the benthos) in determining their response to seasonal changes in the environment.

One factor that may underlie the observed decrease in ***M*** coverage during the Wet Season (Figure 4.5, Table 4.3) is increased turbulence in the water column due to winter storms, a condition that makes resuspension of ***M*** into water column more likely. In fact, the resuspension of mats of microphytobenthos in the fishpond water column is a fairly common occurrence during the Wet Season (personal observation). A second contributing factor may be competition from benthic macroalgae.

With the shift from the Dry Season to the Wet Season, the expansion of the area covered by ***G***, in concert with the retreat of ***A*** coverage area from the Dry to the Wet Seasons, suggests that *G. salic*ornia

is more freshwater tolerant than *Acanthophora spicifera.* This is consistent with findings of the NOAA-DAR-LAS Project report by Ruttenberg et al (2011), who observed an increase in monospecific stands of *G. salicornia* across Kāne'ohe Bay at the end of the Wet Season. However, when one considers the areal distribution of the two benthic macroalgae with more context, such as their location relative to environmental parameters, the picture is more complex than simply tolerance of freshwater input driving dominance of one species over the other. The monospecific patches of ***A*** occur immediately proximal to the river mākāhā, and another monospecific patch of ***A*** occurs in the extreme southern portion of the fishpond, an area that shows signs of groundwater input (Young 2011). These latter observations would lead one to believe that in fact ***A*** is the macroalgal species that is more freshwater tolerant, despite the fact that pond-wide, the areal extent of ***G*** increases during the wet season while the total area covered by ***A*** contracts. One possibility is that water temperature, rather than salinity, is the driving factor dictating which species of benthic macroalgae dominates. The mean temperature of the fishpond is colder during the wet season than during the dry season. Pinpointing which environmental parameter might exert control over species shifts in macroalgal cover will require additional work, including experimental work determining growth rate and proliferation under different salinity and temperature conditions. The central area of the fishpond, where salinity levels are intermediate between end-member extremes (Young 2011), is the region where mixed canopy algal stands are observed (i.e., where ***A*** and ***G*** occupy a 1:1 ratio of the space). Algae in this region are not exposed to the same extremes in salinity (freshwater-dominated versus saltwater-dominated) as their monospecific counterparts that partition closer to the edges of the fishpond. The confluence of environmental parameters in this central pond region seem to create a situation in which neither species is able to out-compete the other for dominance. While the mixed canopy areas constitute a smaller fraction of total algal biomass relative to the monospecific stands, the mixed-canopy stands can

cover a fairly large area of the fishpond (33% and 41% in the Dry and Wet Seasons, respectively) and may therefore make a substantial contribution to nitrate (***N***) redistribution.

4.2. Nitrate Uptake Assessments

4.2.1. Nitrate Uptake Rates

The positive relationship between the nitrate uptake rate constant (*S*) and bulk flow (Figure 4.8) is consistent with previous studies (Thomas & Atkinson 1997, Hurd 2000, Cornelisen & Thomas 2006). The increase in *S* with increasing flow speeds also indicates that the rate of nitrate uptake by benthic primary producers in the system is limited by the delivery of nitrate to their uptake surfaces.

Scatter in the uptake data about the best-fit curve of *S* versus bulk flow (Figure 4.8) is attributed to variability in the flume-enclosed algal communities. Each flume experiment enclosed a unique algal community, each distinct both in composition and biomass. In addition, different categories of the community of primary producers (e.g. benthic macroalgae versus water column microalgae) exhibit variable responses to water flow velocity. As a consequence of the various combinations of these factors, the rate of nitrate drawdown by the community captured within the flume for each separate experiment is expected to be variable.

Time series data of flume nitrate concentration reveal that either the water within the fume was not well-mixed at the beginning of the experiments, or that there was an artifact of some sort arising from the sampling system. It is also possible that the trolling motor disturbed the sediments sufficiently to release inorganic nutrients at the sediment-water interface and introduce some nitrate into the water enclosed by the flume. As such, we were not able to assess a decline in nitrate concentration within the

first 15 minutes of the experiment. It is for this reason that we instead evaluated nitrate decline over the entire experiment period (45 minutes).

Among the specific benthic algal components (e.g., ***G***, ***A***, or ***M***), individual responses to flow regime may vary widely depending upon morphological traits. Consistent with prior studies which found that organism size and location in the water column relative to flow impacts how organisms respond to the hydrodynamic environment (Hurd 2000), the data presented here suggest that morphological and/or physiological differences between different algal components play a role in observed differences in uptake rates. For example, *G. salicornia* has a more rigid morphology than *A. spicifera,* and this difference in flexibility causes these two benthic algae to interact differently with flowing water. The higher uptake rates observed for *A. spicifera* may be explained by this difference, as follows. Flexible structures bend when they interact with flow, and in bending they expose more of their surface are to shear and moving water. As flow rates increase, so too does the bending, and consequently the area exposed for uptake. The higher overall nitrate uptake rates, and the widening difference in uptake rate between ***A*** and ***G*** as bulk flow increases (Figure 4.9D), thus can be understood as a consequence of the less rigid morphology of ***A***.

For the range of flow velocities assessed in the experimental flume studies, based solely on nitrate uptake rates, *A. spicifera* has the largest potential among the benthic components to influence nitrate removal from the water column (Figures 4.9 and 4.10). While differences in uptake rates may serve as an obvious reference point for making predictions about nitrate distribution, uptake rates are only a part of the equation that governs how much nitrate is removed from the water column. The total ***N*** removed by any algal component is a product of its uptake rate (which may or may not be flow-dependent) and its biomass. Thus, at any given time or place, the process of uptake is determined by a

combination of water flow rate, algal biomass, and algal nitrate uptake rates. Having determined algal biomass through field surveys, and flow-dependent nitrate uptake rates through flume experiments, it is also necessary to include in our interpretations an analysis of the flow within the fishpond. To this end, the proportion of algal canopies exposed to high flow rates was evaluated (see Section 4.3.2 for discussion).

4.3. Nitrate Distribution Model

4.3.1. Variables and Parameters

The model was simplified by excluding those processes for which there was insufficient data to achieve thorough parameterization. For example, because the doubling rates of the benthic components (macroalgae and MPB) are on the same timescale (7–10 days) as the model runtime (8 days), and because we do not have any mortality data for these components, we do not include specific mortality terms for them. Instead, the uptake rates used are considered to be net uptake rates, reflecting the balance between biomass growth and mortality.

Phytoplankton growth rates substituted into the Monod expression to calculate the half-saturation constant were determined from a combination of experiment and unmanipulated field measurements. Flume ***N*** uptake experiments yielded a mean ***N*** uptake rate for ***P*** of 8.796 x 10^{-3} s^{-1}. Experimental conditions were not nutrient- or light-limited and, as such, these rates were taken as maximum nitrate uptake rates for ***P***. From various studies in Kāneʻohe Bay (Redalje & Laws 1981, Landry et al. 1984, Laws et al. 1984, Selph et al. 2016), mean phytoplankton growth rate is 0.7 ± 0.2 (S.E.) d^{-1} (range = 1.6). This value was taken as representative of typical phytoplankton (***P***) growth rate in Kāneʻohe Bay.

The fact that the uptake rate data (Figure 4.9) exhibit a linear relationship with bulk flow suggests that, for the flow range examined, the algae had not yet reached saturation of their uptake surfaces. In a situation in which nitrate uptake transitions from mass transfer limitation to biological limitation, the expectation is that uptake rates would reach a plateau after saturation of uptake surfaces. None of the benthic algal components examined in the flume experiments displayed a leveling off of uptake rates, suggesting that the components were not biologically limited and that uptake would continue to increase with increasing flow.

The half-saturation constant is an important characteristic of organisms living in nitrogen-limited environments (Eppley et al. 1969) and, except for relatively brief periods after storm inputs when Kāneʻohe Bay is driven towards phosphorus limitation, the bay, including the fishpond, are considered to be nitrogen limited (e.g., Ringuet & Mackenzie 2005, Young 2011). Mulder & Hendriks (2014) explain how closely correlated half-saturation constants are to the nutrient environment in which the algae live (e.g., oligotrophic waters versus eutrophic estuaries), emphasizing that using an appropriate half-saturation constant is likely important to obtaining reasonable and useful results from the model. This parameter is found in the denominator of the Monod expression (Eqn. 6), and so is inversely proportional to the growth/uptake rate.

4.3.2. Algal Interactions with High-flow Regions

Since nitrate uptake by benthic species is flow-dependent (Section 3.2.2), and since we know the total quantity of ***N*** removed is determined not only by uptake rates and algal biomass, but also by water flow rates, defining high-flow regions in the fishpond allows us to consider the potential impact of high flow regions on ***N*** distribution and drawdown. In order to examine the influence of water flow, we assess the juxtaposition of regions of high flow and benthic algal cover within the fishpond. Regions of high flow

were defined as those with mean flow speeds of greater than 0.016ms^{-1}; this is the lowest flow rate assessed during field flume experiments.

For single-species stands of ***G*** (***G***$_{monospecific}$), the area exposed to high flow more than doubled from the Dry to the Wet Season (119%). However, the total ***G*** coverage area (i.e. including G within areas of mixed algal vegetation) exposed to high flow increased by a lesser amount: 82% (Figures 4.19 and 4.20).

For single-species stands of ***A*** (***A***$_{monospecific}$), the area exposed to high flow decreased by 6% from the Dry Season to the Wet Season. When we consider this area together with the area of ***A*** within mixed patches, however, the total coverage area of ***A*** exposed to high flow increased by 6.6%. This means that the shift in ***A*** distribution (algal cover) between the Dry and Wet Season has exposed a slightly larger area of ***A*** to high flow during the Wet Season compared to during the Dry Season.

The proportion of ***M*** exposed to high flow is approximately halved in the Wet Season from its Dry Season value.

Even though the area of coverage of the various components shifts between the Dry and Wet Seasons, the relative proportion of those areas exposed to high flow rates compared to their total area remains relatively constant (*T = -0.36,* P value *= 0.744*).

4.3.3. Interpretations of Model Simulations

4.3.3.1. Overall Water Column Nitrate (N) Drawdown

The first order contrast that was made was to evaluate the impact of seasonality (Dry versus Wet Season) on ***N***-drawdown by algal components within the fishpond. The fact that both ***G*** and ***M*** underwent large changes in coverage area between the seasons (Figure 4.5) led to the expectation that a substantial difference in ***N***-drawdown would be observed. Although the difference in overall nitrate

drawdown between the Dry and Wet Seasons was significant (T-Value = -15.42, P-Value = 0.001), the extent of the difference was not as great as for the coverage area; almost indistinguishable, in fact. Differences in extent of ***G*** and ***M*** cover were more exaggerated in areas exposed to high flow (Figures 4.19 and 4.20), but ***N***-drawdown still did not exhibit a comparable corresponding difference. This latter observation suggests that a mediating factor beyond seasonal differences is important in determining the extent of ***N***-drawdown. Results of the following model simulations support that this mediating factor is algal biomass.

A more mundane explanation for the more subdued difference observed in ***N***-drawdown between the Dry- and Wet Seasons can be posited in view of the potentially imperfect match of timing of sampling and seasonal extremes. If the expanse of algal cover varies on a continuum with respect to time, extent of algal coverage would be expected to shrink or grow in concert with changes in the physical environment that are more or less favorable to algal growth. Depending upon the particular preferences of an algal species for a particular set of environmental characteristics, such as those that characterize the Wet versus the Dry Season (e.g., temperature, salinity), one might expect that particular algal species would be favored in different seasons. Further, under this scenario the extremes of algal coverage of particular algal species would be expected to occur at the height of the season that provides the most favorable environmental conditions. It is important to consider that the algal cover distribution used in the analyses conducted herein may not be indicative of the height of the Dry and Wet seasons. Due to the effort involved in sampling, our sample set is limited to once per season. It must be considered that timing of sampling may have captured algal cover during a transition phase, rather than at the height of the season. If the timing of algal cover surveys and sampling missed the

peak-of-season, and instead captured an intermediate point between seasons, the difference in ***N***-uptake rates observed would not be expected to be maximal.

Adding to the uncertainty about whether timing of sampling in this study coincided with peak Dry or Wet Season is the notion that such a distinction may not be useful to describe seasonality in Hawai'i. Instead, based on an annual study of biogeochemistry in He'eia Fishpond, Young (2011) suggests that a more realistic partitioning of distinctive environmental conditions would be baseline (non-storm) versus storm conditions. Notably, there can be substantial stretches of non-storm conditions during the Wet season (Young 2011). Finally, it is also possible that high variability in environmental conditions within seasons renders the algal cover and subsequent ***N*** drawdown assessed in this study difficult to partition cleanly between two distinct seasons.

4.3.3.2. Dry Season Baseline vs. Wet Season Baseline

Model simulation output clearly shows that it is the interplay between biomass and ***N***-uptake rates that determines which algal component dominates ***N***-uptake from the fishpond. For example, despite the fact that ***P*** has uptake rates orders of magnitude higher than ***G*** (Figure 4.12), ***G*** dominates ***N***-uptake, and is the main player in nitrate drawdown. This underscores the fact that simply assessing nitrate uptake rates in isolation is not sufficient to make predictions about ***N***-drawdown in the system. In this case, the high biomass of ***G*** contributed to its ability to dominate ***N-*** drawdown from the water column. ***G*** mean biomass is *ca.* 11 and 33 times higher than the sum of ***P***, ***A***, and ***M*** mean biomass in the Dry season and the Wet Season, respectively.

Focusing on ***G*** alone, however, it can be seen that uptake rate does have an effect on ***N***-drawdown. The smaller drawdown of ***N*** by ***G*** during the wet season compared to the Dry Season corresponds to a slightly lower mean ***G*** uptake rate in wet season than is observed during the Dry season. Additionally,

the fact that ***G*** and ***A*** mean uptake rates are comparable, but ***A*** removes 98% and 97% less ***N*** than ***G*** in the Dry and Wet Seasons, respectively, strengthens the argument that algal biomass plays a major role in determining the total quantity of ***N*** removed from the water column.

4.3.3.3. 100% Dry Season M Baseline vs. 100% Wet Season M Baseline

Prior to the invasion of non-native macroalgae, microphytobenthos likely dominated the benthic primary producer community in He'eia Fishpond (personal communication, POH). As such, nitrate distribution results of the 100% MPB model simulations have the potential to illuminate the way in which the fishpond system may have operated prior to invasive algae colonization. These simulations therefore have particular relevance to fishpond managers, and may in turn assist them in managing the macroalgal invasion. For example, despite the fact that mean biomass of ***M*** is only 4% higher than the mean biomass of **P** in the Dry Season, and mean nitrate uptake is orders of magnitude higher for ***P*** than for ***M***, the small difference in mean biomass is enough to manifest as a 48% difference in the total ***N*** removed from the water column between ***P*** and ***M***. When the contrast is drawn for the Wet Season, where mean ***M*** biomass is 3% lower than mean ***P*** biomass, we observe 14% less ***N*** removed by ***M*** than by ***P***. Microphytobenthos seems to be very effective at removing nitrate from the water column.

4.3.3.4. Dry Season Baseline vs. 100% M Dry Baseline

Under the baseline nitrate treatment (i.e. no nitrate pulse), 100% M coverage had a comparable effect to that of the typical Dry Season 3-component benthic algal complement on ***N*** drawdown. If these two drastically different algal coverage complements can have a similar effect on ***N*** drawdown, it suggests that ***M*** can effectively regulate nitrate in the fishpond when it is not in competition with macroalgae. A return to pre-invasion algal ecology could therefore be just as effective in regulating nitrate leaving the fishpond onto the nearby reef when there is full microphytobenthos cover. A return to pre-invasion algal ecology has the additional benefit of a fishpond algal cover preferred by many of the desirable native

herbivorous fish (e.g., moi) with which managers hope to repopulate the fishpond. The model result of runs parameterized as 100% ***M*** coverage could therefore provide reassuring evidence to fishpond managers as they move to eliminate invasive macroalgae from the fishpond as part of their restoration efforts. An important outcome of this model study is the indication that removal of invasive macroalgae will not result in an increase in ***N***-export to the adjacent coral reefs, as ***M*** appear to be capable of an efficiency of ***N***-removal comparable to that of the invasive macroalgae.

4.3.3.5. Dry Season Baseline vs. Dry Season Pulse

The dynamics between algal components within the fishpond clearly change under conditions set up when the fishpond receives a storm pulse of nitrate. When typical Dry Season algal cover under baseline nutrient conditions is compared to that during pulse conditions, ***P*** is the only algal component that demonstrates a clear response to the storm-increased nutrient load (Figure 4.15). Since nitrate uptake by ***P*** is not flow-mediated, the simulation output suggests that physiological differences between the algae may be responsible for the upsurge in ***N*** uptake by ***P***. This observation about the extent of the role of different algal physiology raises questions about how the composition of the phytoplankton community might affect nutrient cycling, and how different ***P*** communities may respond to environmental perturbations, such as increased frequency of nutrient loading in coastal regions. These questions are beyond the scope of the current study. Under conditions of increased frequency and/or intensity of nutrient loading, it is unclear at what point the ability of the fishpond to respond to storm nutrient input might be exceeded. If exceeded, the fishpond would not serve as an effective filter for water exiting through the ocean mākāhā onto the nearby reef. Should fishpond nutrient uptake capacity be swamped due to increased nutrient loading, nutrient over-enrichment of the adjacent coral reefs would ensue, conditions which are known to pose health threats to coral reef ecosystems.

4.3.3.6. 100% Dry Season M Pulse vs. 100% Wet Season M Pulse

Given that total ***N*** removal is a product of biomass and uptake rate, the higher ***P*** and ***M*** biomass stimulated under the Wet Season ***N***-pulse simulation relative to the Dry Season ***N***-pulse simulation (Figure 4.16) is expected to result in greater ***N***-drawdown by ***P*** and ***M*** under Wet Season conditions. While M did remove more ***N*** during the Wet Season compared to the Dray Season, no increase in ***N***-drawdown by ***P*** is observed during the Wet Season under ***N***-pulse conditions. In fact, the ***N***-drawdown by ***P*** is lower during the Wet Season than during the Dry Season under ***N***-pulse conditions by 11% (Fig. 16). To resolve this puzzling result, it is instructive to consider factors that affect ***P*** biomass that do not impact ***M*** biomass under these scenarios. The most obvious factor to consider is advection, which will impact free-floating ***P*** but will not impact ***M***, which is a static component of the benthos. The higher concentration of ***P*** undergoing advection may translate into a greater ***P*** loss term at the fishpond walls; this loss may be of sufficient magnitude to depress ***N***-drawdown by ***P*** during the Wet Season ***N*** -pulse scenario.

4.3.3.7. Dry Season – 0.5-day pulse vs. 1-day pulse vs. 2-day pulse

The duration of elevated nutrient levels following a storm pulse to the coastal ocean can vary widely depending upon the intensity of the storm, and the prevailing weather patterns. For example, Young (2011) monitored storm impact on He‘eia Fishpond during a first flush storm in which the nutrient pulse duration was 3 to 4 days. At the other extreme, Ringuet & Mackenzie (2005) estimated recovery time (i.e. the time to return to baseline conditions after a storm) to range from 3 to 8 days for the storm events monitored in that study. In order to make an assessment of the effect of storm pulse duration on ***N*** distribution, model simulations were run in which a 0.5-day pulse, a 1-day pulse, and a 2-day pulse were imposed upon the typical Dry (and Wet) Season 4-component algal complement. While an increase in ***N*** drawdown was observed between the 0.5- and 1-day pulse simulations, no change in

response was observed between the 1-day and 2-day pulse simulations. This result suggests that after 24 hours of increased nitrate input, the uptake systems of the algae have reached capacity, and algal nutrient uptake may have become biologically limited. The results of these variable duration storm-pulse model runs are instructive for understanding how nitrate in the fishpond returns to its background levels after a storm. Under average conditions, ***N*** is reduced via biological uptake and is also lost to the external environment as it escapes the fishpond via flow through the mākāhā. In response to a storm pulse, however, the mechanisms involved in returning the fishpond to baseline conditions likely include a shift in the relative importance of biological versus physical processes. Once algal uptake is saturated, and algae are no longer actively removing significant quantities of ***N*** from the water column, the level of nitrate concentrations within the fishpond will depend on the rate of water exchange with the external environment. The physical process of water exchange between the fishpond and the external environment is impacted by winds, water velocity, tidal phase, and discharge at mākāhā (e.g., (Young 2011, Timmerman et al. in prep). The overall response by the fishpond to environmental perturbations such as nutrient pulses is therefore complex, and requires consideration of multiple factors and further study.

Investigation of the time series of ***N*** in the fishpond (Figure 4.18) reveals that elevated levels of ***N*** last only as long as the applied ***N***-pulse itself. This observation suggests that (1) the algae are efficient at removing ***N*** from water column, (2) the algae are able to readily respond to a nitrate pulse, and (3) the fishpond may require a constant supply of ***N*** in order to maintain its algal complement. We see this rapid drawdown of ***N*** not only after introduction of the ***N*** pulse, but also at the initiation of the model run as well – total nitrate is drawn down to within 0.45% of the starting total ***N*** value before the pulse is even applied.

The model-determined time to return to pre-pulse ***N*** levels differs from that reported by the field study of Young (2011), who found that the time required to return to pre-pulse levels was 4 days. In contrast, in the present modeling study, high levels of N persisted only as long as the pulse. The discrepancy between the current study and the previous work by Young (2011) could be explained by the nature of the model. The model described in this study does not explicitly account for all sources and sinks of ***N*** in the fishpond. Notably, sedimentary sources of ***N*** are not considered in the present model, while the data collected by Young (2011) represent the net effect of ALL contributing factors, including sedimentary remineralization of organic material to produce nitrate (***N***), which then diffuses out of the sediment column as a benthic N-flux (e.g., Briggs 2011, Briggs et al. 2013). The relative importance of the sources and sinks of ***N*** to nitrogen cycling and nitrate distribution within the fishpond is as yet undetermined.

5. Conclusion

N distribution in He'eia fishpond is controlled by multiple factors, the relative importance of which can vary depending upon the nutrient status of the system. Several general trends have been described in this contribution. Under baseline nitrate conditions, *Gracilaria salicornia* dominates nitrate drawdown in the fishpond. The dominance of ***G*** is likely due to its high biomass across the fishpond relative to other algal species. In the absence of this high-biomass macroalga, however, the capacity of phytoplankton and microphytobenthos to draw down nitrate from the water column appears to be comparable to the capacity of ***G***. This bodes well for the management effort to eradicate invasive macroalgae from the fishpond, in that the equivalent ***N***-removal efficiency by ***P*** and ***M*** suggests that ***N***-export to the adjacent coral reef can be maintained in the absence of the invasive macroalgae.

Algal biomass plays an important role in determining how much ***N*** is removed from the water column via incorporation into algal tissues. This observation has direct application for management of the fishpond, since algal removal projects currently are underway as part of fishpond restoration efforts. Partitioning of algal biomass data between high water flow regions versus lower flow regions suggests that the extent and location of algal removal efforts can be an influential contributing factor in the distribution of nitrate between the various algal reservoirs of the system.

The model presented here offers new insights into the behavior of the primary producers in He‘eia fishpond in response to nutrient delivery. It is important to point out, however, that because this study considers nitrate only, it provides a somewhat biased view of algal response to the nutrient regime in the fishpond. In order to provide a more sound and comprehensive basis for management decisions, it will be important to consider the combined effects of multiple nutrients on the fishpond ecosystem. In addition, the overall response of an ecosystem to various perturbations or shifts in nutrient availability is influenced not only by the relative availability of dissolved inorganic forms of nutrients, but also by nutrients present in other forms (dissolved vs. particulate, organic vs. inorganic). As such, it is important to include multi-element assessments in order to both improve prediction power and achieve more accurate descriptions of the vulnerability of the ecosystems (from Global News Group https://marine.rutgers.edu/globalnews/mission.htm).

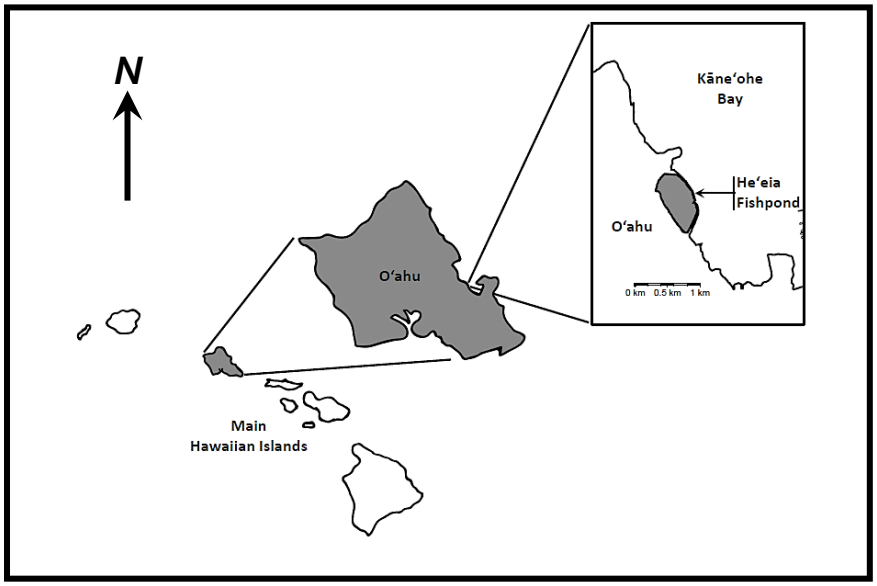

Figure 4.1 Map showing study site at Heʻeia Fishpond (Loko iʻa o Heʻeia). The fishpond is in the southern portion of Kāneʻohe Bay, Oʻahu, Hawaiʻi (21° 26’ 10.07”N, 157° 48’ 27.94”W).

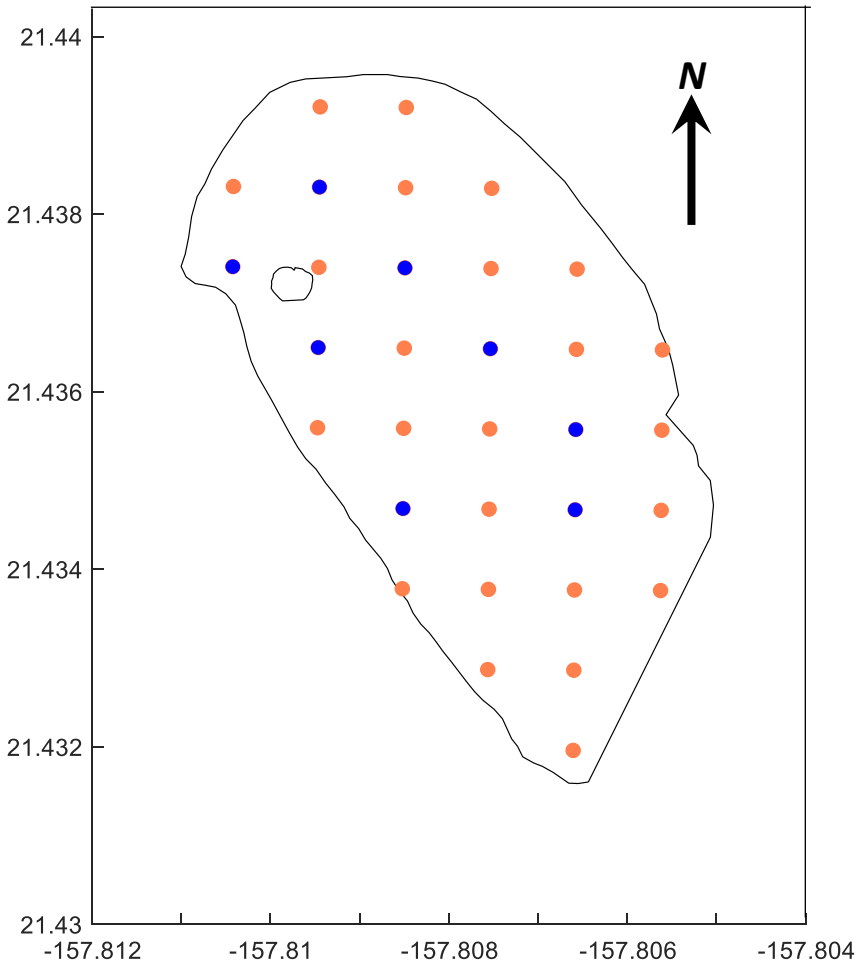

Figure 4.2 Map of He'eia Fishpond showing monthly (blue circles) and seasonal sampling (orange circles) locations for algal cover and biomass.

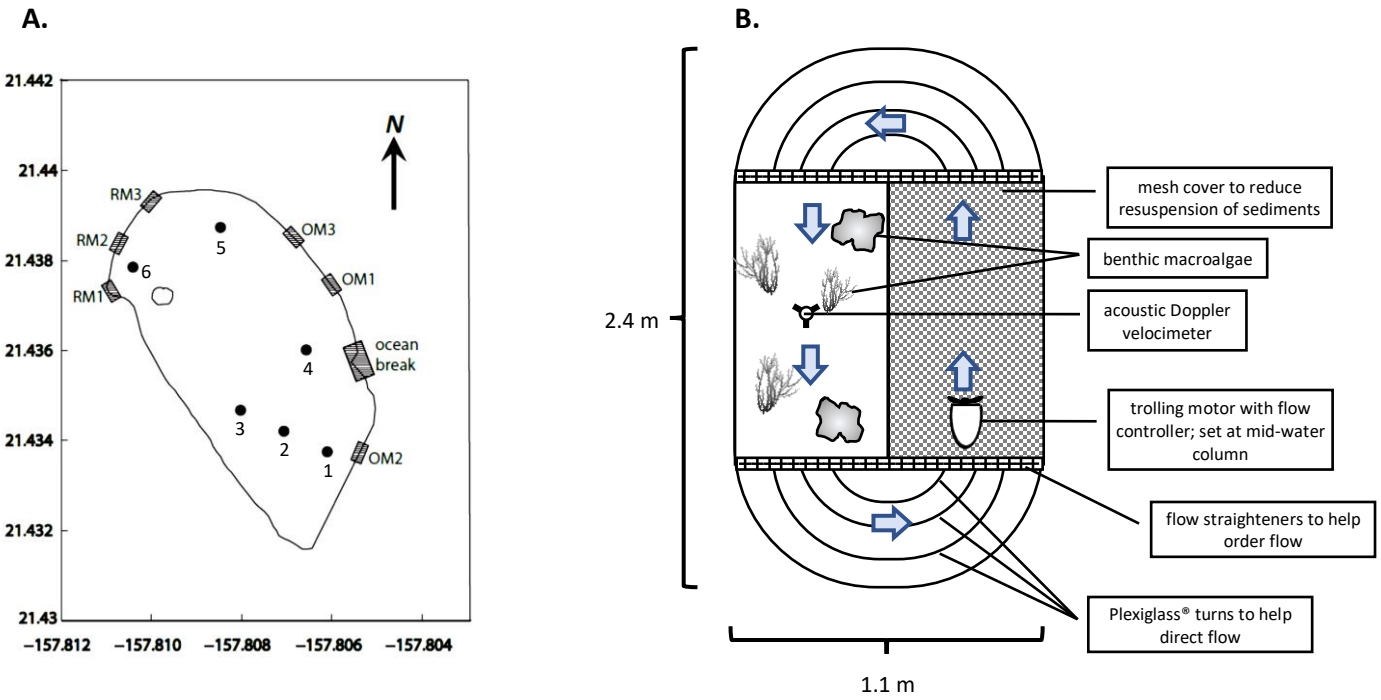

Figure 4.3 A. Map of He'eia Fishpond showing points of water exchange (mākāhā (sluice gates) and break in fishpond wall (▨) and numbered field flume experiment locations (●). RM: River Mākāhā (points of fresh water introduction into the fishpond). OM: Ocean Mākāhā (sites of salt water introduction and water exchange with adjacent coastal ocean water). **B. Plan view of field flume.** The flume was constructed out of clear plexiglass® to allow light penetration and had an aluminum frame. It isolates a 2.6 m^2 area of the natural benthic community and the overlying water column. Blue arrows indicate water flow.

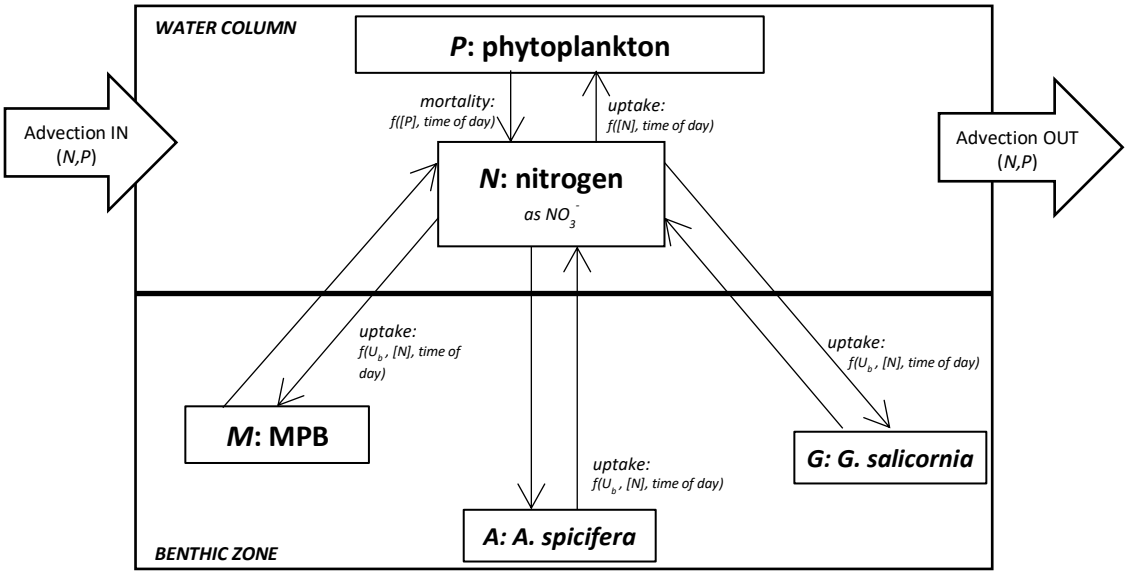

Figure 4.4. Schematic representation of the processes linking nitrogen reservoirs within each model cell. The **model cell** is defined as a 7.3 m x 11.1 m area. **Phytoplankton** (P), **microphytobenthos** (MPB), ***Gracilaria salicornia*** (G), and ***Acanthophora spicifera*** (A) represent nitrogen bound in tissues of autotrophic organisms, while **nitrogen** (N) represents dissolved inorganic nitrogen (as nitrate) in the water column.
Here, the **water column** refers to the entire depth of the water from surface to the sediment-water interface; the **benthic zone** refers to the bottom ecological zone that encompasses the flora and fauna (benthos) living on, in, and at the seabed. We use **bulk flow (U_b)** to refer to the mean water speeds (i.e. over the entire water column) that mediate nitrate uptake by the benthos. **Advection** includes water velocity in both the x- and y- directions to determine movement of dissolved and suspended particles (***N*** and ***P*** respectively).

Nitrogen transfer between reservoirs, within each model cell, is represented by the solid black arrows. Nitrogen and phytoplankton transfer between adjacent model cells, via advection, is shown as the white block arrows. Bulk flow patterns, and thus also advection of dissolved and suspended particles, are established and applied based on empirical data from He'eia Fishpond.

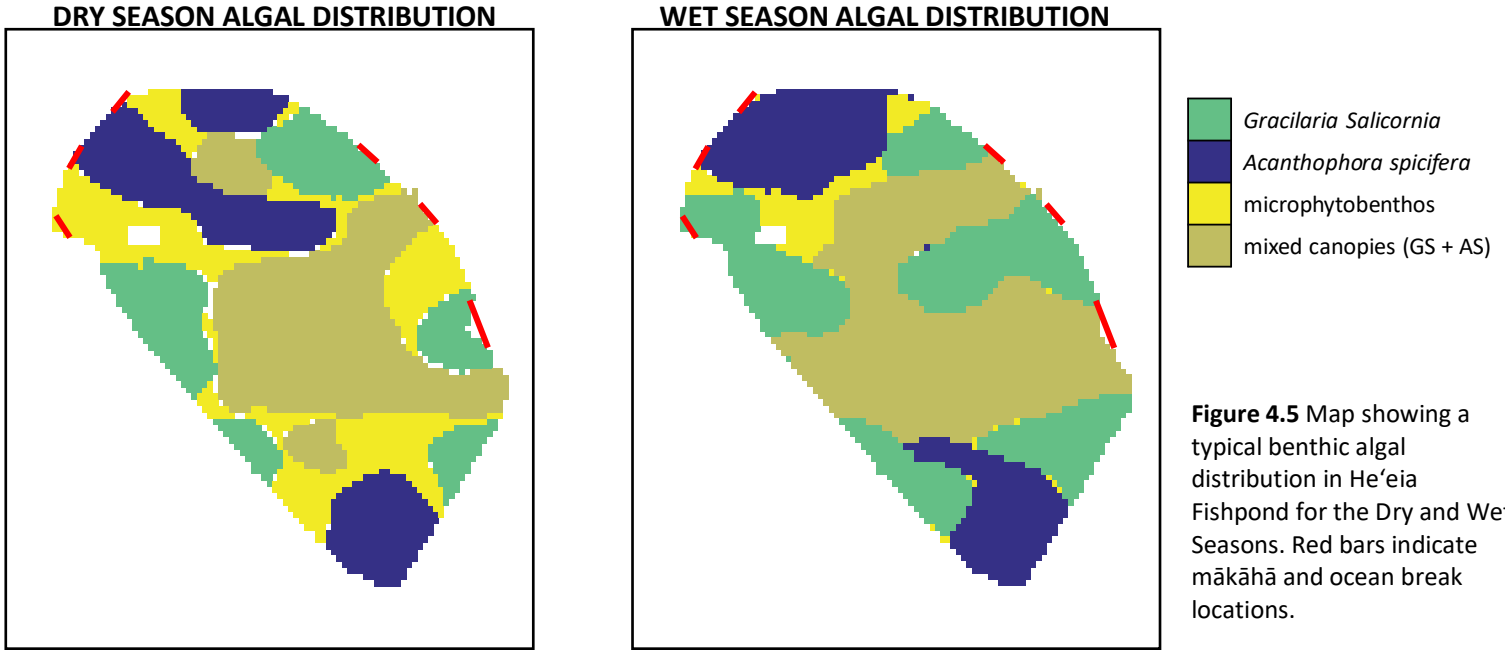

Figure 4.5 Map showing a typical benthic algal distribution in He'eia Fishpond for the Dry and Wet Seasons. Red bars indicate mākāhā and ocean break locations.

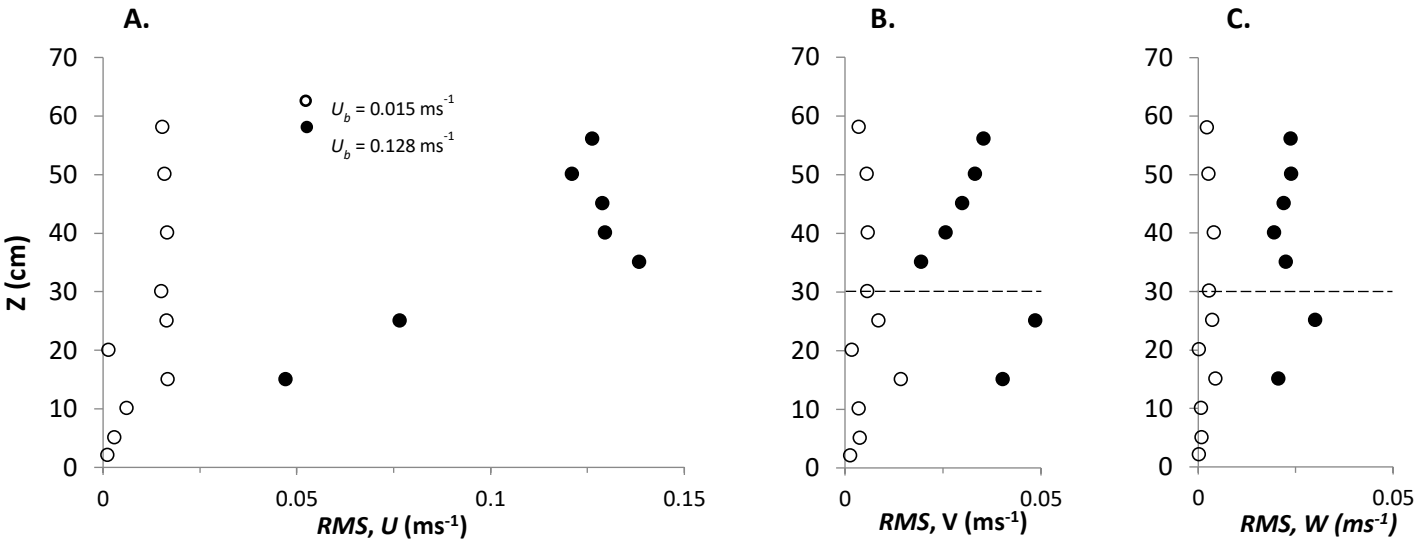

Figure 4.6 Vertical profiles of RMS velocity in A. main (longitudinal), B. transverse (V), and vertical(Z) directions of flow. Open circles represent flow during a low flow experiment (0.015 ms-1) and solid black circles represent flow during a higher flow experiment (0.128 ms^{-1}). The dashed line indicates the mean height of algal canopies. These profiles show how flow is dampened within the canopies and, as expected, increases slightly at the top of the canopy, indicative of an increase in turbulence in this region.

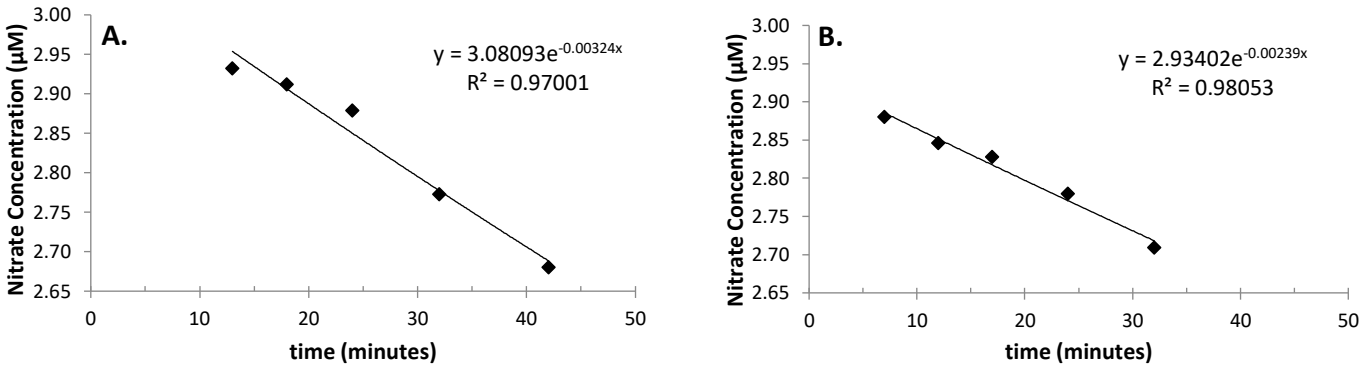

Figure 4.7 Two examples of nitrate drawdown timeseries data within the flume at two flow velocities: A) 0.015 ms^{-1} and B) 0.129 ms^{-1} The nitrate drawdown curve for each experimental run was used to determine a first-order rate constant (*k*), which is the slope of the least-squares regression of log nitrate concentration versus time. k is then used to calculate an uptake rate constant, *S* (ms^{-1}) for the entire community enclosed within the flume. $S = k * Vol/A$, where Vol is the volume of water in the flume and A is the area (in m^2) of exposed benthos within the flume.

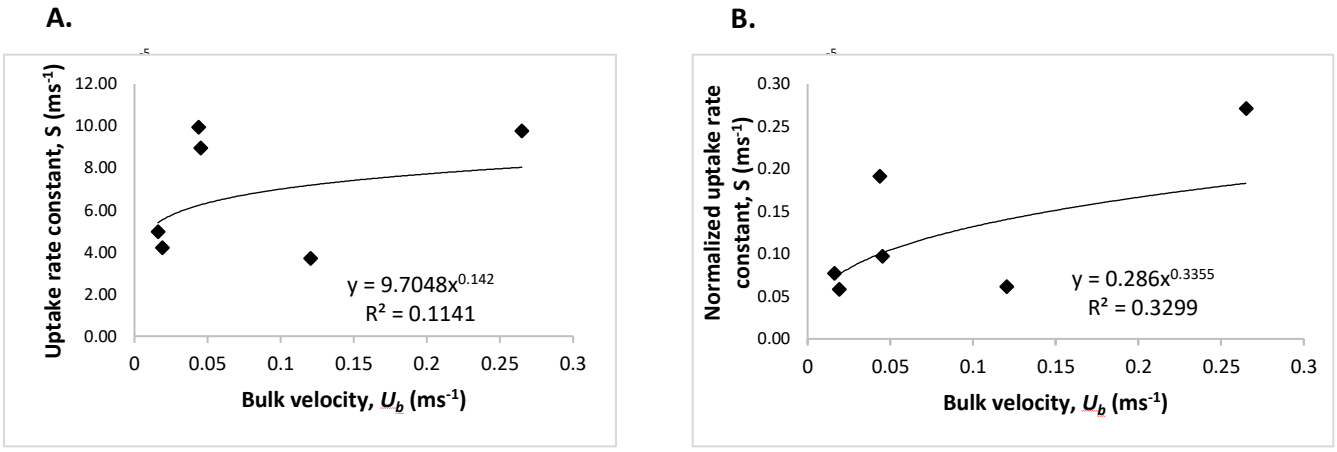

Figure 4.8 A. Nitrate uptake rate constant, S (*S = k * Vol*/A), for entire community as a function of bulk velocity, U_b. B. Nitrate uptake rate constant normalized to % algal cover.

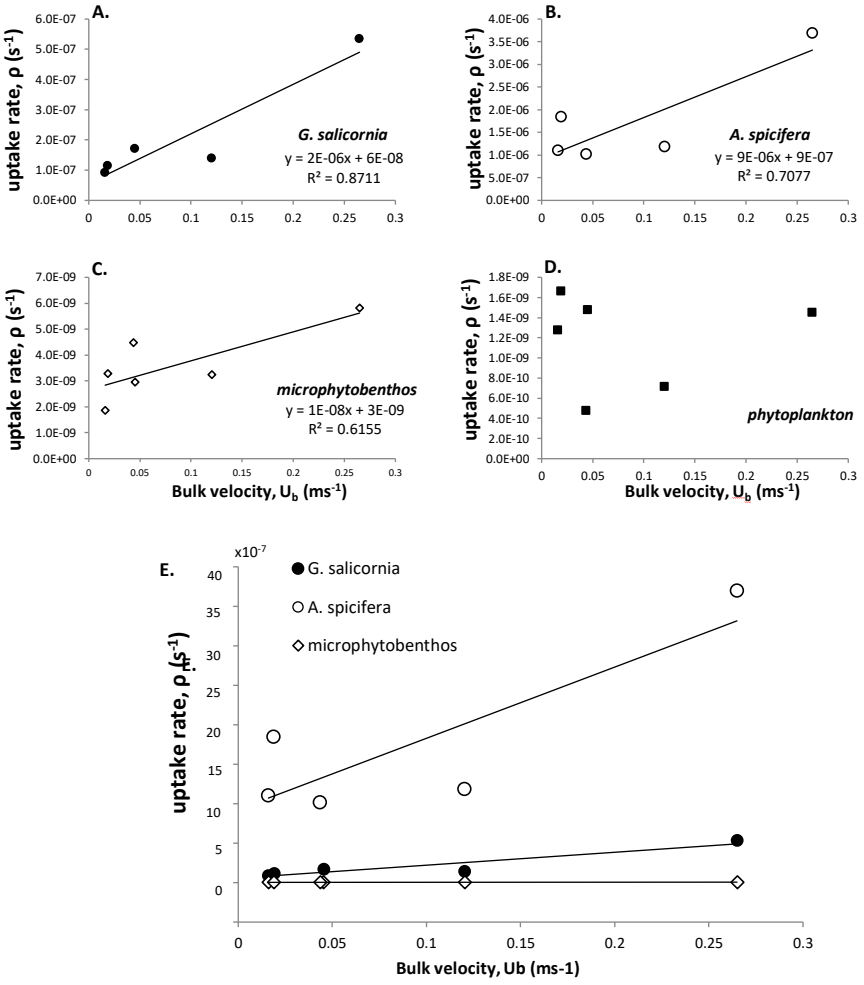

Figure 4.9 Nitrate Uptake by A. *Gracilaria salicornia*, B. *Acanthophora spicifera*, C. microphytobenthic community, and D. phytoplankton community in relation to bulk velocity (U_b). *G. salicornia*, *A. spicifera*, and microphytobenthos, all located at the benthos, exhibit flow-mediated uptake of nitrate. Phytoplankton uptake does not demonstrate any relationship with flow. **E contrasting nitrate uptake by benthic algal components.** Data from A.–D. plotted on the same chart to illustrate differences in the relationship between the nitrate uptake rates of the different benthic algal components and bulk flow. *A. spicifera* (○) had the highest uptake rates, followed by *G. Salicornia* (●), and then microphytobenthos (◊).

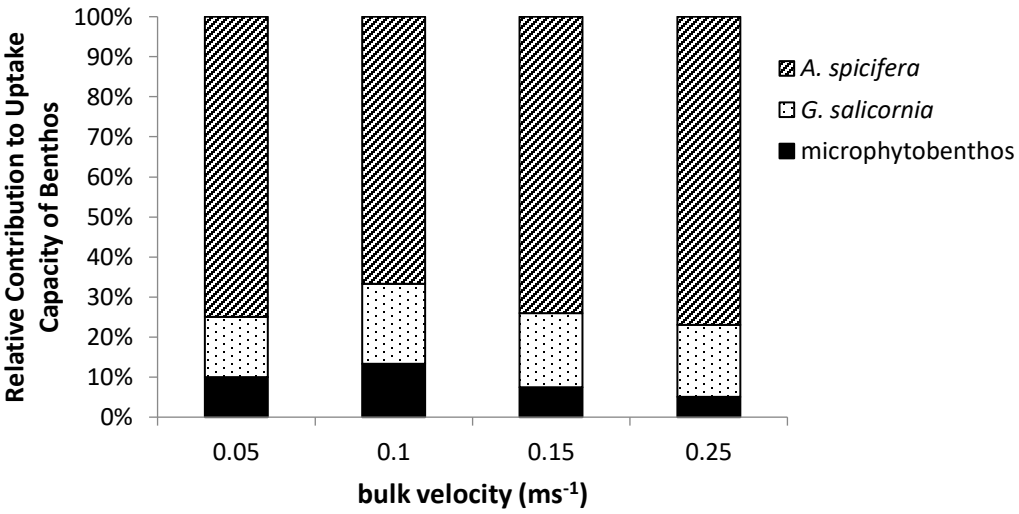

Figure 4.10 Relative contribution of individual components of primary producing community to total nitrate uptake capacity of the benthos. *A. spicifera* accounts for at least 75% of NO_3^- uptake capacity.

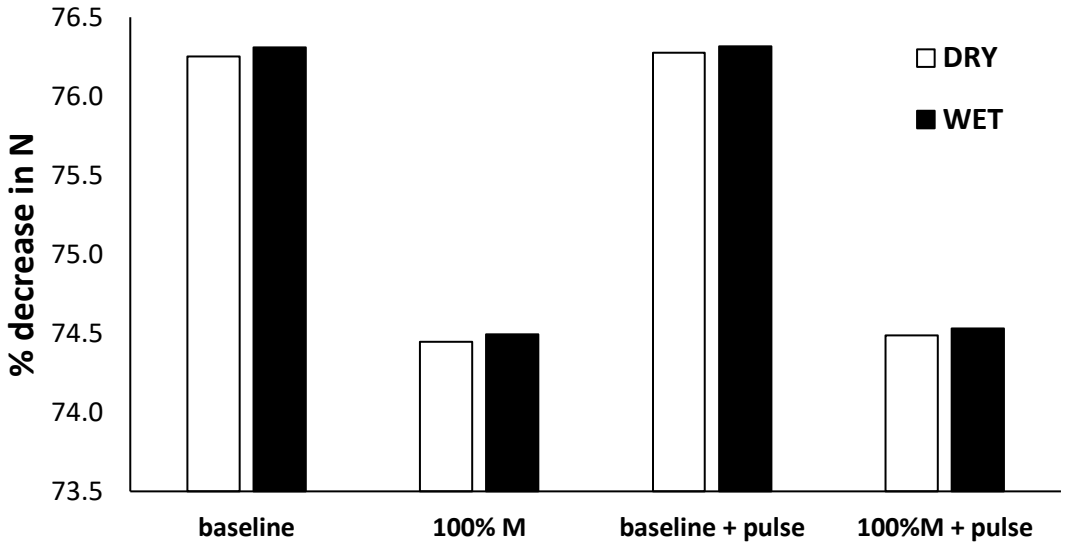

Figure 4.11 Percent decrease in *N* for each model simulation. Simulations run under Dry Season conditions are shown in white bars while those run under Wet Season conditions are shown in sold black bars.

baseline: typical algal distribution for Dry and Wet Seasons, respectively, under mean background nitrate concentration of 0.18µM

100%M: entire fishpond covered only by microphytobenthos; no macroalgae present

+ pulse: indicates the inclusion of a 0.5-day pulse of 40.19µM ***N*** at river mākāhā simulating storm conditions

Overall ***N*** drawdown across the entire fishpond during the Wet Season versus the Dry Season is significantly higher (T-Value = -15.42; P-Value = 0.001).

Overall ***N*** drawdown by 100% ***M*** cover is significantly lower than by typical algal cover, regardless of season (T-Value = 264.56; P-Value < 0.0005)

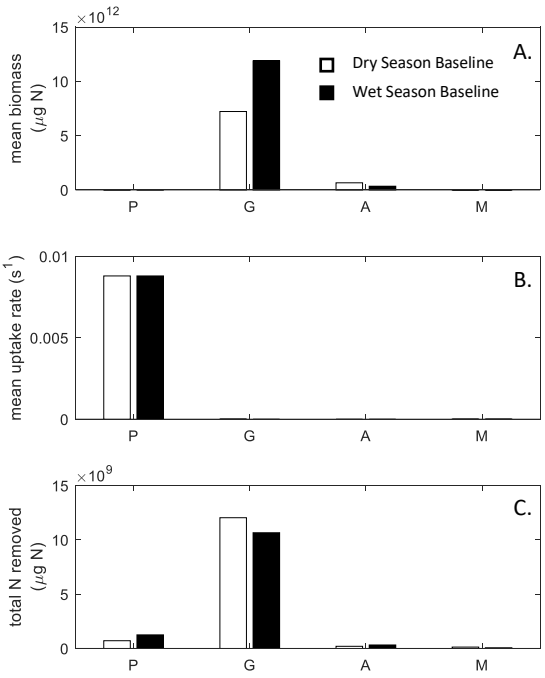

D.

panel ID		P		G		A		M	
		DS baseline	WS baseline	DS baseline	WS baseline	DS baseline	WS baseline	DS baseline	WS baseline
A.	**mean biomass**	1.59E+10	2.25E+10	7.22E+12	1.19E+13	6.56E+11	3.42E+11	4.31E+09	1.42E+09
B.	**mean uptake rate**	8.80E-03	8.80E-03	2.01E-09	1.14E-09	1.25E-09	7.00E-10	8.85E-09	6.01E-09
C.	**total N removed**	7.13E+08	1.25E+09	1.20E+10	1.07E+10	1.98E+08	3.21E+08	1.26E+08	6.02E+07

Figure 4.12. Typical Dry Season algal coverage versus Typical Wet Season algal coverage under baseline nutrient conditions

A. Mean biomass, **B.** mean nitrate uptake rate, and **C.** total N removed for each model primary producing component (***P***, ***G***, ***A***, and ***M***) over the 8-day model run.

D. Table of data plotted in bar charts.

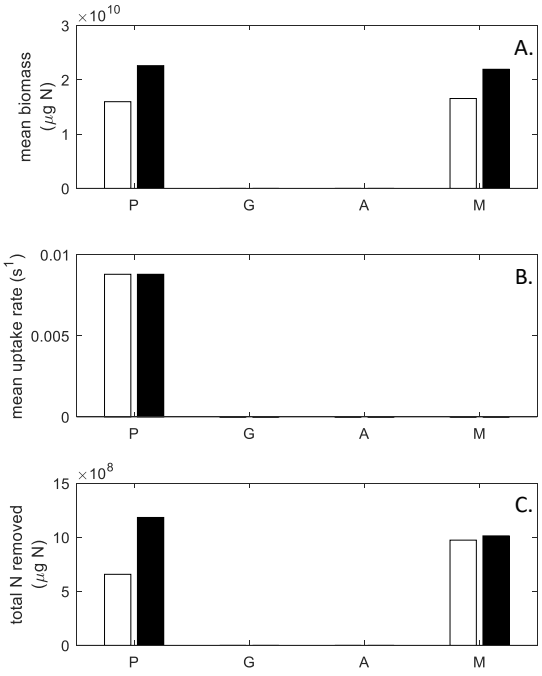

D.

panel ID		P		G		A		M	
		100M Dry baseline	100M Wet baseline	100M Dry baseline	100M Wet baseline	100M Dry baseline	100M Wet baseline	100M Dry baseline	100M Wet baseline
A.	**mean biomass**	1.597E+10	2.261E+10	0	0	0	0	1.655E+10	2.194E+10
B.	**mean uptake rate**	0.0087958	0.0087958	1.01E-08	7.81E-09	6.73E-09	5.20E-09	3.34E-08	2.62E-08
C.	**total N removed**	657414358	1.184E+09	0	0	0	0	973684311	1.013E+09

Figure 4.13. 100 % Dry Season M converge versus 100% Wet Season M coverage under baseline nutrient conditions

A. Mean biomass, **B.** mean nitrate uptake rate, and **C.** total N removed by ***P*** and ***M*** over the 8-day model run.

D. Table of data plotted in bar charts.

Note: Difference in scale relative to the panels in Figure 11

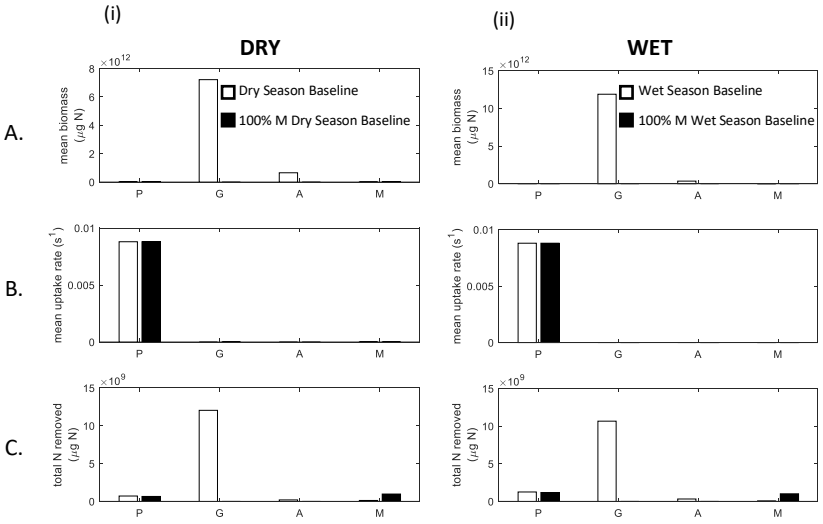

Figure 4.14. (i) Typical Dry Season algal coverage versus 100 % Dry Season M converge under baseline nutrient conditions and (ii) Typical Wet Season algal coverage versus 100 % Wet Season M converge under baseline nutrient conditions

A. Mean biomass, **B.** mean nitrate uptake rate, and **C.** total N removed for each model primary producing component (***P***, ***G***, ***A***, and ***M***) over the 8-day model run. **D.** Table of data plotted in bar charts.

D.

panel ID		P		G		A		M	
		DS baseline	100M Dry baseline	DS baseline	100M Dry baseline	DS baseline	100M Dry baseline	DS baseline	100M Dry baseline
A.	**mean biomass**	1.59E+10	1.597E+10	7.22E+12	0	6.56E+11	0	4.31E+09	1.655E+10
B.	**mean uptake rate**	8.80E-03	0.0087958	2.01E-09	1.01E-08	1.25E-09	6.73E-09	8.85E-09	3.34E-08
C.	**total N removed**	7.13E+08	657414358	1.20E+10	0	1.98E+08	0	1.26E+08	973684311

panel ID		P		G		A		M	
		WS baseline	100M Wet baseline	WS baseline	100M Wet baseline	WS baseline	100M Wet baseline	WS baseline	100M Wet baseline
A.	**mean biomass**	2.25E+10	2.261E+10	1.19E+13	0	3.42E+11	0	1.42E+09	2.194E+10
B.	**mean uptake rate**	8.80E-03	0.0087958	1.14E-09	7.81E-09	7.00E-10	5.20E-09	6.01E-09	2.62E-08
C.	**total N removed**	1.25E+09	1.184E+09	1.07E+10	0	3.21E+08	0	6.02E+07	1.013E+09

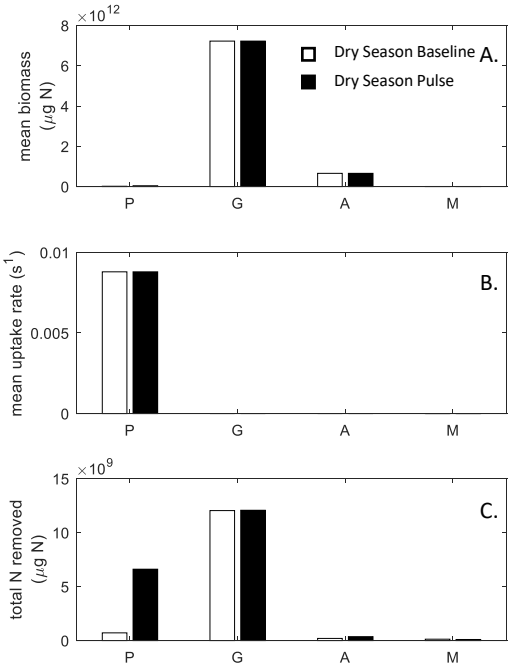

D.

panel ID		P		G		A		M	
		DS baseline	DS pulse	DS baseline	DS pulse	DS baseline	DS pulse	DS baseline	DS pulse
A.	**mean biomass**	1.59E+10	4.08E+10	7.22E+12	7.22E+12	6.56E+11	6.57E+11	4.31E+09	4.30E+09
B.	**mean uptake rate**	8.80E-03	8.80E-03	2.01E-09	2.00E-09	1.25E-09	1.25E-09	8.85E-09	8.72E-09
C.	**total N removed**	7.13E+08	6.61E+09	1.20E+10	1.21E+10	1.98E+08	3.63E+08	1.26E+08	9.93E+07

Figure 4.15. Typical Dry Season algal coverage under baseline nutrient conditions versus under nutrient pulse conditions

A. Mean biomass, **B.** mean nitrate uptake rate, and **C.** total N removed for each model primary producing component (***P***, ***G***, ***A***, and ***M***) over the 8-day model run.

D. Table of data plotted in bar charts.

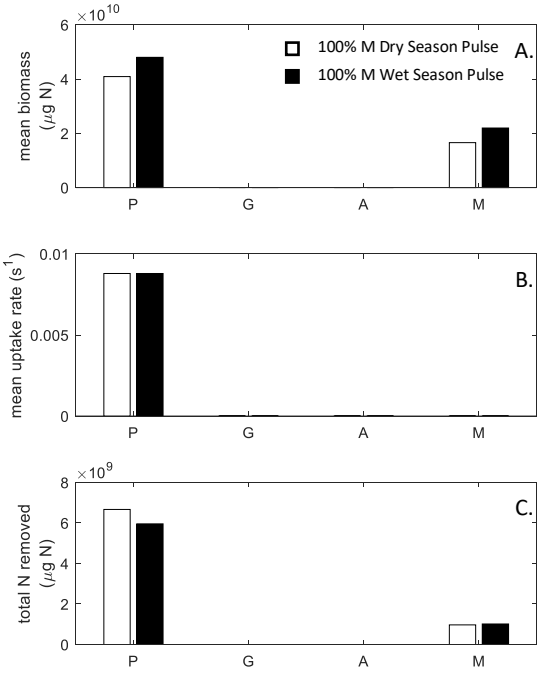

D.

panel ID		P		G		A		M	
		100M dry pulse	100M wet pulse	100M dry pulse	100M wet pulse	100M dry pulse	100M wet pulse	100M dry pulse	100M wet pulse
A.	**mean biomass**	4.09E+10	4.80E+10	0	0	0	0	1.66E+10	2.20E+10
B.	**mean uptake rate**	8.80E-03	8.80E-03	1.03E-08	8.02E-09	6.88E-09	5.35E-09	3.39E-08	2.67E-08
C.	**total N removed**	6.67E+09	5.96E+09	0	0	0	0	9.68E+08	1.01E+09

Figure 4.16. 100 % Dry Season M converge versus 100% Wet Season M coverage under nutrient pulse conditions

A. Mean biomass, **B.** mean nitrate uptake rate, and **C.** total N removed for each model primary producing component (***P***, ***G***, ***A***, and ***M***) over the 8-day model run.

D. Table of data plotted in bar charts.

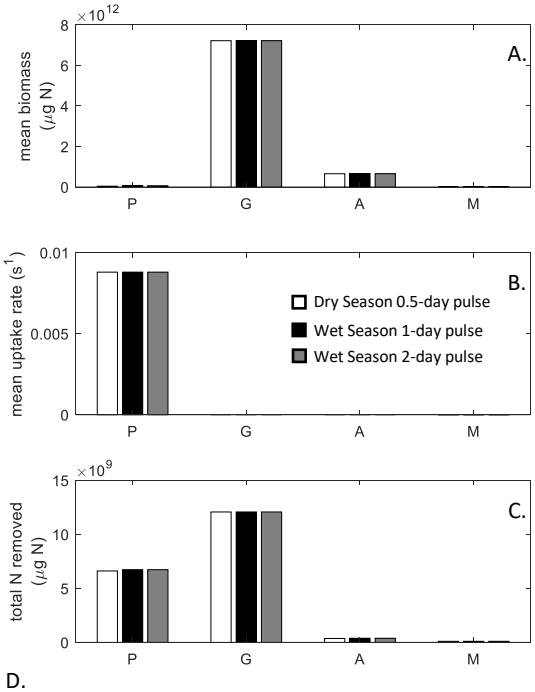

Figure 4.17. Typical Dry Season algal coverage under half-day nutrient pulse conditions versus 1-day nutrient pulse conditions versus 2-day nutrient pulse conditions

A. Mean biomass, **B.** mean nitrate uptake rate, and **C.** total N removed for each model primary producing component (***P***, ***G***, ***A***, and ***M***) over the 8-day model run.
D. Table of data plotted in bar charts.

D.

panel ID		P			G			A			M		
		DS pulse 0.5	DS pulse 1	DS pulse 2	DS pulse 0.5	DS pulse 1	DS pulse 2	DS pulse 0.5	DS pulse 1	DS pulse 2	DS pulse 0.5	DS pulse 1	DS pulse 2
A.	**mean biomass**	4.08052E+10	5.53094E+10	5.53094E+10	7.22195E+12	7.22195E+12	7.22195E+12	6.56552E+11	6.56566E+11	6.56566E+11	4.29529E+09	4.29616E+09	4.29616E+09
B.	**mean uptake rate**	8.79583E-03	8.79583E-03	8.79583E-03	2.00486E-09	2.02044E-09	2.02044E-09	1.25343E-09	1.26418E-09	1.26418E-09	8.72400E-09	8.77800E-09	8.77800E-09
C.	**total N removed**	6.61075E+09	6.73125E+09	6.73125E+09	1.20704E+10	1.20714E+10	1.20714E+10	3.63098E+08	3.82482E+08	3.82482E+08	9.93272E+07	1.00439E+08	1.00439E+08

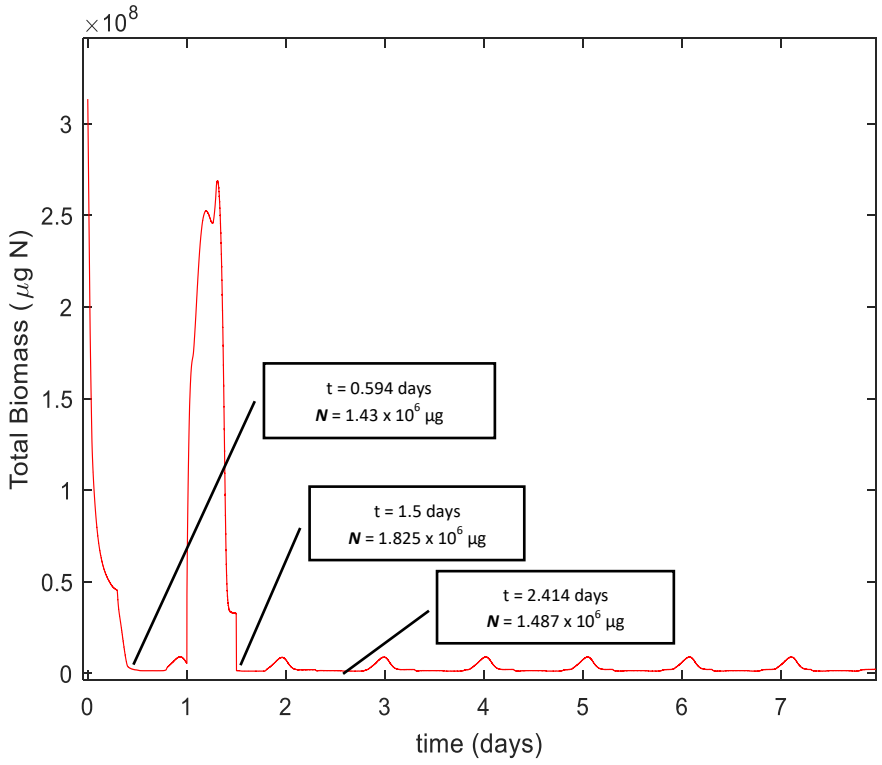

Figure 4.18. Timeseries of total N in the fishpond under 0.5-day nutrient pulse conditions. ***N*** is drawn down fairly rapidly from initial value to approximately 1.4 x10^6 µg N by t = 0.594 days. Once the pulse was introduced at t = 1 day, total N increases but is quickly drawn down to a new low ***N*** level (1.8 x10^6 µg N) by t = 1.5 days and then to approximately 1.5 x10^6 µg N (comparable to the pre-pulse minimum) by t = 2.414 days, about which it cycles. Time taken to reduce the pulse nutrient input is approximately equal to the length of the pulse itself (i.e. 0.5 days).

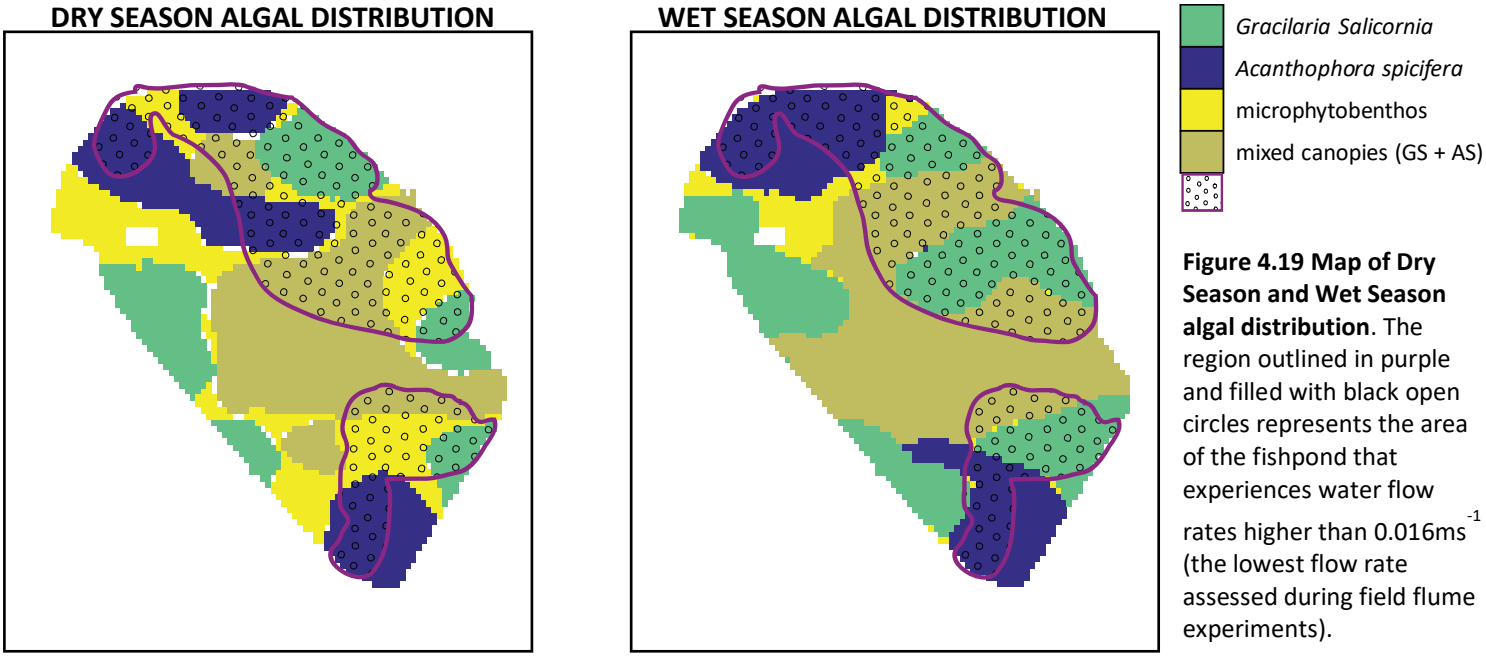

Figure 4.19 Map of Dry Season and Wet Season algal distribution. The region outlined in purple and filled with black open circles represents the area of the fishpond that experiences water flow rates higher than 0.016ms^{-1} (the lowest flow rate assessed during field flume experiments).

	AREA (m^2)			AREA EXPOSED TO HIGH FLOW (m^2)			PROPORTION OF ALGAL AREA EXPOSED TO HIGH FLOW (%)	
	DRY	WET	% difference	DRY	WET	% difference	DRY	WET
$G_{monospecific}$	62440	105179	68.4	23690	51938	119.2	37.9	49.4
$A_{monospecific}$	69359	67243	-3.1	35494	33296	-6.2	51.2	49.5
M	80431	17340	-78.4	35494	3989	-88.8	44.1	23.0
mixed*	105341	131066	24.4	35494	46891	32.1	33.7	35.8
G_{total} *	167781	170712	1.7	41436	75383	81.9	24.7	44.2
A_{total} *	174701	132776	-24.0	53241	56741	6.6	30.5	42.7

***mixed** refers to areas of mixed macroalgal canopies in which the biomass of **A** and **G** are halved to simulate a 50/50 occupancy of the space. G_{total} and A_{total} refer to the total areas of **G** and **A** respectively, which include where they occur as mono-specific stands and where they occur as part of the mixed canopy*

Figure 4.20 Bar charts showing seasonal differences in benthic algal cover for each algal species observed. A. Fishpond-wide coverage **B.** Areas exposed to high flow (> 0.016ms^{-1}).

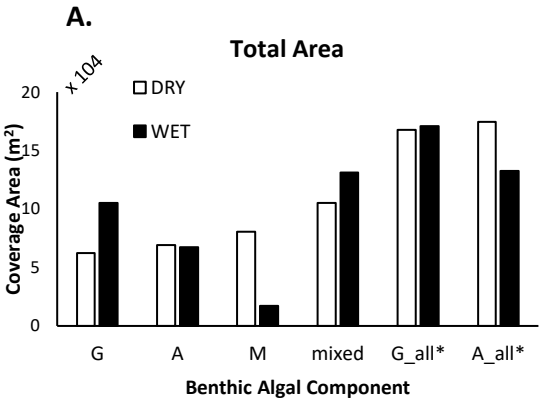

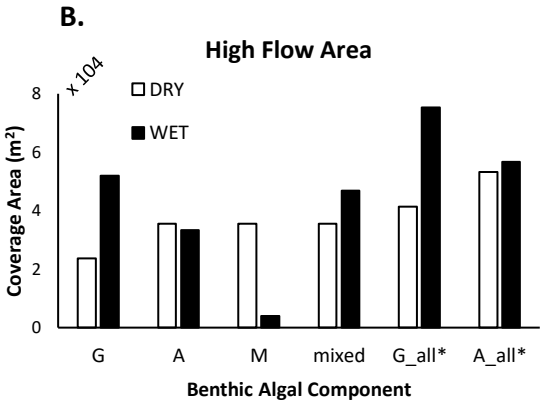

Table 4.1 Nitrate reservoirs defined for model. The value of any of these variables, at time (t) and position (x,y), is based upon a system of equations that define nitrate uptake (i.e. transfer from N to P, G, A, and M reservoirs) and algal mortality (i.e. transfer from P reservoirs to N). See equations (1) – (5.1).

Reservoir	Model Units	Location
Nitrogen as nitrate (***N***)	µg N m^{-3}	water column
Phytoplankton (***P***)	µg N m^{-3}	water column
Microphytobenthos (***M***)	µg N m^{-3}	benthos
Gracilaria salicornina (***G***)	µg N m^{-3}	benthos
Acanthophora spicifera (***A***)	µg N m^{-3}	benthos

Scenario #	Scenario ID	Scenario Description	Season	P	G	A	M
0	Null	• N only; no algae	N/A				
1	Dry Season baseline	• Dry Season algal distribution	DRY	x	x	x	x
2	Wet Season baseline	• Wet Season algal distribution	WET	x	x	x	x
3	100% MPB – Dry Season concentration	• 100% MPB cover • Dry Season MPB concentration	DRY	x			x
4	100% MPB – Wet Season concentration	• 100% MPB cover • Wet Season MPB concentration	WET	x			x
0P	Null + nitrate pulse	• N only; no algae • 40.19µM nitrate pulse (day 2-5)	N/A				
1P	Dry Season baseline + nitrate pulse	• Dry Season algal distribution • 40.19µM nitrate pulse (day 2-5)	DRY	x	x	x	x
2P	Wet Season baseline + nitrate pulse	• Wet Season algal distribution • 40.19µM nitrate pulse (day 2-5)	WET	x	x	x	x
3P	100% MPB – Dry Season concentration + nitrate pulse	• 100% MPB cover • Dry Season MPB concentration • 40.19µM nitrate pulse (day 2-5)	DRY	x			x
4P	100% MPB – Wet Season concentration + nitrate pulse	• 100% MPB cover • Wet Season MPB concentration • 40.19µM nitrate pulse (day 2-5)	WET	x			x

Table 4.2 Summary of Model Simulations.

The following conditions apply to all scenario runs:
*initialized at 0.18µM N (baseline nitrate concentration)
*length of run = 8 days
*N: nitrate in water column
*P: phytoplankton-bound nitrate nitrogen
*G: *G. salicornia*-bound nitrate nitrogen
*A: *A. spicifera*-bound nitrate nitrogen
*M: microphytobenthos-bound nitrate nitrogen

Table 4.3 Comparison of algal cover in He'eia Fishpond between Dry and Wet Seasons

	AREA (m^2)		
	DRY	**WET**	**% difference**
$G_{monospecific}$	62439.59	105178.5	68.4
$A_{monospecific}$	69359.23	67242.63	-3.1
M	80430.65	17339.81	-78.4
mixed*	105341.4	131066.1	24.4
G_{total}*	167780.9	170711.6	1.7
A_{total}*	174700.6	132775.7	-24.0

****mixed** refers to areas of mixed macroalgal canopies in which the biomass of **A** and **G** are halved to simulate a 50/50 occupancy of the space. G_{total} and A_{total} refer to the total areas of **G** and **A** respectively, which include where they occur as mono-specific stands and where they occur as part of the mixed canopy*

	bulk flow, U_b (ms^{-1})	water depth (m)	Δ [NO_3^-] (µM)	Δ t (s)	first order rate constant, k	Pearson's correlation coefficient, r	p-value	algal % cover					uptake rate constant, S (ms^{-1})	S normalized to algal cover (ms^{-1})
								G	*A*	mixed canopy, *G* + *A*	bare sediment	total macroalgal cover		
1	0.016	0.69	-0.252	1785	5.256E-05	-0.987	0.002	16	6	42	36	64	4.96E-05	7.75E-02
2	0.045	0.65	-0.604	2108	1.002E-04	-0.995	<0.0005	92	0	0	8	92	8.95E-05	9.73E-02
3	0.120	0.68	-0.171	1525	3.968E-05	-0.993	0.001	30	30	0	40	60	3.69E-05	6.15E-02
4	0.019	0.55	-0.381	1478	5.626E-05	-0.587	0.413	2	70	0	28	72	4.21E-05	5.85E-02
5	0.265	0.61	-0.69	1873	1.180E-04	-0.934	0.02	4	32	0	64	36	9.76E-05	2.71E-01
6	0.044	0.70	-0.347	1330	1.039E-04	-0.998	0.002	0	52	0	48	52	9.95E-05	1.91E-01

Table 4.4 Nitrate drawdown summary for field flume experiments.

CHAPTER 5 – CONCLUSION

The hydrodynamic environment in which algae live plays a critical role in the nature of algal response to environmental perturbations, such as acute or sustained changes in nutrient delivery to their uptake surfaces. As such, water flow patterns may indirectly impact the resilience of algal populations and communities. For cases in which nutrient uptake rates correlate closely to water flow rates, it may be possible to use water flow patterns as predictors for community response. This can potentially be an asset in conservation efforts, since water flow is often easier and faster to measure than algal nutrient uptake and growth rates. Using water flow patterns as a proxy for nutrient delivery and community response could be a particularly useful strategy for large-scale predictions. The dissertation research presented here is structured as a systematic progression from the study of an individual alga up to investigation of an ecosystem comprised of multiple types of algae. This progressive structure allows assessment of biological response on multiple ecological scales.

A field study conducted in shallow coastal waters surrounding Moku o Loʻe, an island within Kāneʻohe Bay, O'ahu, establishes unequivocally that *Gracilaria salicornia*, an invasive macroalga with rigid thalli, attenuates water flow rates within the understory of its canopy. Water flow within the canopy was 98% lower than flow adjacent to and above the canopy, near the surface, where freestream flow is characteristic. The reduced within-canopy water flow rate, and the resulting geochemical environment that develops, are sustained long enough that the high-nutrient low-flow environment within the *G. salicornia* canopy can be considered a microhabitat. The observation of a gradient in Nitrate Reductase activity in *G. salicornia* tissues that correlates with within-canopy dissolved nitrogen gradients strongly suggests that the alga is responding directly to the nutrient regime within the microenvironment that it creates. The establishment of microhabitats has potentially significant implications for nutrient

availability to other primary producers within the ecosystem, as well as for the organisms that reside within the algal canopies. As such, *G. salicornia* can be considered an ecosystem engineer.

Results obtained by an experimental study of the macroalgal epiphyte community on *Padina thivye* demonstrated that not only were there differential responses by members of the epiphyte community to variable nitrate flux, but that these differences in activity translated into shifts in community structure on timescales as short as a day. Although the epiphyte community on the macroalgae is dominated by diatoms, it is still quite diverse. Mean community diversity was high (Shannon Entropy, H' = 3.83 ± 0.18 SD based on the nitrate reductase marker) compared to other epiphyte communities such as those measured in Mabrouk et al. (2014), with Shannon Diversities and "true diversities" ranging from 3.18 to 4.04 and 26.15 to 56.77, respectively, across all gene loci and samples. Changes in the relative abundances of community members were also observed between different experimental treatments. Specifically, treatments characterized by higher nitrate flux stimulated larger changes in community structure than those with lower nitrate flux. Additionally, a change in the identity of the dominant species was observed in the higher flux treatment. Some members of the epiphyte assemblage were observed to respond more rapidly than others; this differential response is likely due to differences in their physiology. The observation made here that epiphyte communities respond rapidly to changes in environmental conditions in a way that alters their community structure, and the fact that these communities can play a significant role in nutrient cycling, implies that the overall response of a system to changes in the nutrient environment is the sum of the response of multiple components of the community. Development and application of a place-specific functional gene microarray, similar to the one used in this study, allows whole community response to environmental

changes to be quantified and, as such, is a promising approach to evaluating ecosystem response to environmental perturbations.

By scaling up the algal response concepts to the system level, and incorporating empirical measurements derived from assessments of individual and community response into a numerical model, it is possible to make predictions about how different algal complements of an ecosystem will influence overall nitrate availability. Such a combined experimental/modeling approach was taken in a study of He'eia Fishpond, a native Hawaiian fishpond in Kāne'ohe Bay. The results of field flume experiments revealed that nitrate uptake rates for all three benthic algal components, (*G. salicornia* (***G***), *A. spicifera* (***A***), and microphytobenthos (***M***)), two of which are invasive species (***G*** and ***A***), are impacted by water flow rate. The nitrate uptake rates of all benthic algae correlate positively with bulk flow rates. *A. spicifera* displays significantly higher flow-mediated uptake rates than either *G. salicornia* or the microphytobenthos. When these flow mediated uptake rate data are utilized to inform the one-dimensional model of nitrate uptake in He'eia Fishpond, however, model results suggest that *G. salicornia* dominates nitrate drawdown within the fishpond, despite its slower nitrate uptake rate. Macroalgal census data take within the pond indicate that *G. salicornia* total biomass is higher than that of *A. spicifera*, and it is argued that the larger biomass of *G. salicornia* is responsible for its dominance in nitrate uptake within the pond.

One model simulation of particular interest to managers of He'eia Fishpond, who are endeavoring to return the fishpond to its pre-impacted state, before invasion of non-native macroalgae such as *G. salicornia* and *A. spicifera,* is a scenario in which the fishpond hosts only phytoplankton and microphytobenthos (MPB); the invasive macroalgae are absent. Results of this model scenario suggest that the MPB community is capable of drawing down just as much nitrate from the water column as the

invasive macroalgae, when not in competition with the macroalgae. This is a particularly significant finding as it relates to forecasting what removal of invasive algae from He'eia Fishpond might mean for transport of nitrate onto the coral reef flat that abuts the fishpond. As managers of the fishpond move forward with restoration efforts aimed at removal of invasive macroalgae, these model results suggest that transition of the fishpond from a macroalgal-dominated to an MPB-dominated system will not change the quantity of nitrate-nitrogen currently being released by the fishpond on to the adjacent coral reef system.

Results of model simulations designed to investigate how the different algal components respond to a storm nutrient pulse reveal that the phytoplankton component of the primary producer community is the most responsive to a post-storm nitrate pulse. The Phytoplankton component increased its total nitrate uptake from 7.13 $x10^8$ µg N during baseline conditions to 6.61 x 10^9 µg N after delivery of a nitrate pulse, which represents an increase of 83%. In an attempt to investigate how storm pulses of different strengths might impact nitrate uptake by pond primary producers, several storm pulse model simulations were run in which the duration of the pulse was varied from 0.5 to 4 days. The length of the nitrate pulse had a clear effect on the total nitrate removed from the water column. We determined that a 24-hour pulse is sufficient to effectively saturate nitrate uptake by the algae. Any additional nitrate introduced beyond this threshold did not result in additional increases in nitrate uptake by the algae.

The hierarchical design of this study (transitioning from Individual to Community to Ecosystem scales of investigation) facilitated an organic synthesis and application of the data collected and concepts involved in biophysical interactions between algae and flowing water. The flow attenuation generated by benthic algal canopies correlates with elevated dissolved nutrient concentrations within the benthic

algal canopies assessed. Benthic algal canopies may therefore serve as ecosystem engineers via their effect on the accumulation and distribution of dissolved inorganic nutrients. It may be that *G. salicornia* outcompetes native species not only by some inherent physiological advantage, and/or because it is undergrazed, but by exerting mechanical control on nutrient distribution that reduces the nutrient pool that is available to other algae. The high biomass and extensive coverage of *G. salicornia* have the potential to amplify this effect. Marine macroalgal epiphytes are responsive to changes in their geochemical environment and, as such, their ecology is an important consideration in determining the ability of systems to respond to, and recover from, perturbations such as increased nutrient concentrations. This is particularly relevant since increased nutrient loading in coastal areas is an environmental concern globally, and is projected to worsen.

The straightforward nature of the nitrate distribution model developed for He'eia Fishpond makes it accessible as a management tool for non-scientists. In addition, it could be adopted as an educational tool for students and the general public, alike. An important goal underpinning this dissertation research was to generate a set of research questions and results that would have meaning for the local stakeholders of the ecosystems under study, and to find ways that the research could contribute to the community. It is hoped that this combination of fundamental research results with the numerical model, designed for a system of societal and cultural value that is currently undergoing restoration (He'eia Fishpond), might begin to achieve this goal.

Appendix I – Canopy Hydrodynamics Data Validation

Table A1.T1 Inside-canopy Fluorescein Dye Retention measurements and calculated dye decay rates (k) for the twelve (12) algal canopies assessed. Submergence ratio = water depth/canopy height. Decay rate obtained from the exponential regression of the dye intensity (C) described by $C = e^{-kt}$, where k = decay rate, and t = time in seconds.

canopy #	*Canopy Dimensions (m)*			*water*	*submergence*	*decay*
	length	*width*	*height*	*depth (m)*	*ratio*	*rate, k (s^{-1})*
1	0.21	0.17	0.09	0.47	5.2	-0.01838
2	0.245	0.195	0.07	0.535	7.6	-0.01310
3	0.35	0.285	0.065	0.455	7.0	-0.01095
4	0.43	0.33	0.14	0.585	4.2	-0.01069
5	0.36	0.2	0.1	0.545	5.5	-0.02571
6	0.22	0.21	0.165	0.6	3.6	-0.02877
7	0.27	0.26	0.13	0.58	4.5	-0.02099
8	0.32	0.21	0.09	0.67	7.4	-0.02565
9	0.31	0.27	0.1	0.63	6.3	-0.01424
10	0.16	0.14	0.11	0.72	6.5	-0.02267
11	0.28	0.21	0.12	0.7	5.8	-0.01394
12	0.31	0.25	0.12	0.73	6.1	-0.01279

Table A1.T2 Hydrodynamic Data Validation test and inside-canopy ADV data quality parameter ranges.

	Bucket Test	*Freestream Flow Test*	*Beam Obstruction Test*	*Inside-canopy Measured Ranges*
signal amplitude *(counts)*	50 – 150	50 – 70	100 – 200	20 – 180
beam correlation *(%)*	95 – 100	>80	0 – 100	60 – 100
SNR *(dB)*	20 – 60	10 – 50	25 – 75	5 – 70

Appendix II – Graphical Abstract

Graphical Abstract summarizing the physical and biogeochemical processes taking place at the sediment-water interface

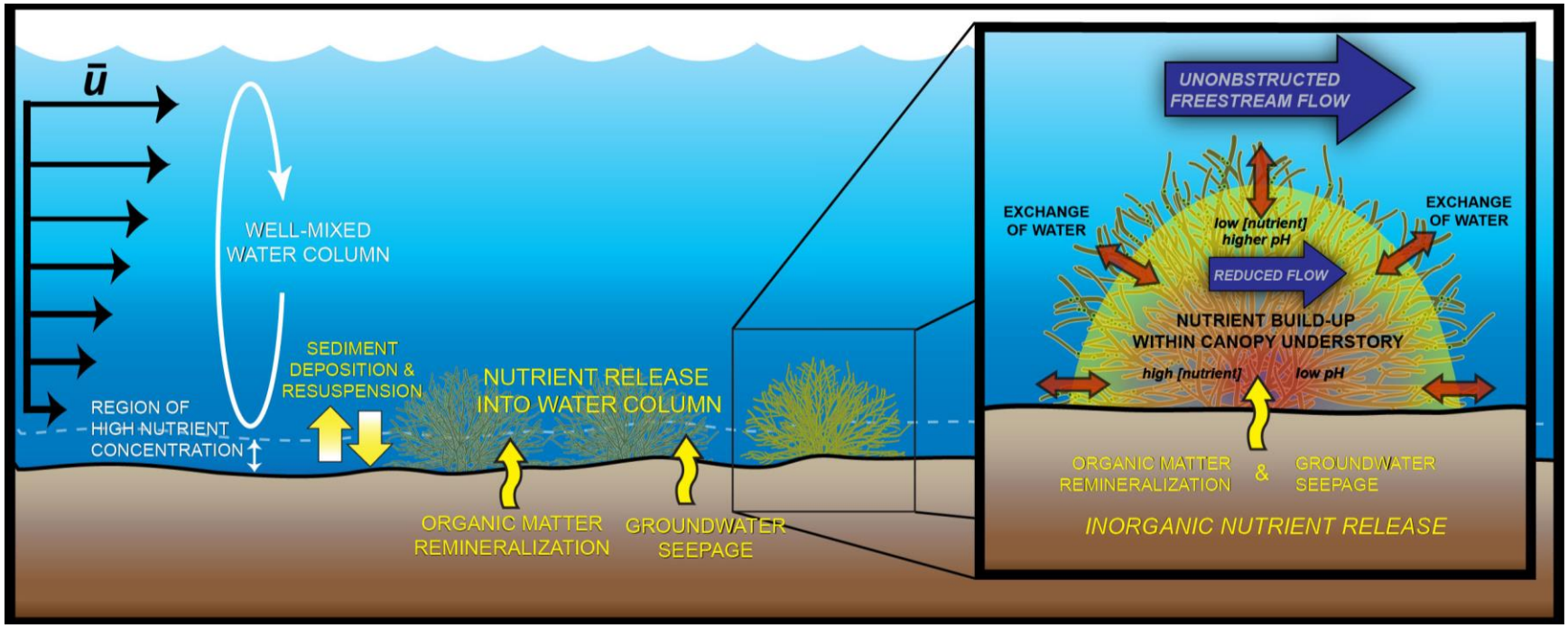

Appendix III – Flume Experiment Sampling Scheme

This appendix provides details of the paired flume experiment sampling scheme.

A3.T1 Table showing sampling scheme over 10-day experiment

SMPL ID (timepoint)	Sample description	water	Enzyme activity	DNA	Actual Time
WC	Field sample from collection site	✓	✓	✓	day before
LBKGD	Lab Background (acclimation container)	✓	✓	✓	N/A
FBKGD	Flume Background (before spike)	✓	✗	✗	N/A
T_0	00 mins	✓	✓	✓	11:00am
T_1	20 mins	✓	✓	✓	11:20am
T_2	40 mins	✓	✓	✓	11:40am
T_3	1 hr	✓	✓	✓	12:00 noon
T_4	3 hrs	✓	✓	✓	02:00pm
T_5	6 hrs	✓	✓	✓	05:00pm
T_6	12 hrs	✓	✓	✓	11:00pm
T_7	18 hrs	✓	✓	✓	05:00am
T_8	24 hrs (1d)	✓	✓	✓	11:00am
T_9	48 hrs (2d)	✓	✓	✓	11:00am
T_{10}	72 hrs (3d)	✓	✓	✓	11:00am
T_{11}	96 hrs (4d)	✓	✓	✓	11:00am
T_{12}	120 hrs (5d)	✓	✓	✓	11:00am
T_{13}	144 hrs (6d)	✓	✓	✓	11:00am
T_{14}	168 hrs (7d)	✓	✓	✓	11:00am
T_{15}	192 hrs (8d)	✓	✓	✓	11:00am
T_{16}	216 hrs (9d)	✓	✓	✓	11:00am
T_{17}	240 hrs (10d)	✓	✓	✓	11:00am

Appendix IV – Epiphyte vs. Macroalgae Host Enzyme Activity

In this appendix, supporting data is presented that demonstrate elevated epiphyte nitrate reductase enzyme activity compared to the macroalgal host.

A.

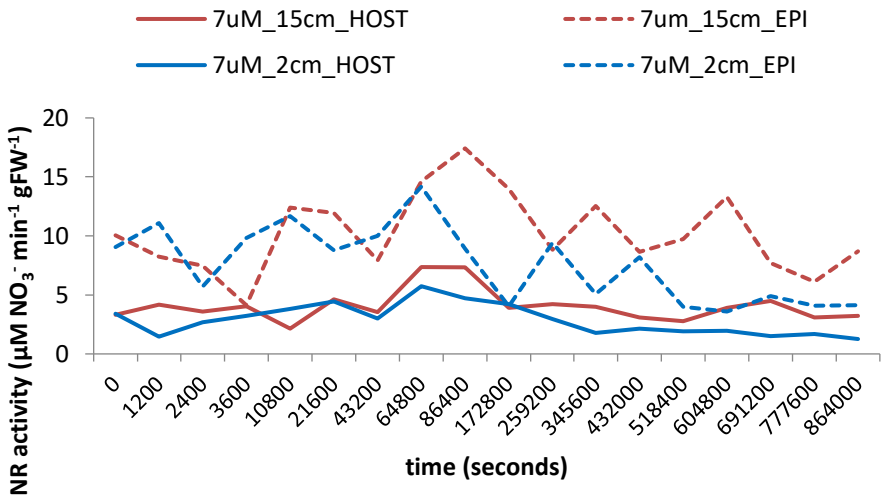

B.

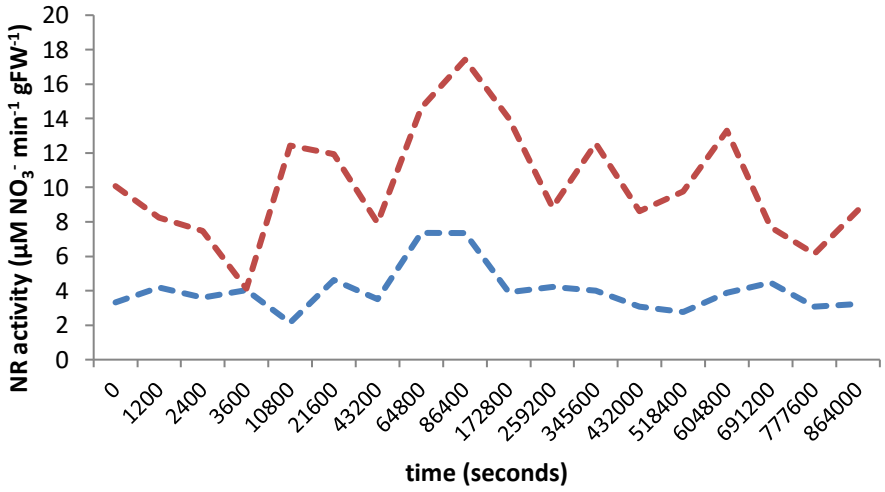

C.

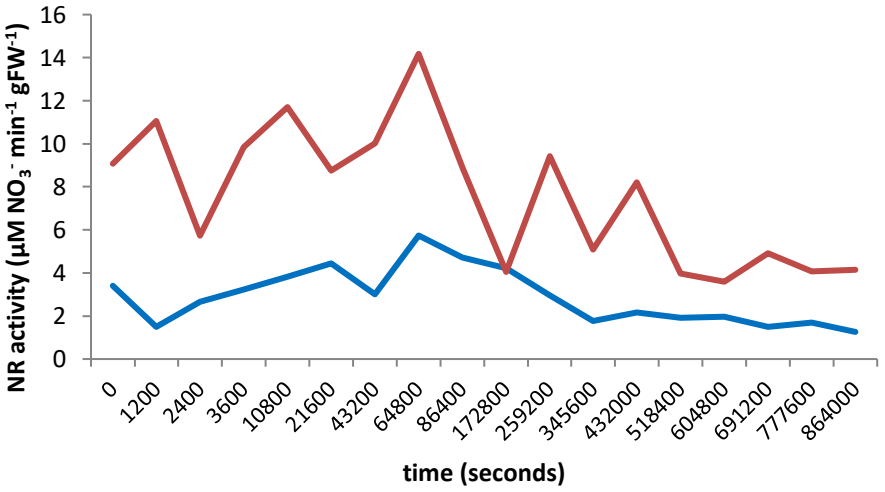

Figure A4.F1. (A) Time series of nitrate reductase activity for macroalgal host and epiphyte communities during a paired 10-day flume experiment. Nitrate concentration was set at 7 µM in both the **(B)** high flow (0.15 cms^{-1}; dashed lines) and **(C)** low flow (0.02 ms^{-1}); solid lines) flumes. Host activity is shown in blue and epiphyte activity is shown in red. For a given nitrate flux (i.e., concentration-flow combination), epiphyte NR activity is consistently higher than that of its macroalgal host.

Appendix V – Functional Gene Microarray Glossary

In this appendix, supplemental information to help clarify the terminology used frequently with functional gene microarray analysis is provided.

Box 1. **Functional Gene:** A gene that encodes an enzyme involved in some metabolic function, as contrasted to ribosomal genes, which encode a portion of the ribosome. The functional gene sequences upon which the probes were based were mostly obtained from clone libraries derived from PCR amplification, either from cultivated strains or from DNA extracted from environmental samples.

Probe: 70 bp oligonucleotide sequence designed to hybridize with sequences having >87% identity to the probe sequence. The probes were selected using an algorithm (Bulow *et al.* 2008) that identifies the 70-mer region of greatest variability within the aligned sequences, then iteratively identifies the set of sequences that represent all of the aligned sequences with the minimum number of probes and the minimum number of overlaps between sequences represented by individual probes. For example, 639 chromophyte *rbcL* sequences were aligned and the algorithm allows them to be represented by 78 probes.

Probe set: A group of probes identified as hybridizing with targets defined by phylogenetic affiliation. For example, all diatom *rbcL* genes should hybridize with one of the probes in the Diatom *rbcL* probe set. In reality, the probe set is not definitive because it is based on known sequences. Nevertheless, sequences which have >87% identity with the probe will be detected, even if the identity of those sequences are unknown.

Archetype: The group of sequences that hybridize to an individual probe. The probe is identified by the name of a single sequence, but it hybridizes to closely related sequences, and that group of target sequences is referred to as an archetype. The archetype includes an unknown number of individual sequences, which vary in identity with the probe from 87 to 100%. Therefore, the archetype is most likely composed of multiple different sequences, not only the one for which the probe with which they hybridize is named.

Figure A5.F1. Glossary of terms relevant to the phytoarray used in this study (after Ward and Van Oostende (2016).

Appendix VI – Nitrate Distribution Model Variables and Parameters

Table A6.T1 Table of Model Variables and Parameters, values and sources

ID	description	mean value / expression	range	units	source
VARIABLES					
N	Free dissolved nitrate in the water column	--	--	µg N m^{-3}	--
P	Phytoplankton-bound nitrate nitrogen	--	Dry Season: P = 22.959e03 to 186.370e03 Wet Season: P = 43.776e03 to 255.031e03	µg N m^{-3}	this study
G	*G. salicornia*-bound nitrate nitrogen	--	Dry Season: G = 0.186e03 to 2345.935e03 Wet Season: G = 0.0146e03 to 36.121e03	µg N m^{-3}	this study
A	*A. spicifera*-bound nitrate nitrogen	--	Dry Season: A = 0.087e03 to 208.962e03 Wet Season: A = 0.029e03 to 55.63e03	µg N m^{-3}	this study
M	microphytobenthos-bound nitrate nitrogen	--	Dry Season: M = 14.03e03 to 33.37e03 Wet Season: M = 13.37e03 to 42.34e03	µg N m^{-3}	this study
PARAMETERS					
Nbar	-- mean background nitrate concentration.	2.52 x10^3 µgN m^{-3} (0.18 µM)	--	µg N m^{-3}	- average of baseline (i.e. non-storm) surface and bottom water NO_3^- + NO_2^- across the area of the fishpond over the course of a year-long monitoring study (Young 2011)

ID	**description**	**mean value / expression**	**range**	**units**	**source**
sun	-- sine function applied to uptake -- allows the modulation of grazing rates and uptake rates based on time of day; uptake only takes place during daylight hours	sun = sin (omega*times + 7*3600); -- omega=((2*pi)/86400) -- times: vector of model timesteps	--	µgN m^{-3}	--
kp	half saturation constant for phytoplankton nitrate uptake	3600892.422	--	µgN m^{-3}	this study
kg	half saturation constant for *G. salicornia* nitrate uptake	1.194606535	--	µgN m^{-3}	this study
ka	half saturation constant for *A. spicifera* nitrate uptake	9.440917935	--	µgN m^{-3}	this study
km	half saturation constant for microphytobenthos nitrate uptake	0.002850092	--	µgN m^{-3}	this study
prho	8.79583 $x10^{-03}$	specific nitrate uptake rate by phytoplankton	--	µg N removed/µg N tissue/s or s^{-1}	-- values obtained empirically from isotope analysis of field flume experiments.
grho	1.84198 $x10^{-08}$*speed + litgrho litgrho = ln(1.6)/(7*86400) (60% increase over 7 days)	flow-dependent GS specific nitrate uptake rate	--	µg N removed/µg N tissue/s or s^{-1}	-- values obtained empirically from isotope analysis of field flume experiments and scaled by literature valued
arho	1.04213 $x10^{-07}$*speed + litarho litarho = ln(1.4)/(7*86400) (40% increase over 7 days)	flow-dependent AS specific nitrate uptake rate	--	µg N removed/µg N tissue/s or s^{-1}	-- values obtained empirically from isotope analysis of field flume experiments and scaled by literature valued

ID	description	mean value / expression	range	units	source
mrho	1.29620 x10^{-10}*speed + litmrho litmrho = ln(2)/(3.5*86400) (one doubling in 3.5 days)	flow-dependent MPB specific nitrate uptake rate	--	µg N removed/µg N tissue/s or s^{-1}	-- values obtained empirically from isotope analysis of field flume experiments and scaled by literature valued
q1	mortality rate for phytoplankton	1.61762 x10^{-06}	--	s^{-1}	0.15 and 0.88 d^{-1} (Obayashi & Tanoue 2005)

Table A6.T2 Field Flume Experiment Isotope Data Summary

Expt #	xRMS [ms-1]	Average [NO3] over 15 minutes	Component	%N in tissue	δ ^{15}N	Uptake rate, V [g N removed (g N tissue)$^{-1}$ s^{-1}]	Specific uptake rate, ρ [g N removed (g dry wt)$^{-1}$ s^{-1}]
1	0.0160	2.097	*G. salicornia*	0.85982	12.5	1.043E-07	8.965E-08
			A spicifera	0.99366	136.3	1.103E-06	1.096E-06
			microphytobenthos	0.07752	2.9	2.392E-08	1.855E-09
			phytoplankton	0.06868	224.0	1.852E-06	1.272E-07
4	0.0189	2.949	*G. salicornia*	1.29052	10.6	8.76E-08	1.131E-07
			A spicifera	1.46049	155.2	1.259E-06	1.838E-06
			microphytobenthos	0.09255	4.3	3.549E-08	3.284E-09
			phytoplankton	0.07478	258.4	2.219E-06	1.66E-07
6	0.0436	3.284	*G. salicornia*	--	--	--	--
			A spicifera	2.05991	63.6	4.908E-07	1.011E-06
			microphytobenthos	0.19426	2.8	2.311E-08	4.489E-09
			phytoplankton	0.13790	53.6	3.447E-07	4.754E-08
2	0.0453	2.701	*G. salicornia*	1.07479	19.1	1.587E-07	1.706E-07
			A spicifera	--	--	--	--
			microphytobenthos	0.12838	2.8	2.31E-08	2.966E-09
			phytoplankton	0.10508	169.9	1.404E-06	1.476E-07
3	0.1202	2.783	*G. salicornia*	1.051	15.8	1.315E-07	1.382E-07
			A spicifera	1.45569	100.5	8.076E-07	1.176E-06
			microphytobenthos	0.12287	3.2	2.64E-08	3.244E-09
			phytoplankton	0.12411	69.7	5.757E-07	7.145E-08
5	0.2650	3.358	*G. salicornia*	0.87314	73.9	8.76E-08	1.131E-07
			A spicifera	0.95793	470.4	3.852E-06	3.69E-06
			microphytobenthos	0.15995	4.4	3.631E-08	5.808E-09
			phytoplankton	0.13261	127.5	1.094E-06	1.451E-07

References

Ackerman JD, Okubo A (1993) Reduced Mixing in a Marine Macrophyte Canopy. Funct Ecol 7:305–309

Allen J (1998) Mangroves as alien species: the case of Hawaii. Glob Ecol Biogeogr Lett 7:61–71

Aller RC (1994) Bioturbation and remineralization of sedimentary organic matter: effects of redox oscillation. Chem Geol 114:331–345

Anderson DM, Glibert PM, Burkholder JM (2002) Harmful algal blooms and eutrophication: Nutrient sources, composition, and consequences. Estuaries 25:704–726

Arnold KE, Murray SN (1980) Relationships between irradiance and photosynthesis for marine benthic green algae (Chlorophyta) of differing morphologies. J Exp Mar Biol Ecol 43:183–192

Barnes RSK, Barnes MKS (2012) Shore height and differentials between macrobenthic assemblages in vegetated and unvegetated areas of an intertidal sandflat. Estuar Coast Shelf Sci 106:112–120

Bathen KH (1968) A descriptive study of the physical oceanography of Kaneohe Bay, Oahu, Hawaii.

Beach KS, Borgeas HB, Nishimura NJ, Smith CM (1997) In vivo absorbance spectra and the ecophysiology of reef macroalgae. Coral Reefs 16:21–28

Berner RA (1980) Early diagenesis: A theoretical approach. Princeton University Press

Bilger RW, Atkinson MJ (1995) Effects of nutrient loading on mass-transfer rates to a coral-reef community. Limnol Oceanogr 40:279–289

Boucher G, Clavier J, Garrigue C (1994) Estimation of bottom ammonium affinity in the New Caledonia lagoon. Coral Reefs 13:13–19

Boudreau BP (1997) A one-dimensional model for bed-boundary layer particle exchange. J Mar Syst 11:279–303

Bouma T, De Vries M, Low E, Peralta G, Tanczos I, Van de Koppel J, Herman PMJ (2005) Trade-offs related to ecosystem engineering: a case study on stiffness of emerging macrophytes. Ecology 86:2187–2199

Briggs RA (2011) Organic matter remineralization in coastal sediments in and around Kane ʻohe bay, Hawai ʻi.

Briggs RA, Ruttenberg KC, Glazer BT, Ricardo AE (2013) Constraining Sources of Organic Matter to Tropical Coastal Sediments: Consideration of Nontraditional End-members. Aquat Geochem 19:543–563

Bulow SE, Francis CA, Jackson GA, Ward BB (2008) Sediment denitrifier community composition and nirS gene expression investigated with functional gene microarrays. Environ Microbiol 10:3057–3069

Burdige DJ (2006) Geochemistry of marine sediments. Princeton University Press Princeton

Campbell WH (1999) Nitrate Reductase Structure, Function and Regulation: Bridging the Gap between Biochemistry and Physiology. Annu Rev Plant Physiol Plant Mol Biol 50:277–303

Chícharo MA, Chícharo L (2008) RNA:DNA Ratio and Other Nucleic Acid Derived Indices in Marine Ecology. Int J Mol Sci 9:1453–1471

Cornelisen CD, Thomas FIM (2002) Ammonium Uptake by Seagrass Epiphytes: Isolation of the Effects of Water Velocity Using an Isotope Label. Limnol Oceanogr 47:1223–1229

Cornelisen CD, Thomas FI (2004) Ammonium and nitrate uptake by leaves of the seagrass< i> Thalassia testudinum: impact of hydrodynamic regime and epiphyte cover on uptake rates. J Mar Syst 49:177–194

Cornelisen CD, Thomas FIM (2006) Water flow enhances ammonium and nitrate uptake in a seagrass community. Mar Ecol Prog Ser 312:1–13

Dahlgren CP, Eggleston DB (2001) Spatio-temporal variability in abundance, size and microhabitat associations of early juvenile Nassau grouper Epinephelus striatus in an off-reef nursery system. Mar Ecol Prog Ser 217:145–156

De Carlo EH, Hoover DJ, Young CW, Hoover RS, Mackenzie FT (2007) Impact of storm runoff from tropical watersheds on coastal water quality and productivity. Appl Geochem 22:1777–1797

D'Elia CF, DeBoer JA (1978) Nutritional Studies of Two Red Algae .II. Kinetics of Ammonium and Nitrate Uptake. J Phycol 14:266–272

Diaz RJ, Rosenberg R (2008) Spreading Dead Zones and Consequences for Marine Ecosystems. Science 321:926–929

Duarte CM, Losada IJ, Hendriks IE, Mazarrasa I, Marba N (2013) The role of coastal plant communities for climate change mitigation and adaptation. Nat Clim Change 3:961–968

Dulai H, Kleven A, Ruttenberg K, Briggs R, Thomas F (2016) Evaluation of Submarine Groundwater Discharge as a Coastal Nutrient Source and Its Role in Coastal Groundwater Quality and Quantity. In: Fares A (ed) Emerging Issues in Groundwater Resources. Springer International Publishing, Cham, p 187–221

Ellingsen KE, Hewitt JE, Thrush SF (2007) Rare species, habitat diversity and functional redundancy in marine benthos. J Sea Res 58:291–301

Eppley RW, Rogers JN, McCarthy JJ (1969) Half-saturation constants for uptake of nitrate and ammonium by marine phytoplankton. Limnol Oceanogr 14:912–920

Eutrophication in Europe's coastal waters Topic report 7/2001 (2001) European Environment Agency

Fagan KE, Mackenzie FT (2007) Air–sea CO 2 exchange in a subtropical estuarine-coral reef system, Kaneohe Bay, Oahu, Hawaii. Mar Chem 106:174–191

Falter JL, Sansone FJ (2000) Hydraulic control of pore water geochemistry within the oxic-suboxic zone of a permeable sediment. Limnol Oceanogr 45:550–557

Flores E, Frías J, Rubio L, Herrero A (2005) Photosynthetic nitrate assimilation in cyanobacteria. Photosynth Res 83:117–133

Flores E, Guerrero M, Losada M (1980) Short-term ammonium inhibition of nitrate utilization by Anacystis nidulans and other cyanobacteria. Arch Microbiol 128:137–144

Foley CJ, Bradley DL, Höök TO (2016) A review and assessment of the potential use of RNA:DNA ratios to assess the condition of entrained fish larvae. Ecol Indic 60:346–357

Fonseca G, Hutchings P, Gallucci F (2011) Meiobenthic communities of seagrass beds (Zostera capricorni) and unvegetated sediments along the coast of New South Wales, Australia. Estuar Coast Shelf Sci 91:69–77

Fukunaga A, Peyton KA, Thomas FIM (2014) Epifaunal community structure and ammonium uptake compared for the invasive algae, Gracilaria salicornia and Acanthophora specifera, and the native alga, Padina thivyi. J Exp Mar Biol Ecol 456:78–86

Gambi MC, Lorenti M, Russo GF, Scipione MB, Zupo V (1992) Depth and Seasonal Distribution of Some Groups of the Vagile Fauna of the Posidonia oceanica Leaf Stratum: Structural and Trophic Analyses. Mar Ecol 13:17–39

Ghisalberti M, Nepf HM (2002) Mixing layers and coherent structures in vegetated aquatic flows. J Geophys Res Oceans 107:3–1

Ghisalberti M, Nepf H (2009) Shallow Flows Over a Permeable Medium: The Hydrodynamics of Submerged Aquatic Canopies. Transp Porous Media 78:309–326

Giambelluca TW, Nullet MA, Schroeder TA, University of Hawaii at Manoa. Water Resources Research Center, University of Hawaii at Manoa. Department of Meteorology, Hawaii. Division of Water and Land Development (1986) Rainfall atlas of Hawai‘i.

Giraud X, Le Quéré C, Cunha LC da (2008) Importance of coastal nutrient supply for global ocean biogeochemistry. Glob Biogeochem Cycles 22:n/a-n/a

Goering JJ, Parker PL (1972) NITROGEN FIXATION BY EPIPHYTES ON SEA GRASSES1. Limnol Oceanogr 17:320–323

Goring DG, Nikora VI (2002) Despiking acoustic Doppler velocimeter data. J Hydraul Eng 128:117–126

Granbom M, Chow F, Lopes PF, Oliveira MC de, Colepicolo P, Paula EJ de, Pedersén M (2004) Characterisation of nitrate reductase in the marine macroalga Kappaphycus alvarezii (Rhodophyta). Aquat Bot 78:295–305

Grebmeier JM, McRoy CP, Feder HM (1988) Pelagic-benthic coupling on the shelf of the northern Bering and Chukchi seas. 1. Food supply source and benthic biomass. Mar Ecol Prog Ser Oldendorf 48:57–67

Harley CD, Randall Hughes A, Hultgren KM, Miner BG, Sorte CJ, Thornber CS, Rodriguez LF, Tomanek L, Williams SL (2006) The impacts of climate change in coastal marine systems. Ecol Lett 9:228–241

Harris KR, Newitt PJ (1997) Self-Diffusion of Water at Low Temperatures and High Pressure. J Chem Eng Data 42:346–348

Hawaii Agricultural Land Use Study Released (2016) State Hawaii Dep Agric

Hill MO (1973) Diversity and Evenness: A Unifying Notation and Its Consequences. Ecology 54:427–432

Holtappels M, Kuypers MMM, Schlüter M, Brüchert V (2011) Measurement and interpretation of solute concentration gradients in the benthic boundary layer. Limnol Oceanogr Methods 9:1–13

Holz M, Heil SR, Sacco A (2000) Temperature-dependent self-diffusion coefficients of water and six selected molecular liquids for calibration in accurate 1H NMR PFG measurements. Phys Chem Chem Phys 2:4740–4742

Hoover D, Mackenzie F (2009) Fluvial fluxes of water, suspended particulate matter, and nutrients and potential impacts on tropical coastal water biogeochemistry: Oahu, Hawai 'I. Aquat Geochem 15:547–570

Howarth RW, Marino R (2006) Nitrogen as the limiting nutrient for eutrophication in coastal marine ecosystems: Evolving views over three decades. Limnol Oceanogr 51:364–376

Huettel M, Røy H, Precht E, Ehrenhauss S (2003) Hydrodynamical impact on biogeochemical processes in aquatic sediments. Hydrobiologia 494:231–236

Hurd CL (2000) Water Motion, Marine Macroalgal Physiology, and Production. J Phycol 36:453–472

Hurd CL, Harrison PJ, Druehl LD (1996) Effect of seawater velocity on inorganic nitrogen uptake by morphologically distinct forms of Macrocystis integrifolia from wave-sheltered and exposed sites. Mar Biol 126:205–214

Jacoby C, Walters L, Baker S, BYler K (2004) A Primer on Invasive Species in Coastal and Marine Waters.

Jorissen FJ, Stigter HC de, Widmark JGV (1995) A conceptual model explaining benthic foraminiferal microhabitats. Sel Pap Fifth Int Symp Foraminifera 26:3–15

Jost L (2006) Entropy and diversity. Oikos 113:363–375

Karez R, Engelbert S, Sommer U (2000) Co-consumption and protective coating: two new proposed effects of epiphytes on their macroalgal hosts in mesograzer-epiphyte-host interactions. Mar Ecol Prog Ser 205:85–93

Kregting LT, Bass AL, Guadayol Ò, Yund PO, Thomas FI (2013) Effects of Oscillatory Flow on Fertilization in the Green Sea Urchin Strongylocentrotus droebachiensis. PloS One 8:e76082

Landry MR, Haas LW, Fagerness VL (1984) Dynamics of microbial plankton communities: experiments in Kaneohe Bay, Hawaii. Mar Ecol Prog Ser 16:127–133

Lapointe BE, Barile PJ, Littler MM, Littler DS (2005) Macroalgal blooms on southeast Florida coral reefs: II. Cross-shelf discrimination of nitrogen sources indicates widespread assimilation of sewage nitrogen. Harmful Algae 4:1106–1122

Lapointe BE, Bedford BJ (2011) Stormwater nutrient inputs favor growth of non-native macroalgae (Rhodophyta) on O'ahu, Hawaiian Islands. Harmful Algae 10:310–318

Lapointe BE, O'Connell J (1989) Nutrient-enhanced growth of Cladophora prolifera in harrington sound, bermuda: Eutrophication of a confined, phosphorus-limited marine ecosystem. Estuar Coast Shelf Sci 28:347–360

Larkum A, Orth R, Duarte C (2006) Seagrasses: Biology, Ecology and Conservation.

Larned ST (1998) Nitrogen- versus phosphorus-limited growth and sources of nutrients for coral reef macroalgae. Mar Biol 132:409–421

Larned ST, Stimson J (1996) Nitrogen-limited growth in the coral reef chlorophyte Dictyosphaeriacavernosa, and the effect of exposure to sediment-derived nitrogen on growth. Mar Ecol Prog Ser 145:95–108

Lavery PS, Reid T, Hyndes GA, Van Elven BR (2007) Effect of leaf movement on epiphytic algal biomass of seagrass leaves. Mar Ecol Prog Ser 338:97–106

Laws EA, Redalje D, Haas L, Bienfang P, Eppley R, Harrison W, Karl D, Marra J (1984) High phytoplankton growth and production rates in oligotrophic Hawaiian coastal waters. Limnol Oceanogr 29:1161–1169

Lee K-S, Park SR, Kim YK (2007) Effects of irradiance, temperature, and nutrients on growth dynamics of seagrasses: a review. J Exp Mar Biol Ecol 350:144–175

Levin SA (1981) Mechanisms for the Generation and Maintenance of Diversity in Ecological Communities. In: The Mathematical theory of the dynamics of biological populations II : based on the proceedings of a conference on the mathematical theory of the dynamics of biological

populations organised by The Institute of Mathematics and Its Applications and held in Oxford, 1st-3rd July, 1980. Academic Press, London ; New York, p 173–194

Levin SA (2000) Multiple Scales and the Maintenance of Biodiversity. Ecosystems 3:498–506

Lewis JB (1987) Measurements of Groundwater Seepage Flux Onto a Coral Reef: Spatial and Temporal Variations. Limnol Oceanogr 32:1165–1169

Lowe RJ, Koseff JR, Monismith SG (2005) Oscillatory flow through submerged canopies: 1. Velocity structure. J Geophys Res Oceans 1978–2012 110

Mabrouk L, Ben Brahim M, Hamza A, Mahfoudhi M, Bradai MN (2014) A Comparison of Abundance and Diversity of Epiphytic Microalgal Assemblages on the Leaves of the Seagrasses Posidonia oceanica (L.) and Cymodocea nodosa (Ucria) Asch in Eastern Tunisia. J Mar Biol 2014

Mabrouk L, Hamza A, Brahim MB, Bradai M-N (2011) Temporal and depth distribution of microepiphytes on Posidonia oceanica (L.) Delile leaves in a meadow off Tunisia. Mar Ecol 32:148–161

Mabrouk L, Hamza A, Mahfoudi M, Bradai M-N (2012) Spatial and temporal variations of epiphytic Ostreopsis siamensis on Posidonia oceanica (L.) Delile leaves in Mahdia (Tunisia). Cah Biol Mar 53:419–427

Marcus NH, Boero F (1998) Minireview: The Importance of Benthic-Pelagic Coupling and the Forgotten Role of Life Cycles in Coastal Aquatic Systems. Limnol Oceanogr 43:763–768

Marino D, Montresor M, International Society for Diatom Research (1995) Proceedings of the Thirteenth International Diatom Symposium: Maratea, Italy, 1st-7th September 1994. Biopress Limited

Martinez JA, Smith CM, Richmond RH (2012) Invasive algal mats degrade coral reef physical habitat quality. Estuar Coast Shelf Sci 99:42–49

Marx J, Herrnkind W (1985) Factors Regulating Microhabitat Use by Young Juvenile Spiny Lobsters, Panulirus argus: Food and Shelter. J Crustac Biol 5:650–657

McCoy D, McManus MA, Kotubetey K, Kawelo AH, Young C, D'Andrea B, Ruttenberg KC, Alegado R 'Anolani (2017) Large-scale climatic effects on traditional Hawaiian fishpond aquaculture. PLOS ONE 12:e0187951

McLelland SJ, Nicholas AP (2000) A new method for evaluating errors in high-frequency ADV measurements. Hydrol Process 14:351–366

Mendez FJ, Losada IJ (2004) An empirical model to estimate the propagation of random breaking and nonbreaking waves over vegetation fields. Coast Eng 51:103–118

Miller S, Shima J, Phillips N (2012) Effects of microhabitat availability on estimates of density of a reef fish: implications for assessments of marine protected areas. Hydrobiologia 685:173–190

Moncreiff CA, Sullivan MJ (2001) Trophic importance of epiphytic algae in subtropical seagrass beds: evidence from multiple stable isotope analyses. Mar Ecol Prog Ser 215:93–106

Montfrans J van, Wetzel RL, Orth RJ (1984) Epiphyte-Grazer Relationships in Seagrass Meadows: Consequences for Seagrass Growth and Production. Estuaries 7:289–309

Mulder C, Hendriks AJ (2014) Half-saturation constants in functional responses. Glob Ecol Conserv 2:161–169

Murphy JL (2012) Linking Benthic Algae to Sediment Oxidation-Reduction Dynamics: Implications for Sediment-Water Interface Nutrient Cycling. Ann Arbor 1001:48106–1346

Nelson TA (1997) Epiphyte-Grazer Interactions on Zostera marina (Anthophyta: monocotyledones): Effects of Density on Community Function. J Phycol 33:743–752

Nepf H (1999) Drag, turbulence, and diffusion in flow through emergent vegetation. Water Resour Res 35:479–489

Ni-Ni-Win, Hanyuda T, Arai S, Uchimura M, Prathep A, Draisma SGA, Phang SM, Abbott IA, Millar AJK, Kawai H (2011) A Taxonomic study of the genus Padina (Dictyotales, Phaeophyceae) including the Descriptions of Four New Species From Japan, Hawaii, And The Andaman Sea. J Phycol 47:1193–1209

Nortek AS (2015) Comprehensive Manual. Nortek Vangkroken 2 1351 Rud Nor

Obayashi Y, Tanoue E (2002) Growth and mortality rates of phytoplankton in the northwestern North Pacific estimated by the dilution method and HPLC pigment analysis. J Exp Mar Biol Ecol 280:33–52

Ohashi Y, Shi W, Takatani N, Aichi M, Maeda S, Watanabe S, Yoshikawa H, Omata T (2011) Regulation of nitrate assimilation in cyanobacteria. J Exp Bot 62:1411–1424

Ormond RFG, Roberts JM, Jan R-Q (1996) Behavioural differences in microhabitat use by damselfishes (Pomacentridae): implications for reef fish biodiveristy. Mar Biodivers 202:85–95

Ostrander CE, McManus MA, DeCarlo EH, Mackenzie FT (2008) Temporal and spatial variability of freshwater plumes in a semienclosed estuarine–bay system. Estuaries Coasts 31:192

Paul M, Bouma T, Amos C (2012) Wave attenuation by submerged vegetation: -combining the effect of organism traits and tidal current. Mar Ecol Prog Ser 444:31–41

Percuoco VP, Kalnejais LH, Officer LV (2015) Nutrient release from the sediments of the Great Bay Estuary, N.H. USA. Estuar Coast Shelf Sci 161:76–87

Pittman S, McAlpine C (2003) Movements of marine fish and decapod crustaceans: Process, theory and application. In: Advances in Marine Biology. Academic Press, p 205–294

Prado P, Alcoverro T, Martínez-Crego B, Vergés A, Pérez M, Romero J (2007) Macrograzers strongly influence patterns of epiphytic assemblages in seagrass meadows. Biol Ecol Seagrasses 350:130–143

Prado P, Alcoverro T, Romero J (2008) Seasonal response of Posidonia oceanica epiphyte assemblages to nutrient increase. Mar Ecol Prog Ser 359:89–98

Price S (1983) Atlas of Hawaii, 2nd edn. University of Hawaii Press

Prinos P, Stratigaki V, Manca E, Losada I, López Lara J, Sclavo M, Cáceres Rabionet I, Sánchez-Arcilla Conejo A (2010) Wave propagation over Posidonia oceanica: large scale experiments.

Rabalais NN, Turner RE, JustiĆ D, Dortch Q, Wiseman WJ, Sen Gupta BK (1996) Nutrient changes in the Mississippi River and system responses on the adjacent continental shelf. Estuaries 19:386–407

Redalje DG, Laws EA (1981) A new method for estimating phytoplankton growth rates and carbon biomass. Mar Biol 62:73–79

Ringuet S, Mackenzie FT (2005) Controls on nutrient and phytoplankton dynamics during normal flow and storm runoff conditions, southern Kaneohe Bay, Hawaii. Estuaries 28:327–337

Rodgers S, Cox EF (1999) Rate of Spread of Introduced Rhodophytes Kappaphycus alvarezii, Kappaphycus striatum, and Gracilaria salicornia and Their Current Distribution in Kane'ohe Bay, O'ahu Hawai'i.

Ruttenberg K, Briggs R (2012) Impact of Nutrient Biogeochemistry on Invasive Algal Distributions Along an Anthropogenic Impact Gradient, Kaneohe Bay, Hawaii.

Scavia D, Field JC, Boesch DF, Buddemeier RW, Burkett V, Cayan DR, Fogarty M, Harwell MA, Howarth RW, Mason C (2002) Climate change impacts on US coastal and marine ecosystems. Estuaries 25:149–164

Seitzinger SP, Kroeze C, Bouwman AF, Caraco N, Dentener F, Styles RV (2002) Global Patterns of Dissolved Inorganic and Particulate Nitrogen Inputs to Coastal Systems: Recent Conditions and Future Projections. Estuaries 25:640–655

Selph KE, Jungbluth M, Goetze E, Chang S, Uchida M, Kolker G (2016) Phytoplankton and microzooplankton growth and grazing dynamics in Kaneohe Bay, Hawaii, a subtropical estuarine coastal embayment

Seymour JR, Marcos and, Stocker R (2009) Resource Patch Formation and Exploitation throughout the Marine Microbial Food Web. Am Nat 173:E15–E29

Sherameti I, Sopory SK, Trebicka A, Pfannschmidt T, Oelmüller R (2002) Photosynthetic Electron Transport Determines Nitrate Reductase Gene Expression and Activity in Higher Plants. J Biol Chem 277:46594–46600

Siple MC, Donahue MJ (2013) Invasive mangrove removal and recovery: Food web effects across a chronosequence. J Exp Mar Biol Ecol 448:128–135

Smith JE, Hunter CL, Conklin EJ, Most R, Sauvage T, Squair C, Smith CM (2004) Ecology of the invasive red alga Gracilaria salicornia (Rhodophyta) on O'ahu, Hawai'i. Pac Sci 58:325–343

Smith JE, Hunter CL, Smith CM (2002) Distribution and reproductive characteristics of nonindigenous and invasive marine algae in the Hawaiian Islands. Pac Sci 56:299–315

Smith SV, Kimmerer WJ, Laws EA, Brock RE, Walsh TW (1981) Kaneohe Bay sewage diversion experiment: perspectives on ecosystem responses to nutritional perturbation. Pac Sci 35:279–395

Stiansen JE, Sundby S (2001) Improved methods for generating and estimating turbulence in tanks suitable for fish larvae experiments. Sci Mar 65:151–167

Stimson J, Larned S. (2000) Nitrogen efflux from the sediments of a subtropical bay and the potential contribution to macroalgal nutrient requirements. J Exp Mar Biol Ecol 252:159–180

Stimson J, Larned S, Conklin E (2001) Effects of herbivory, nutrient levels, and introduced algae on the distribution and abundance of the invasive macroalga Dictyosphaeria cavernosa in Kaneohe Bay, Hawaii. Coral Reefs 19:343–357

Stimson J, Larned S, McDermid K (1996) Seasonal growth of the coral reef macroalga Dictyosphaeria cavernosa (Forskål) Børgesen and the effects of nutrient availability, temperature and herbivory on growth rate. J Exp Mar Biol Ecol 196:53–77

Strickland JDH (John DH (1972) A practical handbook of seawater analysis, (TR Parsons and JDH Strickland, Eds.).

Taroncher-Oldenburg G, Griner EM, Francis CA, Ward BB (2003) Oligonucleotide microarray for the study of functional gene diversity in the nitrogen cycle in the environment. Appl Environ Microbiol 69:1159–1171

The battle for the coast (2010) World Ocean Rev 1–Overview

Thomas FIM, Atkinson MJ (1997) Ammonium Uptake by Coral Reefs: Effects of Water Velocity and Surface Roughness on Mass Transfer. Limnol Oceanogr 42:81–88

Throndsen J (1997) Chapter 5 - The Planktonic Marine Flagellates A2 - Tomas, Carmelo R. In: Identifying Marine Phytoplankton. Academic Press, San Diego, p 591–729

Tofts PS, Lloyd D, Clark CA, Barker GJ, Parker GJM, McConville P, Baldock C, Pope JM (2000) Test liquids for quantitative MRI measurements of self-diffusion coefficient in vivo. Magn Reson Med 43:368–374

Trujillo AP, Thurman HV (2013) Essentials of Oceanography, 11th edn. Prentice Hall

Valiela I, McClelland J, Hauxwell J, Behr PJ, Hersh D, Foreman K (1997) Macroalgal blooms in shallow estuaries: Controls and ecophysiological and ecosystem consequences. Limnol Oceanogr 42:1105–1118

Vaudo JJ, Heithaus MR (2013) Microhabitat Selection by Marine Mesoconsumers in a Thermally Heterogeneous Habitat: Behavioral Thermoregulation or Avoiding Predation Risk? PLoS ONE 8:e61907

Verduin JJ, Backhaus JO (2000) Dynamics of Plant–Flow Interactions for the Seagrass Amphibolis antarctica: Field Observations and Model Simulations. Estuar Coast Shelf Sci 50:185–204

Vogel S (1996) Life in Moving Fluids: The Physical Biology of Flow, 467 pp, 2nd edn. Princeton University Press

Wahl TL (2003) Discussion of "Despiking acoustic doppler velocimeter data" by Derek G. Goring and Vladimir I. Nikora. J Hydraul Eng 129:484–487

Wallsgrove R, Penn D (2012) Water Resources and Climate Change Adaptation in Hawai 'i: Adaptive Tools in the Current Law and Policy Framework. Univ Hawai 'i Cent Isl Adapt Policy

Ward B, Bouskill N (2011) The utility of functional gene arrays for assessing community composition, relative abundance, and distribution of ammonia-oxidizing bacteria and archaea. Methods Enzymol 496:373–396

Ward BB, Van Oostende N (2016) Phytoplankton assemblage during the North Atlantic spring bloom assessed from functional gene analysis. J Plankton Res 38:1135–1150

Weitzman J, Aveni-Deforge K, Koseff J, Thomas F (2013) Uptake of dissolved inorganic nitrogen by shallow seagrass communities exposed to wave-driven unsteady flow. Mar Ecol Prog Ser 475:65–83

Wheeler WN (1980) Effect of boundary layer transport on the fixation of carbon by the giant kelp Macrocystis pyrifera. Mar Biol 56:103–110

Wheeler WN (1988) Algal productivity and hydrodynamics-a synthesis. Prog Phycol Res 6:23–58

Williams S, Carpenter R (1988) Nitrogen-limited primary productivity of coral reef algal turfs: potential contribution of ammonium excreted by Diadema antillarum. Mar Ecol Prog Ser Oldendorf 47:145–152

Woodbury AM (1933) Biotic Relationships of Zion Canyon, Utah with Special Reference to Succession. Ecol Monogr 3:151–245

Wu L, Kellogg L, Devol AH, Tiedje JM, Zhou J (2008) Microarray-Based Characterization of Microbial Community Functional Structure and Heterogeneity in Marine Sediments from the Gulf of Mexico. Appl Environ Microbiol 74:4516–4529

Yamamuro M (1999) Importance of epiphytic cyanobacteria as food sources for heterotrophs in a tropical seagrass bed. Coral Reefs 18:263–271

Young CW (2011) Perturbation of nutrient inventories and phytoplankton community composition during storm events in a tropical coastal system: He'eia Fishpond, O'ahu, Hawai'i. [Honolulu]:[University of Hawaii at Manoa],[May 2011]

Young EB, Dring MJ, Berges JA (2007) Distinct patterns of nitrate reductase activity in brown algae: light and ammonium sensitivity in Laminaria digitata is absent in Fucus species1. J Phycol 43:1200–1208

Young EB, Lavery PS, Elven B van, Dring MJ, Berges JA (2005) Nitrate reductase activity in macroalgae and its vertical distribution in macroalgal epiphytes of seagrasses. Mar Ecol Prog Ser 288:103–114

Zajac RN, Vozarik JM, Gibbons BR (2013) Spatial and Temporal Patterns in Macrofaunal Diversity Components Relative to Sea Floor Landscape Structure. PLoS ONE 8:e65823